NUMERICAL SIMULATION OF A DIRECT EXPANSION GEOTHERMAL HEAT PUMP USING CARBON DIOXIDE IN A TRANSCRITICAL CYCLE

A Thesis
Submitted to the Graduate Faculty
of the
North Dakota State University
of Agriculture and Applied Science

By

Brian Thomas Austin

In Partial Fulfillment of the Requirements
for the Degree of
MASTER OF SCIENCE

Major Department:
Mechanical Engineering

May 2011

Fargo, North Dakota

North Dakota State University
Graduate School

Title

Numerical Simulation of a Direct Expansion Geothermal Heat Pump

Using Carbon Dioxide in a Transcritical Cycle

By

Brian Austin

The Supervisory Committee certifies that this ***disquisition*** complies with North Dakota State University's regulations and meets the accepted standards for the degree of

MASTER OF SCIENCE

ABSTRACT

Austin, Brian Thomas, M.S., Department of Mechanical Engineering, College of Engineering and Architecture, North Dakota State University, May 2011. Numerical Simulation of a Direct Expansion Geothermal Heat Pump Using Carbon Dioxide in a Transcritical Cycle. Major Professor: Dr. Sumathy Krishnan.

Many of the synthetic refrigerants used in heat pump and air conditioning systems are potent greenhouse gases. In light of the increasing concern regarding climate change, there has been an increased interest in natural refrigerants such as carbon dioxide which have a comparatively negligible impact on climate change. Direct expansion geothermal heat pumps require a very large volume of refrigerant, making the use of a natural refrigerant particularly beneficial from an environmental perspective.

In this study a numerical model has been developed to analyze the steady state performance of a direct expansion geothermal heat pump water heater using carbon dioxide in a transcritical cycle. The system incorporates a compressor, a counter-flow gas cooler, an expansion device and a ground heat exchanger which is the system evaporator. The model was developed by means of thermodynamic, heat transfer and fluid flow analysis of each component of the system. A comparison between predicted component performance and experimental results available in the literature indicated that the simulation can provide a reasonably accurate representation of an actual system. Given this verification, the simulation was used to gain an understanding of the direct expansion CO_2 geothermal heat pump's performance under varying design

and operating parameters. The salient parameters which were studied include: compressor speed, ground coil length, number of ground circuits and gas cooler length. The effect of monthly soil temperature variation was also investigated.

The parametric study revealed several factors which are important for system optimization. First, at any given soil temperature an optimum mean evaporation temperature exists; even a small deviation from this optimum can have a significant impact on coefficient of performance. Another important factor is the number of evaporator circuits. Finally, the gas cooler and evaporator capacities were shown to have a large impact on performance; heat exchanger capacities should be matched for optimum performance. Utilizing the findings of the study, an optimized system was simulated and compared to the baseline. The optimized system achieved a coefficient of performance of 2.58, representing an 18% improvement over the baseline system. Heating capacity increased 17% to 12.3 kW. The study suggests that with further research and optimization, carbon dioxide can perform well in a direct expansion geothermal heat pump and is a suitable replacement for more environmentally degrading refrigerants.

ACKNOWLEDGEMENTS

A sincere thank you to Dr. Sumathy for her encouragement and patience through this process. Thank you to Dr. Pryor, Dr. Stewart and Dr. Akhatov for being a part of my committee. My appreciation also goes out to each of the professors who taught the courses I enrolled in during my graduate studies. A big thank you to Donna Alby, Tanya Ericson and Tiffany Neuharth in the Mechanical Engineering Office for all their help during my two years here at NDSU. Donna especially was always able to answer my questions or point me in the right direction. The office always had a supply of animal crackers and I certainly ate my share. Thanks.

Thank you to God for curiosity, learning, knowledge, and for this opportunity. Finally, thank you to my friends and family who make life fun. I am especially grateful to my parents Robert and Audrey Austin. Their encouragement has been consistent throughout my wandering journey. I am grateful for their love and support.

TABLE OF CONTENTS

LIST OF TABLES

LIST OF FIGURES

NOMENCLATURE

A	Surface area (m^2)
bd	Bond Number
Bo	Boiling Number
C	Heat capacity rate ($kJ/s \cdot K$)
COP	Coefficient of Performance
c_p	Specific heat capacity ($kJ/kg \cdot K$)
d	Diameter (m)
d_h	Hydraulic diameter
e	Error
f	Friction factor
F_p	Heat transfer enhancement factor
G	Mass flux ($kg/m^2 \cdot s$)
g	Gravitational acceleration (m/s^2)
h	Specific enthalpy (kJ/kg)
h_{fg}	Enthalpy of vaporization (kJ/kg)
k	Thermal conductivity ($kW/m \cdot K$)
L	Length (m)
$\dot{m}$	Mass flow rate (kg/s)
N	Compressor speed (htz)
NTU	Number of transfer units
Nu	Nusselt number
P	Pressure (kPa)
Pr	Prandl number
q	Heat flux (kW/m^2)
$\dot{Q}$	Heat transfer rate (kW)
$\dot{Q}_i$	Heat extraction rate of Ground Heat Exchanger (kW)
$\dot{Q}_o$	Heating capacity of system (kW)

R	Heat capacity ratio
Re	Reynolds number
T	Temperature (K)
T_{soil}	Soil temperature (K)
$\bar{T}_{ev}$	Mean evaporation temperature (K)
ΔT_{app}	Approach temperature difference (K)
u	Velocity (m/s)
U	Overall heat transfer coefficient (kW/m^2·K)
$\dot{V}$	Volumetric Flow Rate (m^3/s)
V_s	Swept volume of compressor (m^3)
$\dot{W}$	Power (kW)
x	Quality
Xtt	Two-phase multiplier
Z	Height (m)

Greek Letters

α	Heat transfer coefficient (kW/m^2·K)
α_{sa}	Nucleate Pool-Boiling Ht Trans Coef. (kW/m^2·K)
β	Contact angle (degrees)
Δ	Difference
ϵ	Heat exchanger effectiveness
η_{mech}	Mechanical efficiency
η_s	Isentropic efficiency
η_{tot}	Total compressor efficiency
η_{vol}	Volumetric compressor efficiency
σ	Surface tension (N/m)
ρ	Density (kg/ m^3)
ϕ_{lo}	Liquid only 2-phase multiplier
φ	Nucleate boiling factor
μ	Viscosity (Pa·s)

Subscripts

atm	Atmospheric
b	Bulk
c	CO_2
calc	Calculated
comp	Compressor
crit	Critical
e	Exit
est	Estimated
ev	Evaporator
g	Gaseous state
i	Inner / inlet
isen	Isentropic
l	Liquid
lo	Liquid only
max	Maximum
min	Minimum
o	Outer / outlet
pc	Pseudo-critical
sat	Saturation
suc	Suction
sup	Superheat
v	Vapor
w	Water

1. INTRODUCTION

1.1. General Introduction

Climate change has become a major issue for business, industry and the general populous. Debate on climate change typically focuses on carbon dioxide (CO_2) emissions because, as the byproduct of fossil fuel combustion and many industrial processes, the amount of CO_2 given off is so vast. Qualitatively, however, CO_2's impact on climate change is actually much smaller than many other atmospheric gases. Global warming potential (GWP) is a relative measure of the heat trapping effect of a gas in comparison to an equal mass of carbon dioxide over a given quantity of time in the atmosphere [1]. Many refrigerants used in air conditioning, refrigeration and heat pump systems today have GWPs more than one-thousand times greater than that of CO_2 (Table 1). While the energy savings provided by heat pumps are beneficial in terms of mitigating climate change, continued use of these refrigerants is detrimental. Increasingly, refrigerants with high GWP are coming under scrutiny. The European Union, for instance, passed legislation in 2007 which will phase out refrigerants with GWP greater than 150 in mobile applications [2][3].

Table 1. Global warming potential of various refrigerants

Refrigerant	CO_2	R-407C	R-410A	R-22	Ammonia	R134a	R-404A
GWP	1	1610	1725	1700	0	1300	3260

Driven in part by these concerns, new refrigerants are being sought out and "old" refrigerants are being reinvestigated. Interestingly, carbon dioxide has shown

strong potential as a climate-friendly alternative refrigerant. CO_2 is a non-toxic, non-flammable, natural substance with a low GWP and zero impact on the ozone layer. It is also inexpensive and readily available. Modern research on CO_2 as a refrigerant began in 1990 when Lorentzen [4] proposed a transcritical refrigeration cycle. Since then, research has investigated a wide variety of CO_2-based heat pump and air conditioning systems. These studies have led to improved efficiencies and even some commercialized systems; CO_2 heat pump water heaters have been commercially available in Japan for nearly a decade [5][6].

One type of system which could stand to benefit from the use of CO_2 is a direct expansion geothermal heat pump (DX-GHP). In a DX-GHP the refrigerant passes directly through the buried ground coils and evaporation occurs therein. This is distinct from a conventional geothermal heat pump which uses a secondary loop to absorb heat from the ground. Since the entire ground heat exchanger (GHX) is filled with refrigerant, several times more refrigerant is required than in a conventional heat pump. This large refrigerant charge makes the use of an environmentally benign refrigerant even more important. CO_2's low cost, low environmental impact and particular thermophysical properties make it appropriate for this application.

In the current study, a detailed theoretical model was developed for the purpose of analyzing a direct expansion transcritical CO_2 geothermal heat pump. The model was developed based on the governing thermodynamic and heat transport equations pertaining to the four processes of the transcritical heat pump cycle. Accuracy of the model was verified through a comparison to published experimental data. Simulations were then carried out in order to investigate the impacts of various

design and operational parameters on the system performance and heat output. Parameters investigated include: compressor speed, evaporator tube diameter, evaporator coil length, number of evaporator circuits, mean evaporation temperature, degree of superheat, and the interrelation of evaporator and gas cooler lengths.

1.2. System Description

Figure 1 shows a schematic diagram of the direct-expansion transcritical CO_2 geothermal heat pump (CGHP) being investigated in this study. The CGHP is analyzed for water heating under steady state operation for the winter conditions of Fargo, North Dakota. The CGHP incorporates four main system components: compressor, gas cooler, expansion valve and evaporator. System operation proceeds according to the principals of the transcritical heat pump cycle.

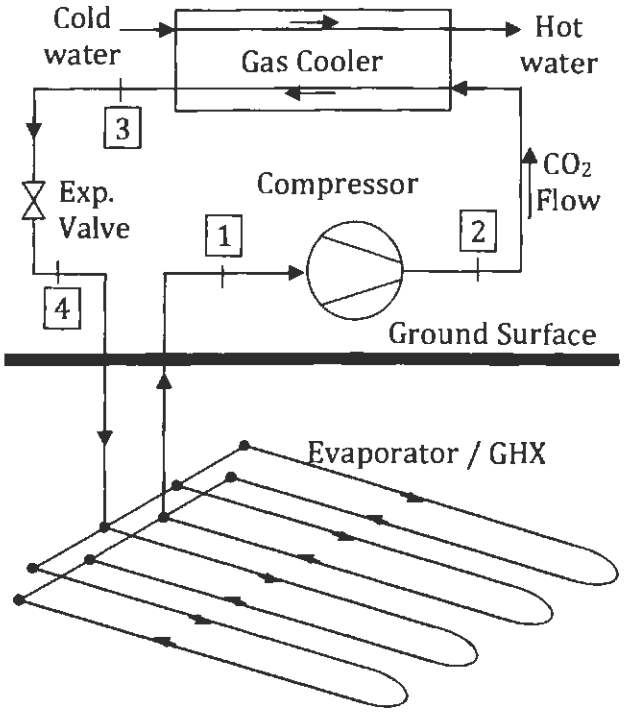

Figure 1. Schematic diagram of the system investigated in this study

The transcritical heat pump cycle is shown on the pressure-enthalpy diagram of Figure 2. To begin a cycle, heat is absorbed from the soil by evaporation of CO_2 in the GHX which consists of multiple circuits connected in parallel. The CO_2 vapor is then compressed to supercritical pressure, with a corresponding temperature rise. The high pressure, high temperature vapor then rejects heat to the water by single-phase supercritical cooling in the counter-flow gas cooler. Low temperature, high pressure CO_2 then exits the gas cooler and is throttled to the evaporator pressure, thus completing the cycle.

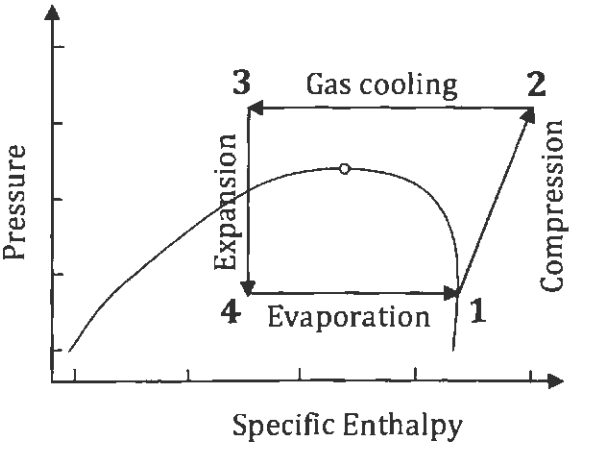

Figure 2. P-h diagram of transcritical heat pump cycle

1.3. Outline of Thesis

The thesis is presented in six chapters. Following the introduction, Chapter 2 proceeds with a review of the technologies which are integrated into the system being studied. Chapter 3 provides an outline of the study's objectives. Chapter Four gives a detailed description of the system analysis and the theoretical model development. Chapter 5 presents the simulation results including: the model validation, the

outcomes and implications of the parametric study, a comparison to refrigerant R410A, and an analysis of monthly system variation. The final chapter highlights the important findings of this study and proposes areas for future research.

2. LITERATURE REVIEW

The science and technology of a direct expansion geothermal heat pump using carbon dioxide in a transcritical cycle comes from various different fields of study. This chapter attempts to provide a basic understanding of each of these technologies and to address the more important technologies with a more in depth background and a review of relevant research.

2.1. The Conventional Heat Pump Cycle

The heat pump (HP) is not a new idea. The concept of a HP is often credited to Lord Kelvin, but he did not demonstrate the concept [7]. Heat pump and refrigeration cycles are essentially identical so the histories are closely linked; however, refrigeration was developed much earlier. The first commercial HP installation was in the Equitable Building of Portland, Oregon in 1948 [8].

Unlike combustion-based and electrical resistance heating systems, a heat pump does not generate heat; rather, heat is transferred from an external source (a heat sink) and delivered to the fluid which is being heated, typically air or water. The heat sink is usually outdoor air at the ambient temperature, and this type of system is referred to as an air-source heat pump. It is important to note that the heat source temperature is lower than the desired output temperature.

The transfer of heat energy from low temperature to high temperature is accomplished via a working fluid (refrigerant) undergoing four thermodynamic processes in a cycle. As shown on the pressure-enthalpy diagram in Figure 3, these

processes are: evaporation, compression, condensation and expansion. Heat is absorbed from the heat sink by evaporation of the refrigerant. This low temperature vapor is then compressed to a higher pressure and temperature such that heat can be rejected to the heated fluid by condensation of the refrigerant. The high temperature liquid is then throttled to a low pressure and temperature in order to complete the cycle. As shown in Figure 4 a basic HP system consists of four components corresponding to each of the cycle processes.

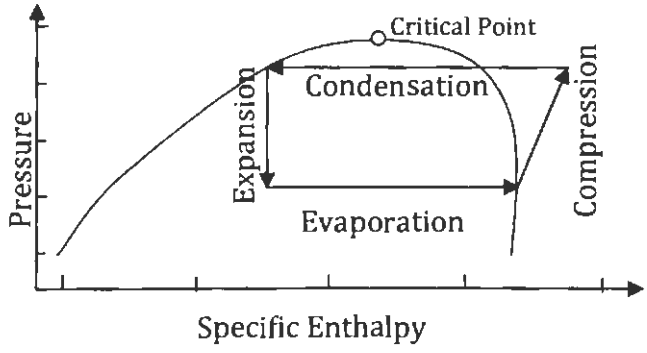

Figure 3. Pressure-Enthalpy diagram of heat pump cycle

The energy required to drive a HP cycle is that which is input to the compressor. The beauty of a HP is that the delivered heat energy can be several times greater than the energy required by the compressor. The measure of a HP's efficiency is the coefficient of performance (COP) which is defined as follows:

$$COP = \frac{Heating\ Capacity}{Power\ Input} \tag{1}$$

where heating capacity is the rate at which heat is delivered by the HP. With COP values of 3 or even greater, a HP is much more efficient than an electrical resistance heater which can achieve a maximum COP of one.

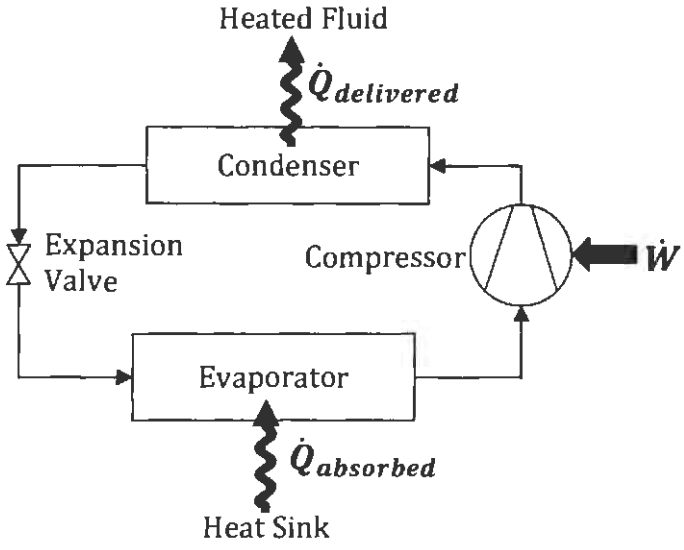

Figure 4. Heat pump system diagram

The HP cycle discussed in this section is known as a subcritical cycle because the refrigerant temperature and pressure are below the critical temperature and pressure during the entire cycle. Observing Figure 3, critical temperature (T_{crit}) and pressure (P_{crit}) can be understood by noting that the critical point is located at the peak of the vapor dome. At the critical point the saturated liquid and saturated vapor states are identical [9], and the fluid is said to be in the supercritical-phase when both temperature and pressure are above this point.

Most refrigerants have a critical temperature that is well above the normal operating range of a heat pump or refrigeration cycle, and heat pumps using these refrigerants are designed to always operate in a subcritical manner. Carbon dioxide, on the other hand, has a very low T_{crit} (31.1°C) and therefore is used most effectively in a cycle where heat rejection occurs at temperatures and pressures greater than T_{crit} and P_{crit}. This is known as a transcritical cycle.

2.2. The Transcritical Heat Pump Cycle

Similar to the conventional cycle, a transcritical HP cycle consists of four thermodynamic processes and heat absorption occurs through evaporation of the working fluid. However, in a transcritical cycle, the refrigerant vapor leaving the evaporator is compressed to a pressure and temperature greater than T_{crit} and P_{crit}. Because no condensation occurs in the supercritical region, heat rejection occurs by single phase (sensible) cooling, referred to as gas cooling. Figure 5 shows the transcritical heat pump cycle on a pressure-enthalpy diagram. Comparing Figure 5 and Figure 3, it can be observed that the only distinction between the two cycles is the replacement of the condensing process with the gas cooling process.

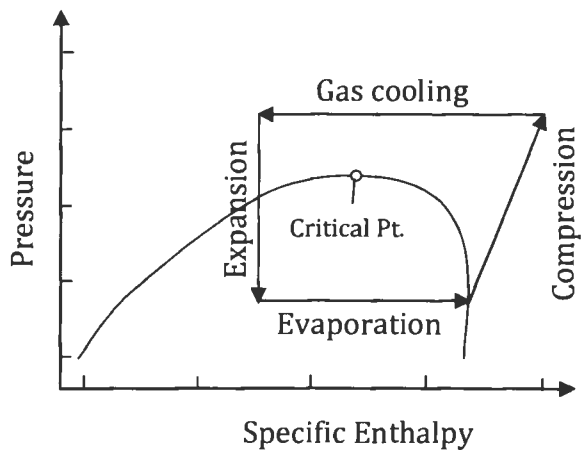

Figure 5. Pressure-Enthalpy diagram of a transcritical heat pump cycle

The benefit of a transcritical cycle can be understood by observing Figure 6 which shows the heat of vaporization for CO_2 at various temperatures [10]. The figure implies that as the condensing temperature nears T_{crit} (31.1°C) the amount of heat which can be rejected greatly decreases. Correspondingly, the amount of heat

which can be absorbed will also reduce. Thus, for a CO_2 HP system operating subcritically, the maximum delivery temperature is unsuitably low. For refrigeration applications, the performance of an air-cooled, subcritical CO_2 system decreases dramatically as ambient temperatures near T_{crit}. In fact, performance degrades at a much lower ambient temperature because the condensing temperature must be greater than the ambient. When CO_2 is instead used in a transcritical cycle, the heat rejection temperature can be increased, thus increasing the potential for heat pump applications and improving the performance in refrigeration applications.

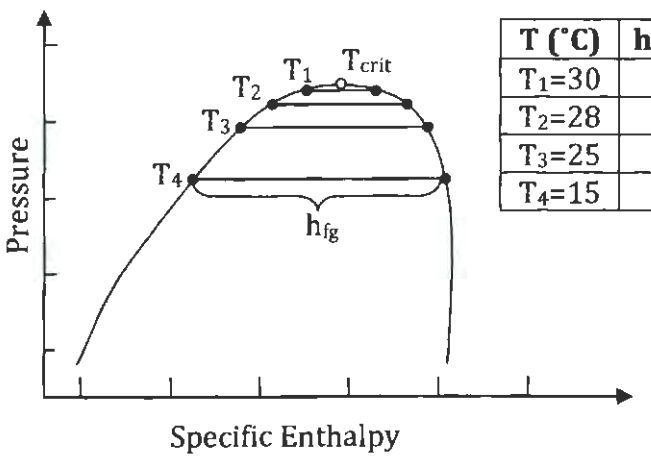

T (°C)	h_{fg} (kJ/kg)
T_1=30	60.6
T_2=28	91.6
T_3=25	119.6
T_4=15	177.7

Figure 6. P-h diagram showing change in heat of vaporization near T_{crit} [10]

The next section provides some background on the use of CO_2 as a refrigerant including how its low critical temperature limited its usefulness and how the transcritical cycle has brought about new interest in CO_2.

2.3. Historical Use of CO_2 as a Refrigerant

Heat pump systems are closely related to refrigeration systems, but vapor compression cycles were developed for refrigeration long before the concept was

applied to heating. Likewise, refrigerant fluids were developed for refrigeration rather than heating. A detailed history of CO_2's role in refrigeration development was given by Pearson [11].

In the modern naming scheme for refrigerants, CO_2 has been given the label R744. Long before this label however, CO_2 was being used in some of the first commercially viable vapor compression refrigeration systems. Other early refrigerants included ether, ammonia, sulfur dioxide and methyl chloride. CO_2 was first used in a vapor compression refrigeration by Thaddeus Lowe in 1866. The high working pressures of CO_2 were a hindrance to implementation, allowing ammonia and sulfur dioxide systems to become established first. Ammonia systems were generally efficient, but they were quite large and ammonia's toxic nature presented a safety hazard. In comparison, CO_2 required more fuel and more robust components, but the systems were much smaller and CO_2 leaks did not pose a health risk [11].

Due to the safety and compactness of CO_2 systems, ships began to use CO_2 for refrigeration in the 1880s and 90s, while on land ammonia was dominant. A further reason for the divergence of ammonia to land-based refrigeration and CO_2 to marine systems relates to condensing temperature and means of condensing. As discussed in Section 2.2, the low critical temperature of CO_2 results in decreased refrigeration capacity as condensing temperature near 31°C. CO_2 was thus restricted to applications where river or sea water was available for cooling. Ammonia, on the other hand, could operate under a wider range of condenser temperatures, which allowed for the use of evaporative coolers when a body of water was unavailable [11].

The land and sea trend continued into the early 1900s when ammonia's improved safety record and better manufacturing caused acceptance of ammonia refrigeration on ships. By the 1930s ammonia plants were preferred even at sea and the use of CO_2 for refrigeration further decreased. The final demise of CO_2 in refrigeration was caused by synthetic refrigerants. R12 and R11 were first introduced for commercial use in 1931 and 1932 [12]. They were non-toxic, non-flammable and operated efficiently over a range of temperatures. Synthetic refrigerants began to displace CO_2 and by the 1950s and 60s came to dominate in all but industrial refrigeration systems.

Interest in CO_2 was renewed in the early 1990s in part due to the phase-out of ozone depleting refrigerants. Norwegian professor Gustav Lorentzen has received much of the credit for the new attention given to CO_2, however, there were others studying CO_2 at the same time. Lorentzen published a patent application for a trans-critical CO_2 automotive air conditioning system in 1990 [4]. Lorentzen's transcritical cycle eliminates the problem of capacity and efficiency loss that subcritical systems have when operating with heat rejection temperatures near the critical point. Technological and manufacturing improvements make it possible now to achieve the high pressures required for transcritical operation. One of the first transcritical CO_2 systems was a prototype automotive air conditioning system built and tested by Lorentzen & Pettersen [13]. The system was further reported by Pettersen [14]. Performance was similar to that of an R12 system and encouraged the further development of the transcritical CO_2 system.

Research into CO_2 refrigeration, air-conditioning and heat pump systems continues, but some CO_2 systems have already been successfully commercialized. For nearly a decade, transcritical CO_2 heat pump water heaters have been commercially available in Japan. Introduced in 2001, over 1 million of the EcoCute water heaters had been sold by 2007 [5] and sales topped 2 million in October of 2009 [6]. Vending machines using a transcritical CO_2 refrigeration cycle are becoming more common in Japan and throughout Europe. In December of 2009 The CocaCola Company announced it would phase out fluorinated refrigerants in all new vending machines by 2015, switching primarily to CO_2 systems [15]. In addition, CO_2 commonly serves as the low temperature refrigerant in cascade type industrial refrigeration systems, and CO_2 is increasingly used as a secondary fluid in food display applications where harmful refrigerants must be kept separate for safety reasons [12].

2.4. Thermophysical Characteristics of CO_2

The performance of a heat pump system is impacted by the thermophysical properties of the refrigerant being used. In order to better understand the application of CO_2 in transcritical heat pump systems, this section will provide an overview of some of the unique characteristics of CO_2.

As discussed in previous sections CO_2 has a very low critical temperature, making it appropriate for use in a transcritical cycle. At the same time, the critical pressure of CO_2 is quite high at 7.38 MPa. Furthermore, the entire CO_2 HP cycle is characterized by high working pressures. The evaporator pressure for a CO_2 heat pump is typically in the range of 2-5 MPa, while gas cooler pressure may be up to

15 MPa [16]. For comparison, the condenser pressure for R134a 0.13 MPa at 50°C [17].

High pressure presents design challenges, mainly in terms of compressor capability; however, today's manufacturing technologies allow production of compressors which can meet these demands [18]. In fact, the improved feasibility of the transcritical CO_2 HP cycle is partly the result of improved compressor technology.

The high working pressure leads to some favorable characteristics as well. High pressure results in a high vapor density, which corresponds with a high volumetric heating/refrigerating capacity. Thus, compared to other refrigerants, a smaller volumetric flow rate is required to achieve the same heat output, which in turn allows for smaller components and a more compact system overall [16][18].

The viscosity and thermal conductivity play an important role in determining the heat transfer characteristics of a refrigerant. Comparing CO_2 and R134a at 0°C, CO_2's thermal conductivity is 20% greater at saturated liquid condition and 60% greater at saturated vapor condition. Comparing the viscosity of the two fluids at the same temperature, CO_2's liquid viscosity is 40% lower and vapor values are similar [19]. These characteristics result in favorable heat transfer rates.

Pressure drop in the evaporator causes a decrease in saturation temperature. This lowers the temperature at the evaporator outlet and reduces cycle efficiency. In light of this, the magnitude of the temperature decrease for a given pressure drop is an important factor for the evaporation process. Figure 7 helps illustrate this point. For CO_2, $\frac{dT_{sat}}{dP_{sat}}$ is significantly smaller than for other refrigerants. For example, at 0°C

a 1 kPa decrease in pressure reduces the saturation temperature of CO_2 by 0.01°C while the same pressure drop causes the saturation temperature of R134a to decrease by 0.10°C [18][20].

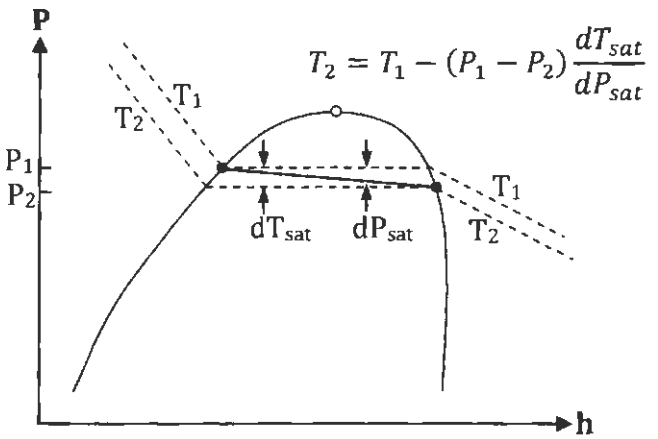

Figure 7. P-h diagram illustrating the decrease in saturation temperature associated with a pressure drop through the evaporator

To understand a refrigerant's behavior in a transcritical heat pump, the supercritical properties must be investigated as well. At supercritical pressures, CO_2's property values vary rapidly with temperature in a region near the pseudo-critical temperature. The pseudo-critical temperature (T_{pc}) is the temperature at which the specific heat reaches a maximum. Figure 8 shows the variation of specific heat (c_p) versus temperature for various pressures. As shown in the figure, for any pressure c_p reaches a maximum at a certain temperature. Furthermore, as the pressure increases this temperature increases and the maximum magnitude of c_p decreases. Yang et al. [21] derived the following equation to calculate the T_{pc}:

$$T_{pc} = -31.40 + 12.15P - 0.6927P^2 + 0.03160P^3 - 0.0007521P^4 \qquad (2)$$

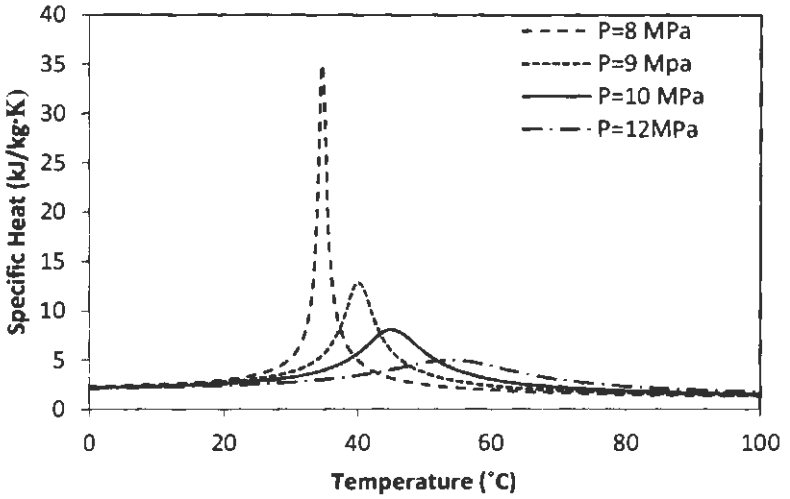

Figure 8. Variation of specific heat with temperature for various pressures [10]

Figure 9 shows that density, thermal conductivity and viscosity also vary rapidly with temperature near T_{pc}. These variations impact the ideal operating conditions of a transcritical HP. For example, the gas cooler should operate in a manner that takes advantage of the large specific heat near T_{pc}. In addition, the rapid variation must be taken into consideration when modeling a supercritical process.

Having laid out the basic principles of a transcritical heat pump systems and a background on the properties of use of CO_2 as a refrigerant, the next sections will provide an overview on the performance and operating characteristics of the transcritical cycle including some of the relevant research.

2.5. Transcritical CO_2 Heat Pumps Fundamentals and Performance

An important operating parameter for a transcritical heat pump is the heat rejection (gas cooler) pressure. Several authors [23-26] used simulation models to investigate the effects of gas cooler pressure. Findings consistently indicate that an

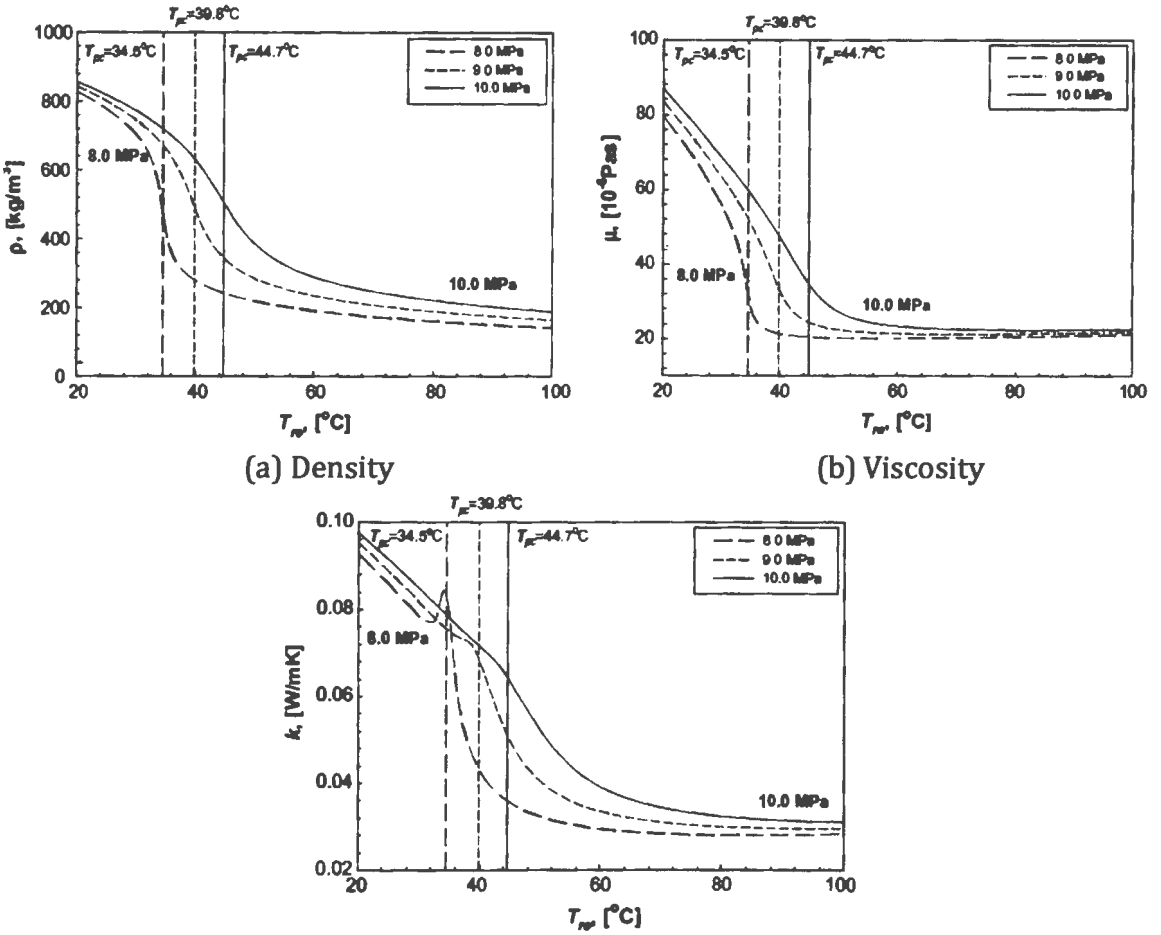

Figure 9. Supercritical property variation of CO_2 with temperature [22]

optimum gas cooler pressure exists for a given gas cooler outlet temperature. As described by Kim et al. [18], this optimum pressure is due to the particular shape of the isotherms in the supercritical region. The effect can be understood by observing Figure 10. For a constant gas cooler outlet temperature, an increase in pressure will increase the amount of heat rejected (line 2-3). At the same time, the compressor work will also increase. The compressor work increases nearly linearly, but due to the shape of the isotherms, the amount of heat rejected increases rapidly at lower

pressures but then more slowly at high pressures. The net effect is that COP will increase up to a certain pressure beyond which it will decrease. Figure 11 further illustrates how the heat rejection pressure impacts heating capacity, compressor power and COP of a transcritical CO_2 heat pump.

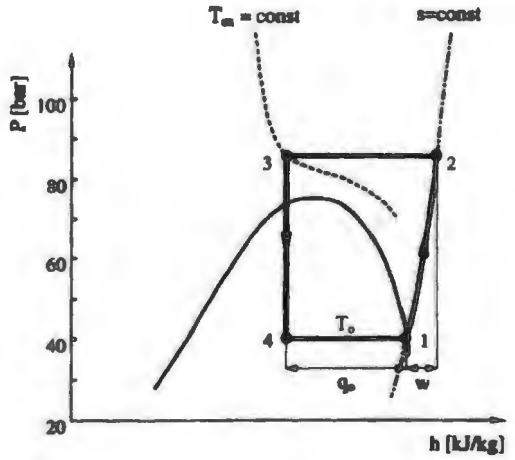

Figure 10. P-h diagram illustrating transcritical cycle and the effect of gas cooler pressure on heating capacity & COP [18]

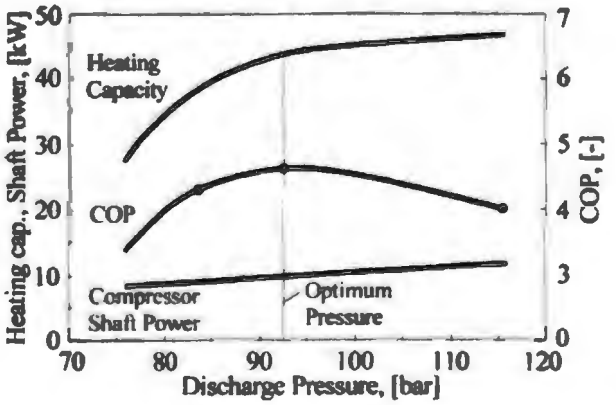

Figure 11. Impacts of gas cooler pressure on compressor power, COP and heating capacity [16]

Heat pumps are commonly used in both air heating and water heating applications, but in the case of the transcritical CO_2 heat pump (TCHP), the particular

characteristics of the gas cooling process make the cycle better suited to water heating. Since heat transfer in the gas cooler occurs by sensible cooling, the temperature profile across the gas cooler is a continuous glide. This is distinct from the latent heat rejection of a condensing process as shown in Figure 12. The continuous temperature glide is advantageous for water heating because the water and CO_2 temperature profiles can be closely matched, thus allowing for reduced entropy generation, improved heat exchanger effectiveness and smaller approach temperatures [27,28].

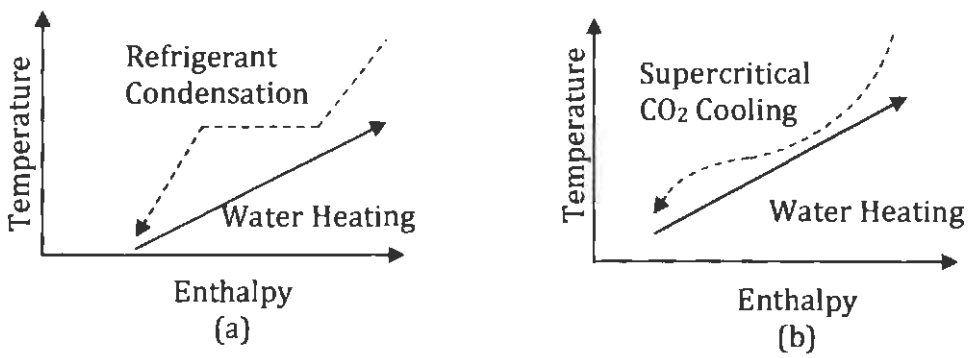

Figure 12. Temperature profile for (a) condensation process; (b) supercritical gas cooling process

Various studies have shown that transcritical CO_2 heat pump water heaters perform with high efficiency and retain acceptable performance even at low evaporating temperatures. The system built and tested by Neksa et al. [29] achieved a COP of up to 4.3 and could still attain a COP of 3.0 when evaporator temperature was reduced to -20°C. Anstett [30] reported on a high-volume test installation which delivered COP between 2.0 and 5.0. With an ambient temperature of -5°C the system delivered water at 70°C with a COP of 2.5.

White et al. [28] investigated a TCHP water heater for high temperature water heating. The experimental system delivered water at 90°C with a COP of 3.0. The limits of high temperature heating using CO_2 and other refrigerants were analyzed by Sarkar et al. [31]. The study concluded that CO_2 was not recommended for output temperatures greater than 200°C due to pressures greater than 20 MPa. In practice, the maximum feasible temperature is actually well below this value.

Besides domestic (tap) water purposes, heated water may be used for space heating such as via hydronic floor heating. Floor heating generally requires a lower water-temperature than other types of hydronic heating. A combined domestic water/hydronic floor heating system was tested by Hihara [32] under various load conditions. Data was used to calculate a seasonal COP of 2.7.

The outlet temperature of the gas cooler has a large impact on the heating capacity and COP of a TCHP. The reason for this is illustrated in Figure 13, which shows that for a small decrease in gas cooler exit temperature there is a significant decrease in the outlet enthalpy. Thus a greater amount of heat can be rejected by the gas cooler. The temperature change also corresponds to a decrease in the enthalpy at the evaporator inlet, and thus more heat is absorbed by the evaporator. Meanwhile, the work required by the compressor remains unchanged. The net effect is an increase in COP. Figure 14 shows that for any gas cooler pressure, COP will increase as exit temperature decreases [18].

The preceding discussion leads to two conclusions for transcritical CO_2 heat pump water heaters: (i) the gas cooler should be a counter-flow heat exchanger; (ii) system COP will improve as water inlet temperature decreases. A counter-flow

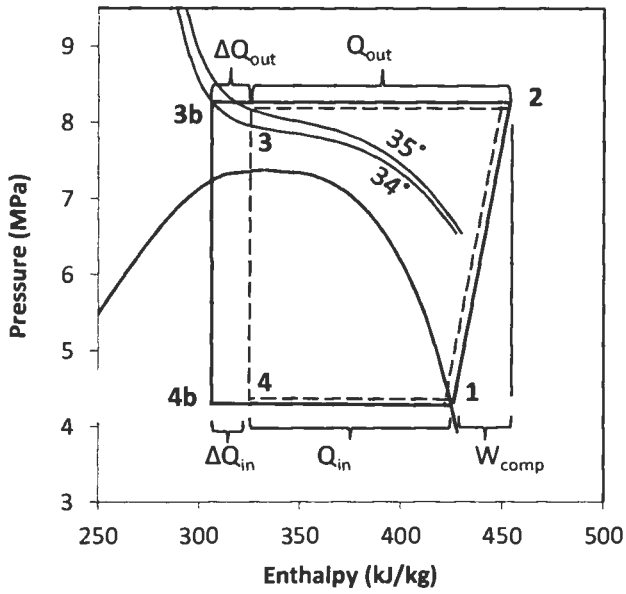

Figure 13. P-h diagram illustrating the change in enthalpy with gas cooler exit temperature [10]

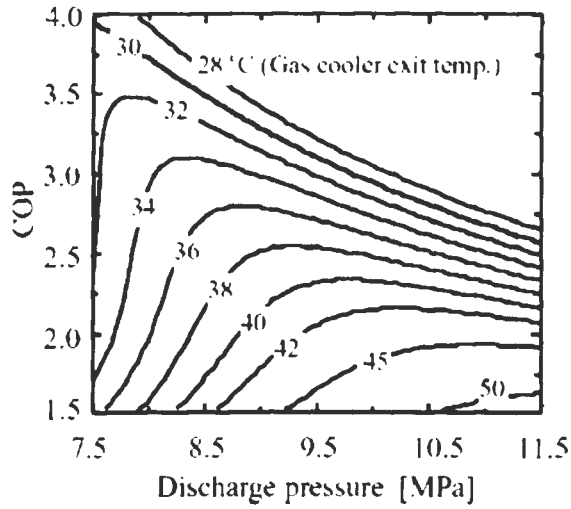

Figure 14. Effect of gas cooler exit temperature on COP of a transcritical cycle [18]

heat exchanger will result in the lowest CO_2 exit temperature and will maximize COP. Furthermore, a counter-flow heat exchanger also produces the greatest water exit

temperature. The benefit of lower water inlet temperature is due to the relationship between the CO_2 outlet and water inlet temperatures in a counter-flow heat exchanger: as water inlet temperature decreases, CO_2 outlet temperature decreases. This effect was shown in a simulation by Laipradit et al. [33].

The results of a test by Fernandez et al. [34] revealed that water reheating is less efficient than initial water heating. In the test, COPs were 30-40% higher when heating incoming water from 15 to 57°C than when reheating from 42 to 57°C. Cecchinato et al. [35] found similar results and concluded that a storage tank characterized by temperature stratification was superior to a mixed tank strategy since the cold water could be drawn from the bottom during reheating.

Stene [36] sought to decrease the gas cooler outlet temperature, and thus increase COP, by partitioning the gas cooler to serve multiple loads: domestic water preheating, space heating and domestic water reheating. COP was greatest for combined mode operation and lowest for space heating only operation. This trend is opposite to that of a heat pump using a conventional refrigerant in which COP is best for space heating only and worst for dual mode.

Sarkar et al. [22] theoretically analyzed a TCHP system designed for simultaneous heating and cooling of water. Any heat pump can be designed to deliver both hot and cold water simultaneously since the evaporator and condenser (or gas cooler) are simultaneously absorbing heat and rejecting heat. This is a very efficient system for applications needing both hot and cold water (such as dairy operations). In a similar study Byrne et al. [37] found that a simultaneous TCHP system used 27% less electricity than two TCHPs serving the heating and cooling functions separately.

Another important parameter for TCHP systems is the refrigerant charge volume. Cho et al. [38] investigated the impacts of charge volume using an experimental system designed for cooling. $COP_{cooling}$ increased as charge volume increased to an optimum point. Beyond the optimum point, there is a slow reduction in $COP_{cooling}$ as the system becomes overcharged. Compared to other refrigerants, CO_2 performance was much more sensitive to under-charged conditions.

A large number of studies have undertaken to improve heat pump performance by modifying the basic system components. A common modification of the basic transcritical CO_2 heat pump system is the addition of a suction line heat exchanger (SLHX). An SLHX is a counter-flow heat exchanger which further reduces the temperature of the gas cooler exit fluid prior to expansion while simultaneously superheating the vapor exiting the evaporator. Figure 15 illustrates the system design. A TCHP simulation by Robinson and Groll [39] showed that the addition of an SLHX improved COP 7%. A simulation by Kim et al. [40] showed that as SLHX length

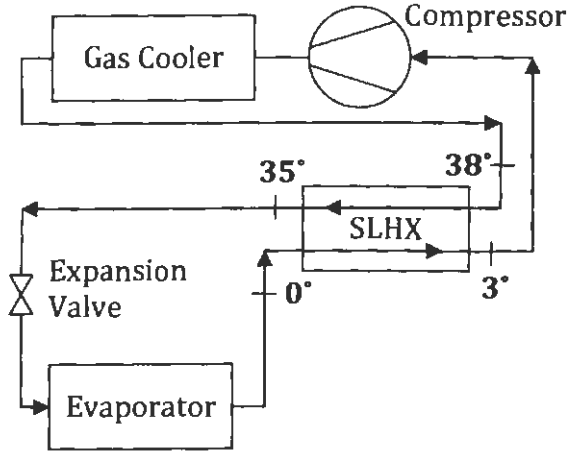

Figure 15. Diagram of a heat pump with suction line heat exchanger (shown with sample temperatures for clarity)

increases the optimum gas cooler pressure decreases. Similar results were obtained by Chen and Gu [41] who reported that as SLHX effectiveness increases, the optimum pressure decreases and the COP increases.

White et al. [28] compared the merits of using an SLHX versus simply increasing the gas cooler size. The COP was roughly equivalent for the two options, but the larger gas cooler delivered a 20% greater heating capacity. Mass flow rate and gas cooler pressure was also greater for the system with the large gas cooler.

2.6. Comparison to Conventional Refrigerants

Several studies compared the performance of CO_2 heat pumps to analogous systems using other refrigerants [31,35,42,43]. Tamura et al. [42] tested an automotive TCHP designed to replace a unit using R134a. Under cooling operation, COPs of the two systems were equal. In heating mode, COP of the CO_2 prototype was 31% greater. The results obtained by Cecchinato et al. [35] also indicated similar performance between CO_2 and R134a; however, the when incoming water temperature was decreased CO_2 system was superior.

The heat output and COP of air-to-air heat pumps using R410A and CO_2 were compared by Richter et al. [43]. The CO_2 system generally had lower COPs, but heating capacity was actually greater for most ambient temperatures. Furthermore, compared to R410A, heating capacity of the TCHP did not drop as dramatically when ambient temperatures decreased.

2.7. Relevant Heat Transfer Correlations

The theoretical analysis of a transcritical CO_2 heat pump system requires the

evaluation of CO_2's heat transfer characteristics during supercritical cooling conditions and evaporation. Well established heat transfer correlations have been experimentally developed, which are commonly used for the prediction of heat transfer coefficients of various fluids including refrigerants. However, experimental studies have shown that many of these correlations do not predict the heat transfer coefficient for supercritical CO_2 with sufficient accuracy. Likewise, many correlations commonly used to predict the evaporative or two-phase flow heat transfer do not match the results of experimental studies with CO_2. The following sections will provide a brief overview of the heat transfer correlations which are applicable to CO_2.

2.7.1. Supercritical Heat Transfer

The variation in viscosity, thermal conductivity, specific heat and density impacts the heat transfer and flow characteristics of CO_2. These variations must be taken into account in heat transfer correlations for supercritical CO_2 cooling.

Early development of a supercritical heat transfer correlation for CO_2 was conducted by Krasnoshchekov et al. [44] on turbulent flow, and Baskov et al. [45] later found that the correlation over-predicted their experimental results. Petrov & Popov [46] developed a new correlation by modifying an earlier Nusselt correlation of Petukhov & Popov [47].

More recently the subject of cooling supercritical CO_2 heat transfer correlation in horizontal channels and microchannels has been investigated by several researchers [48-58]. Yoon et al. [48] conducted an experimental study to determine the heat transfer coefficient for CO_2 flowing in a 7.73mm horizontal tube. Based on

the experimental results a new correlation was proposed which was a modification of the Baskov [45] correlation:

$$Nu = 1.38\, Nu_{wall} \left(\frac{\bar{c}_p}{c_{p,wall}}\right)^{0.86} \left(\frac{\rho_{wall}}{\rho_b}\right)^{0.57} \tag{3}$$

The majority of heat transfer correlations developed for CO_2 require properties to be evaluated at the bulk temperature and at the wall temperature, but in the theoretical evaluation of a heat exchanger the wall temperature is usually unknown. Yoon et al. [48] therefore derived a modification of the Dittus-Boelter [59] correlation which uses the bulk temperature and pseudo-critical temperature for property evaluation. In this correlation the supercritical region is divided into two temperature regions centered on T_{pc}. Evaluation proceeds according to the following equation:

$$\mathrm{Nu_b} = 0.14 Re_b^{0.69} Pr_b^{0.66} \qquad \text{for } T_b > T_{pc} \tag{4}$$

$$\mathrm{Nu_b} = 0.013 Re_b^{1.0}\, Pr_b^{-0.05} \left(\frac{\rho_{pc}}{\rho_b}\right)^{1.6} \qquad \text{for } T_b \leq T_{pc}$$

Similarly, Oh & Son [22] also used the pseudo critical temperature to establish a two region correlation. The correlation is given as:

$$Nu = 0.023 Re_b^{0.7} Pr_b^{2.5} \left(\frac{c_{p,b}}{c_{p,wall}}\right)^{-3.5} \qquad \text{for } T_b > T_{pc} \tag{5}$$

$$Nu = 0.023 Re_b^{0.6} Pr_b^{3.2} \left(\frac{\rho_b}{\rho_{wall}}\right)^{3.7} \left(\frac{c_{p,b}}{c_{p,wall}}\right)^{-4.6} \qquad \text{for } T_b \leq T_{pc} \tag{6}$$

where T_{pc} can be determined by:

$$T_{pc} = -122.6 + 6.124P - 0.1657P^2 + 0.017739P^{2.5} - 0.000560P^3 \tag{7}$$

Pitla et al. [49] accounts for the property variation of supercritical CO_2 by evaluating properties at the fluid bulk temperature and the wall temperature. The heat transfer is finally evaluated as an average of the values multiplied by the conductivity ratio as shown below:

$$Nu_c = \left(\frac{Nu_{wall} + Nu_b}{2}\right)\frac{k_{wall}}{k_b} \tag{8}$$

Nu_{wall} and Nu_{bulk} are calculated by the correlation of Gnielinski [60] for turbulent flow:

$$Nu = \frac{\frac{f}{8}(Re - 1000)Pr}{1.07 + 12.7\left(\frac{f}{8}\right)^{0.5}\left(Pr^{\frac{2}{3}} - 1\right)} \qquad 3000 \leq \text{Re} \leq 5\text{x}10^6 \tag{9}$$

The friction factor in the preceding equation is evaluated using the equation of Petukhov [61]:

$$f = (0.79 \cdot \ln(\text{Re}) - 1.64)^{-2} \qquad 3000 \leq \text{Re} \leq 5\text{x}10^6 \tag{10}$$

2.7.2. Evaporative Heat Transfer

The heat transfer characteristics of CO_2 during evaporation in a horizontal tube have been analyzed by several authors [62-70]. The results of the studies have typically concluded that the generalized correlations for heat transfer do not adequately predict the behavior of CO_2. This has led some authors to develop new predictive correlations specifically for CO_2.

Mastullo et al. [71] compared experimental data to the pressure drop and heat transfer predicted by several correlations. The correlations of Cheng et al. [72] and Jung et al. [73,74] were found to most accurately predict the heat transfer coefficient

of CO_2. The correlation of Jung et al. incorporates the effects of convective heat transfer and nucleate boiling heat transfer as given below:

$$\alpha_c = \varphi \alpha_{sa} + F_p \alpha_l \tag{11}$$

where φ is the nucleate boiling factor:

$$\varphi = 4048 X_{tt}^{1.22} Bo^{1.13} \quad for\ X_{tt} < 1.0 \tag{12}$$

$$\varphi = 2 - 0.1 X_{tt}^{0.28} Bo - 0.33 \quad for\ 1 \leq X_{tt} \leq 5 \tag{13}$$

where X_{tt} is the two-phase multiplier,

$$X_{tt} = \left(\frac{1-x}{x}\right)^{0.9} \left(\frac{\rho_g}{\rho_l}\right)^{0.5} \left(\frac{\mu_l}{\mu_g}\right)^{0.1} \tag{14}$$

and Bo is the boiling number,

$$Bo = \frac{q}{G \cdot h_{fg}} \tag{15}$$

α_{sa} in Eq. (11) is the nucleate pool boiling heat transfer coefficient of Stephan and Abdelsalam [75] calculated as:

$$\alpha_{sa} = 207 \frac{k_l}{bd} \left(\frac{q \cdot bd}{k_l T_{sat}}\right)^{0.745} \left(\frac{\rho_g}{\rho_l}\right)^{0.581} Pr^{0.533} \tag{16}$$

where bd is the Bond number:

$$bd = 0.0146 \beta \left(\frac{2\sigma}{g(\rho_l - \rho_g)}\right)^{0.5} \tag{17}$$

β is the liquid contact angle, set equal to the typical value for refrigerants 35°.

Returning again to Eq. (11), F_p is the heat transfer enhancement factor:

$$F_p = 2.37 \left(0.29 + \frac{1}{X_{tt}}\right)^{0.85} \tag{18}$$

Finally, α_l is the convective heat transfer coefficient of the liquid portion of the flow which is evaluated based on the Dittus-Boelter [59] correlation:

$$\alpha_l = 0.023 \frac{k_l}{d_i} \left(\frac{G(1-x)d_i}{\mu_l} \right)^{0.8} \left(\frac{c_{pl} \cdot \mu_l}{k_l} \right)^{0.4} \tag{19}$$

2.8. Conventional Versus Direct Expansion Geothermal Systems

A geothermal heat pump system is distinguished from an air-source system only by the heat sink from which thermal energy is being absorbed. The geothermal system absorbs heat from the soil, groundwater or surface water. This difference results in changes to the system design, but the heat pump cycle is identical to that of an air-source heat pump.

Figure 16 shows a conventional, closed-loop geothermal heat pump. This type of system utilizes a series of vertical or, as shown, horizontal ground coils through which a liquid solution is pumped in order to absorb heat from the ground. This ground heat exchanger (GHX) is a closed, secondary loop which is separate from the actual heat pump (the primary loop) and requires its own pump to circulate the liquid. The heat absorbed by the GHX is delivered to the heat pump via an intermediate heat exchanger, which functions as the evaporator of the primary loop. The majority of geothermal heat pump systems in the U.S. are 'indirect' systems like the system just described [76].

An alternative to this arrangement is the direct expansion geothermal heat pump (DX-GHP) wherein the secondary loop, pump and intermediate heat exchanger are eliminated, and the refrigerant passes directly through the GHX. In a DX-GHP, heat absorption from the ground occurs by evaporation of the refrigerant directly in

the GHX. Figure 17 shows a schematic diagram of a DX-GHP. Differences between conventional and direct expansion systems can be observed by comparing Figure 16 and Figure 17.

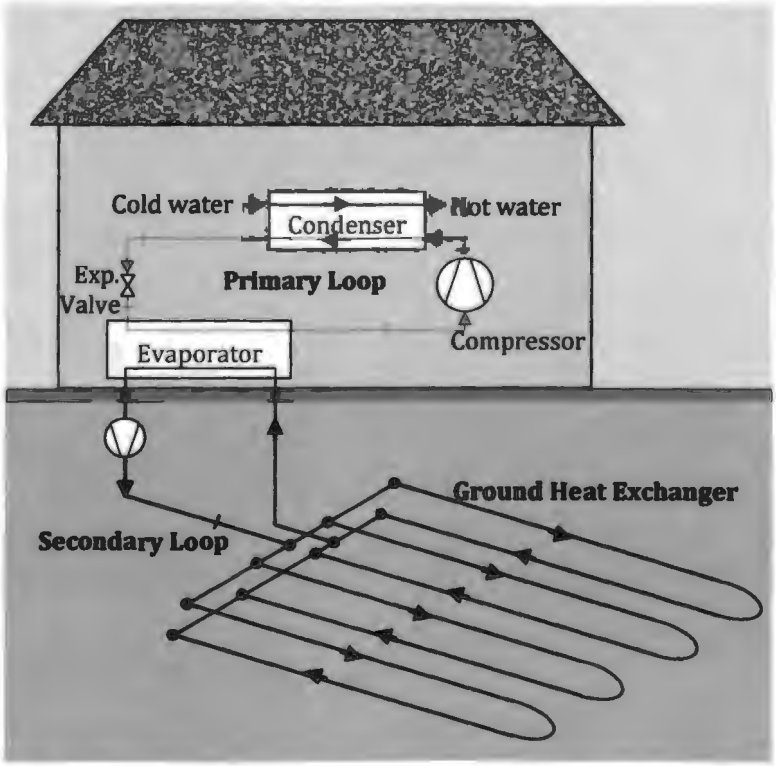

Figure 16. Schematic diagram of a conventional geothermal heat pump

2.9. Direct Expansion Geothermal Heat Pumps

Some of the original research on geothermal heat pumps was based on direct expansion ground coils [77-79]. Since then, the majority of research has focused on indirect systems. Secondary loops became the conventional means of heat extraction from the ground due in part to the benefits of plastic tubing. Plastic tubing is low cost, relatively easy to install and allows for reliable, leak-proof joints, but it is much better

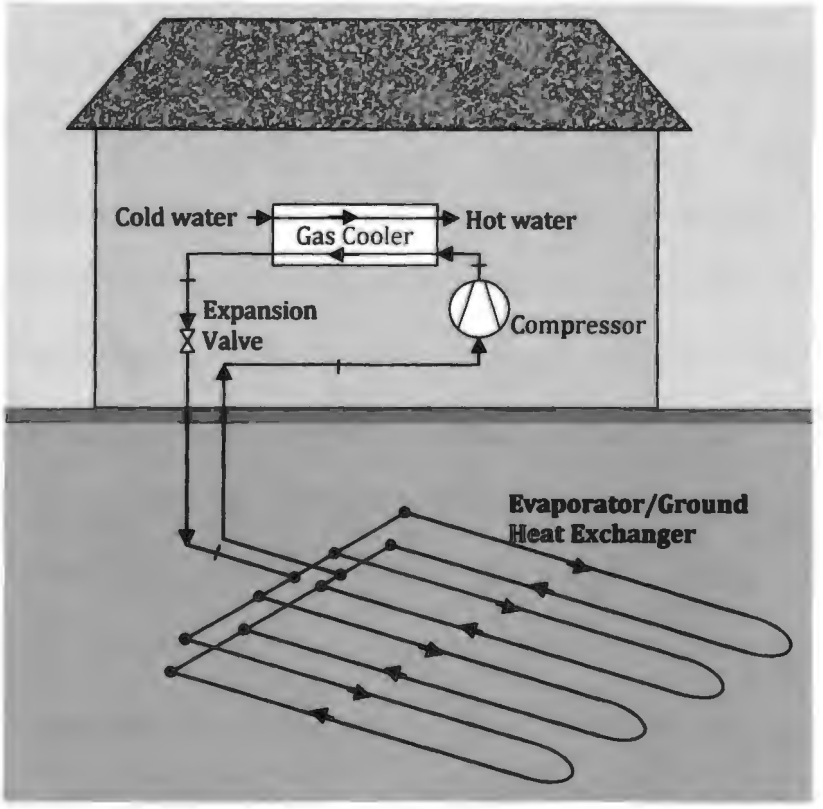

Figure 17. Schematic diagram of a direct-expansion geothermal heat pump

suited to the low pressures of liquid pumping than the higher pressures of an evaporator [80]. Despite the dominance of indirect systems, various studies have investigated DX-GHPs, and the systems are actually relatively common in Austria [81,82]. Appendix A provides a table comparing the performance data from several experimental DX-GHP studies.

Theoretically, a DX-GHP is more efficient than a conventional geothermal heat pump [82]. This is due to the elimination of the intermediate heat exchanger, which allows the evaporation temperature to more closely approach the soil temperature. In addition, energy consumption is further reduced in a DX-GHP by eliminating the

energy required by the secondary pump. The U.S. Energy Information Agency reported average COP of DX-GHPs manufactured in the U.S. as 4.2 while conventional systems had an average of 4.0 [76].

The evaporation process generally can be said to have higher heat transfer rates than the sensible heating of liquid in a ground heat exchanger. This factor combined with the improved efficiency of a direct expansion system can potentially result in shorter GHX lengths compared to a conventional system. One manufacturer of direct expansion systems reported a nominal coil length for vertically oriented GHX as 150 ft/ton compared to 250 ft/ton for indirect-type systems [83].

The copper tubing which is used in a DX-GHP has a much greater thermal conductivity than the plastic tubing used in the GHX of a conventional heat pump. This may be beneficial for the DX-GHP, but only marginally so, since by far the greater thermal resistance is that of the surrounding soil [86]. Furthermore, corrosion problems must be addressed for copper tubes, typically with exterior coatings. Perhaps most important though is the high cost of copper. Minea [85] estimated a 7-10 year payback on period on his experimental system, but only if the cost of tubing could be reduced by 50% (tubing cost was not given, but the expense was partly due to import cost from Europe to Canada). The increased cost of copper tubing over plastic may be somewhat mitigated by reduced excavation costs due to decreased GHX size as compared to an indirect system.

Wang et al. [84] found that the evaporation temperature in a DX-GHP was quite stable due to stable soil temperature. Hence, COP variation was mainly a function of condensing temperature. Goulburn & Fearon [86] concluded that the heat

extraction rate increases as the evaporation temperature decreases, but this also leads to a decrease in COP. They also concluded that if a constant heat extraction rate is desired, the evaporation temperature must decrease at the same rate as the surrounding soil temperature.

Refrigerant distribution in the GHX circuits can be a problem which leads to different heat extraction rates and different evaporation temperatures among the circuits. In a test of a DX-GHP with three vertical circuits Wang et al. [84] found a difference of 10.9°C between the outlet temperatures of the circuits. Many factors may contribute to un-even distribution of refrigerant: header design, couplings, header length between circuits, differences in soil temperature.

The length of the GHX tubes is significantly greater than the evaporator tubes of an air-source heat pump. This leads to increased frictional pressure drop, which also reduces evaporation temperature. Wang et al. [84] measured an average pressure drop of 160 kPa in 30 m U-tube coils (total length 60m); this corresponded to a temperature drop of 11.7°C across the evaporator.

Pressure drop can be reduced while also maintaining the heat extraction capacity by decreasing the length of each circuit but increasing the number of circuits. Several authors [82,84,86] expressed the importance of maintaining a low refrigerant velocity in order to reduce the pressure drop across the evaporator. Refrigerant maldistribution and system instabilities have also been attributed to increased pressure drop [84]. Velocity can be reduced by increasing tube diameter, but this increases refrigerant charge. In addition, Goulburn & Fearon [86] stated that if tube diameter is too large oil return to the compressor is problematic.

Oil return can be problematic in general for DX-GHPs. Oil, which has carried over from the compressor, comes out of the solution and builds up in the evaporator when the refrigerant becomes vapor [86]. This issue may be reduced by maintaining a "wet" condition in the evaporator [82], in other words operating such that evaporation is occurring over as much of the coil length as possible. The refrigerant will thus have very little superheat and will be more likely to carry the oil back to the evaporator.

Johnson et al. [87] found that expansion and contraction of the GHX tubes can lead to air gaps and poor contact with the soil, with the effect of reduced heat transfer. This issue is worse in the case of summer (cooling) operation. Dryout of the soil in summer can also reduce thermal conductivity. In dry locations, a means of maintaining soil moisture content during summer operation may be required [88].

The use of refrigerant directly in the ground heat exchanger also presents some pollution risks. The potential for system leaks is legitimate, and this creates a risk of groundwater contamination [84]. In addition, since the entire GHX must be filled with refrigerant, the charge volume may be as much as ten times greater than a conventional geothermal system [89]. As mentioned in the introduction, many refrigerants have a high GWP, thus the additional refrigerant only to exacerbate the climate change risk. Increased refrigerant also adds to the initial system cost.

2.10. Heat Transfer in the Vicinity of the Ground Heat Exchanger

The performance of any geothermal heat pump is significantly impacted by soil temperature and soil thermal conductivity. Soil temperature varies with location,

depth and season. Horizontally oriented ground heat exchanger coils in the area around Fargo, ND are typically buried 2 - 3.5 m deep [90]. At 2 m, soil temperature fluctuates seasonally from around 3.9 to 13.3°C [91]. There is a time lag between seasonal ambient peak temperature and soil peak temperature. Soil temperature at this depth in Fargo achieves its maximum in mid-September; the minimum is reached in early April.

In addition to the seasonal temperature change, operation of a geothermal heat pump will significantly impact the temperature of the soil surrounding the GHX. As heat is extracted from the ground, soil temperature will decrease as the heating season progresses. This means, COP will be very high early in the heating season and will decrease over the course of the heating season.

Heat transfer in the ground is impacted by many factors including: soil composition, water content, soil freezing, and advection of moisture. Increased water content generally improves the soil conductivity as does freezing [92]. Freezing can also potentially be advantageous as since some of the latent heat given off by the freezing will be absorbed by the GHX [80]. Moisture advection is very beneficial since warm moisture in the soil will replace that which is cooled by the GHX.

Given the many factors affecting heat transfer in the soil, accurate prediction of heat transfer surrounding the GHX is a complex problem. The most common analytical methods of modeling heat transfer surround a tube utilize Kelvin line source theory and cylindrical source theory [93]. In the line source model heat transfer to the evaporator tube is approximated by considering the heat flux to be applied to line at the center of the tube. In the cylindrical model the heat flux is

applied on the surface of a cylinder. In both methods: the heat transfer rate per meter length is considered constant; the tube is considered to be embedded within an infinite or semi-infinite medium with a uniform initial temperature and constant far field temperature; and the temperature distribution (and hence heat flux) is considered axisymmetric [94]. Mei [80] points out some issues with these models: the magnitude of the heat flux must be estimated; the ground temperature is not uniform; the temperature of the fluid in the coil is not constant, thus the heat flux along the length of the coil will not be uniform. Despite these shortcomings, line and cylinder source theory are the basis for many models, and many different modifications have been made on the basic line and cylinder source models.

Mei [80] developed a 2-D model with radially symmetric temperature profile in order analyze the effects of soil freezing around a ground coil under the following assumptions:

1. the soil is homogeneous
2. the soil thermal properties are constant but not necessarily identical in the frozen and non-frozen regions
3. the fluid temperature and velocity are uniform at any coil cross section
4. the coil is buried deep enough that the distance between the ground surface and the coil can be considered as far field
5. only a single coil is in the ground
6. the effect of ground temperature variation happens only at far-field and at the coil burial depth and the effect is radially symmetrical

Models that do not consider axisymmetric heat flux have also been developed. Demir et al. [93] and Esen et al. [95] developed similar numerical models which considered 2-D conduction surrounding the coil by finite difference methodology. The soil was discreetized out to a distance considered to have a constant far-field temperature. Finite element software has also been used for similar treatment of the problem. Pulat et al. [96] used finite element software to consider the thermal interaction of adjacent coils in the ground.

3. OBJECTIVES OF THE STUDY

From the literature, several observations have been made: (i) CO_2 is a refrigerant with low environmental impact (ii) technology has advanced to a point where transcritical CO_2 heat pumps can deliver performance similar to that of heat pumps using conventional refrigerants (iii) direct expansion geothermal heat pumps may perform with efficiencies superior to that of a conventional heat pump (iv) use of DX-GHPs is hindered in part by large refrigerant charge, design issues related to evaporator pressure drop and risk of groundwater contamination.

In light of these observations, this study investigates the potential benefit of a system which merges the two technologies by theoretically analyzing a direct-expansion transcritical geothermal heat pump using CO_2. The objectives of the study are: (i) to conduct an in depth thermodynamic analysis of the system under consideration; (ii) to apply said analysis in the development of a numerical model representing the system's steady state operation; (iii) to simulate the performance of the DX-CGHP using the numerical model; (iv) to investigate the performance impacts of system design and operating parameters and to understand the relative importance of these parameters; (v) to suggest design optimizations based on the findings of the parametric study; (vi) to gain insights regarding the applicability of CO_2 in DX-GHPs; (vii) to understand the evaporative pressure drop characteristics of CO_2 in the ground heat exchanger coils.

4. THERMODYNAMIC ANALYSIS

Figure 1 shows the schematic diagram of the direct expansion transcritical CO_2 geothermal heat pump system being studied. The performance and efficiency of the components and the system as a whole are analyzed using a steady state simulation model. Development of the model begins with a detailed thermodynamic analysis of the cycle, which proceeds by consideration of each process of the system individually. Figure 2 shows the four processes of the cycle – compression, gas cooling, expansion and evaporation - on a p-h diagram. Each process of the cycle must conform to the First Law of Thermodynamics. Hence the analysis begins by detailing the 1st Law energy balance equations for each process, where the component corresponding with each process can be treated as a control volume. Using the control volume approach, the generalized 1st Law Energy Balance is as follows:

$$\dot{Q} + \dot{m}_i \left(h_i + \frac{1}{2}u_i^2 + gZ_i \right) = \dot{W} + \dot{m}_e \left(h_e + \frac{1}{2}u_e^2 + gZ_e \right) \qquad (20)$$

Assuming:

(i) the system is operating under steady state conditions

(ii) changes in kinetic and potential energy are negligible

The energy balance for each process of the cycle reduces to:

$$\dot{Q} = \dot{W} + \dot{m}(h_e - h_i) \qquad (21)$$

In both of the heat exchangers determination of the heat transfer rate in the above equation requires an analysis of the heat transfer characteristics. In of the case

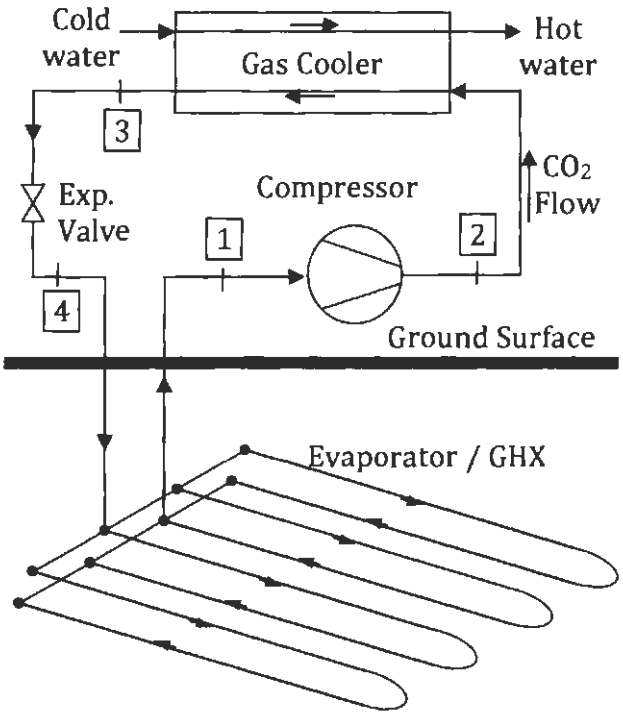

Figure 1. Schematic diagram of the system investigated in this study

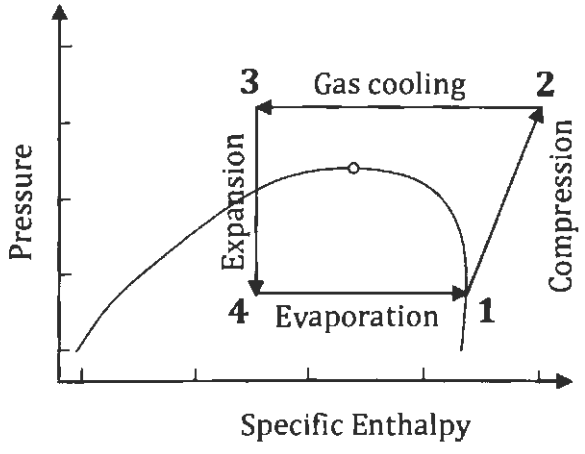

Figure 2. P-h diagram of cycle under investigation in this study

of the gas cooler, heat transfer coefficients are needed for CO_2 and water. In the case of the evaporator, analysis requires heat transfer coefficient of CO_2 and the flux

characteristics of the surrounding soil. Heat transfer coefficients of the fluids are estimated using the Nusselt relationship shown below:

$$\alpha = \frac{Nu \cdot k}{d} \tag{22}$$

where Nu is evaluated using the appropriate empirical correlations available from the literature. Heat transfer in the ground is based on a simplified thermal model of the surround soil. It is also important to analyze the effect of pressure drop of CO_2 in the heat exchangers. Pressure drop is estimated using friction factor correlations available in the literature. Both pressure drop and heat transfer are evaluated based on the assumption that all tubing is smooth.

As shown in Figure 2, the end state of CO_2 in each process of the cycle is equal the beginning state of the next process. This condition is also true for the simulation model based on the assumption that heat loss and pressure drop in connecting tubes between system components is negligible.

In the following sections the theoretical analysis of each component will be detailed. The numerical subscripts in the equations correspond with numbers shown in Figure 2.

4.1. Compression Process

The compressor drives the heat pump cycle and determines the CO_2 flow rate for the system. The analysis proceeds by defining the compressor as a control volume and defining the 1st Law energy balance.

$$\dot{W}_{comp} = \dot{Q}_{loss} + \dot{m}(h_2 - h_1) \tag{23}$$

In developing the thermodynamic model of the compressor, it is helpful to first define some compressor efficiencies. As shown in the following equation, mechanical efficiency specifies the portion of the input power which does work on the fluid.

$$\eta_{mech} = \frac{Work\ Done\ on\ Fluid}{Work\ Input} = \frac{\dot{W}_{comp} - \dot{Q}_{loss}}{\dot{W}_{comp}} \tag{24}$$

Volumetric efficiency is given as:

$$\eta_{vol} = \frac{Actual\ Volumetric\ Flowrate}{Theoretical\ Volumetric\ Flowrate} = \frac{\dot{V}}{(N \cdot V_s)} \tag{25}$$

Isentropic efficiency can be calculated by:

$$\eta_s = \frac{Isentropic\ Enthalpy\ Change}{Actual\ Enthalpy\ Change} = \frac{h_{2s} - h_1}{h_2 - h_1} \tag{26}$$

Total efficiency takes into account both isentropic and mechanical efficiencies.

$$\eta_{tot} = \eta_s \cdot \eta_{mech} \tag{27}$$

The five preceding equations are sufficient to fully analyze the compressor. In the simulation, the outlet temperature, mass flow rate and required power must be determined. The known quantities include the temperature and pressure at the compressor inlet and the pressure at the compressor outlet. In addition, the compressor's total, volumetric and mechanical efficiencies are assumed to correspond with the correlations developed by Oritz, Li & Groll [97] for CO_2. The efficiencies are calculated as functions of the compression ratio as shown in the following equations:

$$\eta_{tot} = -0.26 + 0.7952\left(\frac{P_2}{P_1}\right) - 0.2803\left(\frac{P_2}{P_1}\right)^2 + 0.0414\left(\frac{P_2}{P_1}\right)^3 - 0.0022\left(\frac{P_2}{P_1}\right)^4 \tag{28}$$

$$\eta_{vol} = 0.9207 - 0.0756\left(\frac{P_2}{P_1}\right) + 0.0018\left(\frac{P_2}{P_1}\right)^2 \tag{29}$$

$$\eta_{mech} = 0.9083 - 0.0884\left(\frac{P_2}{P_1}\right) + 0.0051\left(\frac{P_2}{P_1}\right)^2 \quad (30)$$

Solution proceeds by manipulation of Equations (23-27). Thermal losses of the compressor are calculated by rearranging Eq. (24) as follows:

$$\dot{Q}_{loss} = (1 - \eta_{mech})\dot{W}_{comp} \quad (31)$$

By combining Eq. (23), (27) & (31) the compressor power can be calculated by:

$$\dot{W}_{comp} = \frac{\dot{m}_c(h_{2s} - h_1)}{\eta_{tot}} \quad (32)$$

$\dot{m}_c$ can be evaluated using:

$$\dot{m}_c = V_s \cdot \eta_{vol} \cdot N \cdot \rho_1 \quad (33)$$

where V_s is the swept volume, N is the compressor speed and ρ_1 is the suction density. The outlet enthalpy in Eq. (23) can then be solved using the quantities determined in the preceding equations.

$$h_2 = h_1 + \frac{\dot{W}_{comp} - \dot{Q}_{loss}}{\dot{m}_c} \quad (34)$$

Finally, T_2 can be determined since it is a function of h_2 and P_2.

4.2. Gas Cooler

The gas cooler is modeled as a counter-flow, concentric-tube heat exchanger with CO_2 flowing in the inner tube and water flowing through the outer annulus. Heat loss to the surroundings is assumed to be negligible, and as with all heat exchangers, $\dot{W}$ is zero. Thus the 1st Law energy balance for the gas cooler reduces to:

$$\dot{m}_c(h_{c,i} - h_{c,e}) = \dot{m}_w(h_{w,e} - h_{w,i}) \tag{35}$$

Hence the rate of enthalpy change for the two fluids is equal in magnitude but opposite in sign. Furthermore, the rate of enthalpy change is equivalent to the internal heat transfer rate between the two fluids. This heat transfer rate can be calculated by the effectiveness-NTU method for counter-flow as follows:

$$\dot{Q}_{internal} = \epsilon C_{\min}(T_{ci} - T_{wi}) \tag{36}$$

where C_{min} is the smaller heat capacity rate of the two fluids in the gas cooler, and the effectiveness is calculated for counter-flow by:

$$\epsilon = \frac{1 - \exp[-NTU(1-R)]}{1 - C * \exp[-NTU(1-R)]} \tag{37}$$

The Number of Transfer Units in Eq (37) is calculated by,

$$NTU = \frac{UA}{C_{min}} \tag{38}$$

and

$$R = \frac{C_{min}}{C_{max}} \tag{39}$$

The overall heat conductance, UA, is calculated by the inverse sum of the resistivity values, which for the gas cooler are: the convective resistance of CO_2, conductive resistance of the tube-wall and convective resistance of water. The equation is as follows:

$$UA = \left(\frac{1}{\alpha_c A_c} + \frac{\ln\left(\frac{d_o}{d_i}\right)}{2\pi(\Delta L)k_{wall}} + \frac{1}{\alpha_w A_w} \right)^{-1} \tag{40}$$

The two unknown parameters in Eq. (40) are the CO_2-side heat transfer coefficient, α_c, and the water-side heat transfer coefficient, α_w. Estimation of the heat transfer coefficients is by the appropriate heat transfer correlations.

The water-side heat transfer coefficient is predicted by the Nusselt relationship using a correction factor for annular flow as suggested by Petukhov & Roizen [97]:

$$\alpha_w = CF\frac{Nu \cdot k_w}{d_h} \qquad \text{CF} = 0.86\left(\frac{d_i}{d_o}\right)^{-0.16} \qquad d_h = d_0 - d_i \quad (41)$$

Nu is evaluated by the well known Gnielinski [60] correlation for turbulent flow. The correlation was given in Eq. (9) and repeated here for convenience.

$$Nu = \frac{\frac{f}{8}(Re - 1000)Pr}{1.07 + 12.7\left(\frac{f}{8}\right)^{0.5}\left(Pr^{\frac{2}{3}} - 1\right)} \qquad 3000 \leq \text{Re} \leq 5\text{x}10^6 \quad (9)$$

The friction factor is calculated using Pehtukhov [61] as shown below:

$$f = (0.79 \cdot \ln(\text{Re}) - 1.64)^{-2} \qquad 3000 \leq \text{Re} \leq 5\text{x}10^6 \quad (10)$$

As described in Section 2.7.1, the heat transfer characteristics of supercritical CO_2 have been studied extensively and various correlations have been developed for supercritical CO_2 cooling in a horizontal tube. In this analysis the Nusselt correlation of Pitla et al. [49] is used to evaluate the CO_2 heat transfer coefficient in the gas cooler. The equation is repeated here:

$$Nu_c = \left(\frac{Nu_{wall} + Nu_b}{2}\right)\frac{k_{wall}}{k_b} \quad (8)$$

It should be noted that under certain operating conditions CO_2 may cool to subcritical temperatures in a short portion of the gas cooler. Despite this, the above correlation is assumed to be applicable throughout the gas cooler.

The water-side pressure drop is assumed as negligible since the fluid is incompressible and the mass flux is relatively low. Water properties are evaluated at a pressure of 1 atmosphere.

Frictional pressure drop of CO_2 cannot be neglected. ΔP is calculated using a Darcy friction factor as shown below:

$$\Delta P = f \frac{\Delta L}{2\rho_c} \left(\frac{{G_c}^2}{d_i} \right) \tag{42}$$

where friction factor is estimated using the correlation of Blasius [99] for turbulent flow in a smooth tube.

$$f = \frac{0.316}{Re^{1/4}} \quad \text{for } 2300 \leq \text{Re} \leq 2 \times 10^4 \tag{43}$$

$$f = \frac{0.184}{\text{Re}^{1/5}} \quad \text{for Re} \geq 2 \times 10^4 \tag{44}$$

Having developed the theory necessary to analyze the gas cooler, the method of analysis must be addressed. In the simulation, the water inlet-temperature is specified and is assumed to be constant. The CO_2 inlet temperature and pressure are also known since they correspond to the outlet of the compressor. Mass flow rates of both fluids are also known. Ultimately, the exit temperatures of both fluids must be determined.

Certain heat exchanger applications allow for reasonable accuracy through a simple evaluation of an overall heat transfer coefficient. In the case of the CO_2 gas

cooler, heat transfer is highly non-linear and this method is not reasonable. To improve accuracy and to account for the rapid change in properties through the supercritical region, the gas cooler is discreetized along its length into finite control volumes. Each control volume is then analyzed as an independent, finite heat exchanger using the theory outlined above. Figure 18 illustrates a single control volume element of the gas cooler along with the numbering-convention used in the description.

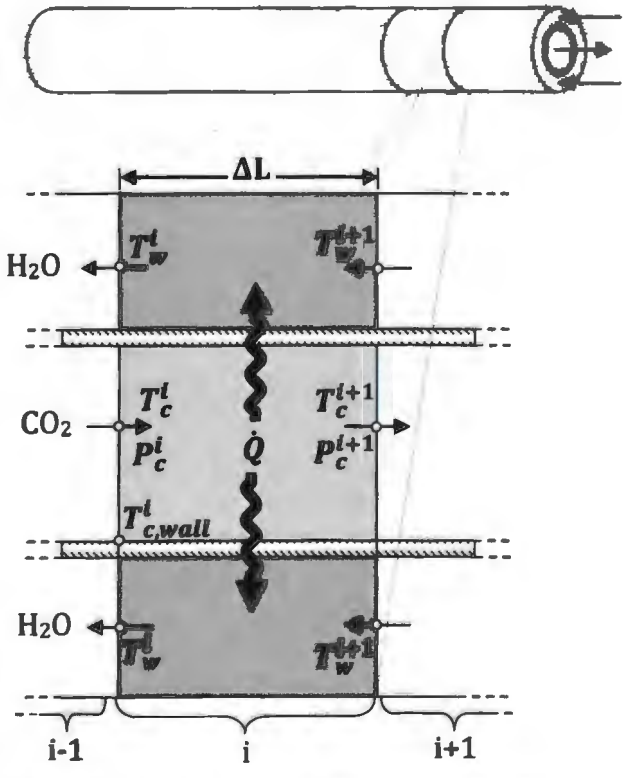

Figure 18. Single control volume element of gas cooler with numbering convention

By using small control volumes, the properties can be considered constant throughout the element. This allows equation (38) to be modified for constant specific heat as follows:

$$\dot{m}_c c_{p,c}\left(T_c^i - T_c^{i+1}\right) = \dot{m}_w c_{p,w}\left(T_w^i - T_w^{i+1}\right) \tag{45}$$

The properties required for the solution (specific heat, viscosity, thermal conductivity, density) are evaluated using the REFPROP 8.0 [10] software package. Water properties are evaluated at T_w^i and P_{atm}; CO_2 bulk properties are evaluated at T_c^i & P_c^i; and CO_2 wall properties at $T_{c,wall}^i$ & P_c^i.

The method proceeds for each element as follows. An inner wall temperature is initially estimated based on CO_2 and water temperatures. CO_2-side and water-side heat transfer coefficients are then calculated which subsequently allows for the evaluation of the overall heat transfer rate, $\dot{Q}^i$, in the element. To check the validity of the wall temperature estimation, the inner wall temperature is then calculated as follows:

$$\left(T_{wall}^i\right)_{calc} = T_c^i - \frac{\dot{Q}^i}{\pi d_i \alpha_c \Delta L} \tag{46}$$

If the calculated and estimated values of T_{wall} are not equal, T_{wall} is updated and the process repeats until the values agree within a specified tolerance. Iteration proceeds by the Secant Method which will be described in Section 0. Once the wall temperature is known, ϵ and NTU can be calculated, and ultimately T_w^{i+1}, T_c^{i+1} & P_c^{i+1} can be determined by combining Eqs. (35) & (45). Finally, these values are passed on to the next element and the procedure repeats until the heat exchanger outlet conditions are obtained. A flow diagram of the procedure is shown in Figure 19.

Turning again to the overall gas cooler, it can be observed that the water exit temperature is unknown. Since volume element calculations begin at the CO_2-inlet,

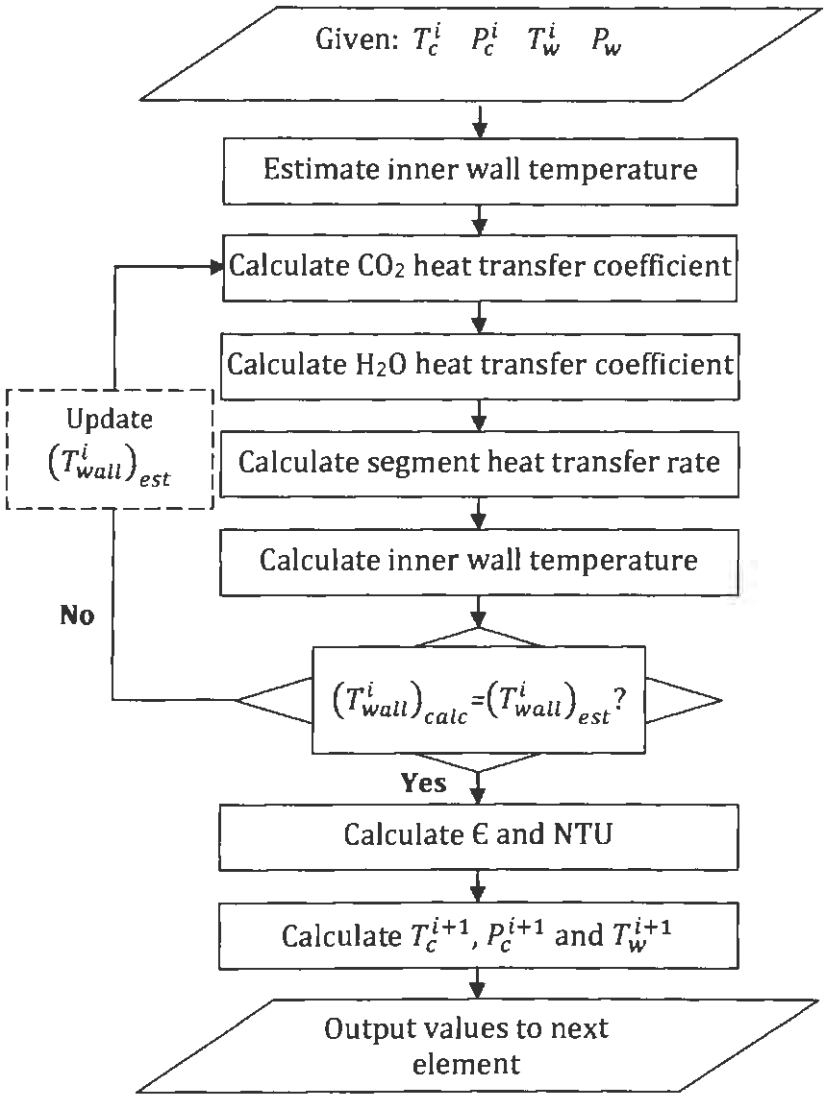

Figure 19. Flow diagram of solution procedure for individual volume elements in gas cooler

this means that T_w^i is unknown. To account for this, an initial value of $T_{w,e}$, is estimated and temperatures across the gas cooler are solved using the procedure described above. The water inlet temperature determined by this estimate is then compared to the actual value. If the error is greater than a specified tolerance, $T_{w,e}$ is updated and the procedure repeats. The new value of $T_{w,e}$ is evaluated using the Secant Method. The process flow for the gas cooling model is shown in Figure 20.

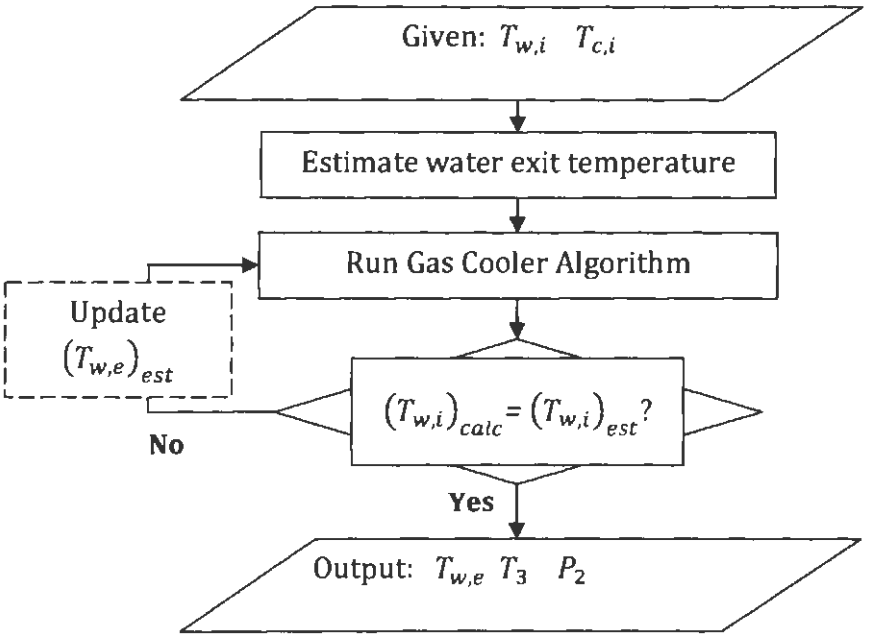

Figure 20. Process flow diagram for gas cooling model

4.3. Expansion Process

The expansion device in a CGHP controls the mass flow rate of CO_2 and the pressure drop as the fluid is throttled from the gas cooler pressure to the evaporator pressure. No work is done during throttling, and conventionally, the process is assumed to be adiabatic. The energy balance therefore reduces to $h_3 = h_4$, and thus the process is isenthalpic.

4.4. Evaporator

The analysis of the evaporation process begins by defining the fluid inside the evaporator tube as the control volume. Unlike the gas cooler, the evaporator is not adiabatic but is receiving heat from the surrounding soil, and this heat transfer must be included in the analysis. Since there is no work done, the first law energy balance can be reduced to the form shown in Eq. 47.

$$\dot{m}_c(h_{c,e} - h_{c,i}) = \dot{Q}_{ev} \tag{47}$$

The rate of heat transfer from the soil can be calculated by the log mean temperature difference method:

$$\dot{Q}_{ev} = UA \frac{(T_{soil} - T_{c,e}) - (T_{soil} - T_{c,i})}{ln \frac{(T_{soil} - T_{c,e})}{(T_{soil} - T_{c,i})}} \tag{48}$$

In the above equation UA is calculated as the inverse sum of the resistivity terms which are: CO_2 convective resistance, conductive resistance of tube-wall and conductive resistance of soil within a 1 m radius of the coil's center. The equation is as follows:

$$UA = \left(\frac{1}{\alpha_c A_c} + \frac{\ln\left(\frac{d_o}{d_i}\right)}{2\pi(\Delta L)k_{wall}} + \frac{\ln\left(\frac{2}{d_0}\right)}{2\pi(\Delta L)k_{soil}} \right)^{-1} \tag{49}$$

Within the evaporator, two flow-regions exist: the two-phase flow region and the superheated vapor region. Different heat transfer and pressure drop correlations are utilized to predict performance in the two distinct regions. In the two-phase region, the heat transfer coefficient is evaluated using the correlation of Jung et al. [73,74] as described in Section 2.7.2 and repeated here.

$$\alpha_c = \varphi \alpha_{sa} + F_p \alpha_l \tag{11}$$

Pressure drop in the two phase region is calculated as follows:

$$\Delta P^i = 2 f_{lo} \frac{\ell}{d_i} \frac{G^2}{\rho_l} \phi_{lo}^2 \tag{50}$$

where f_{lo} is the liquid-only Fanning friction factor, which is evaluated by treating the entire flow as liquid and calculated utilizing the Blasius [99] correlation as shown in

Eq. (51). ϕ_{lo} is the liquid-only two-phase multiplier calculated using the correlation proposed by McAdams et al. [100] as indicated in Eq. (52). The correlation is applicable for flows in which both the two-phase flow and the entire flow as liquid are turbulent.

$$f_{lo} = \frac{0.0791}{Re_{lo}^{0.25}} \quad \text{Re} \geq 2300 \tag{51}$$

$$\phi_{lo}^2 = \left[1 + \left(\frac{\mu_l}{\mu_v} - 1\right)x\right]\left[1 + \left(\frac{\rho_v}{\rho_l} - 1\right)x\right]^{0.1} \tag{52}$$

In the vapor-only region of the evaporator, heat transfer coefficients are calculated using the correlations of Gnielinski [60] and Petukhov [61] given previously by Eqs. (9) & (10) respectively. Pressure drop is calculated using the Fanning friction factor correlation of Blasius [99] as shown previously in Eq. (51), however in this case Reynolds number is calculated for vapor properties.

An important parameter is the degree of superheat at the evaporator exit. The degree of superheat is the difference between CO_2's exit temperature and the saturated vapor temperature at the exit pressure.

$$T_{sup} = T_1 - T_{sat,P1} \tag{53}$$

In this study, evaporator exit temperature, pressure and superheat are known, and the model is developed to determine the CO_2 inlet temperature and pressure. Similar to the gas cooling process, the evaporator is divided into finite control volume elements in order to improve the accuracy of property evaluation and to capture the non-linearity of the heat transfer process. Again, the properties are evaluated based

on the known fluid state for an element (the outlet state in this case) and the inlet temperature and pressure are determined.

Calculation is slightly different in the vapor and two-phase regions. In the vapor region, pressure and temperature are independent and must be calculated separately using the theory outline above. In the two-phase region, T_{sat} and P_{sat} are related; hence for a particular element P_c^{i+1} is evaluated first which can then be used to determine T_c^{i+1}.

4.5. Soil Heat Transfer

In this study, heat transfer in the soil surrounding the evaporator is modeled using the method of Mei [80] as outlined in Section 2.10 with some modification. The model considers conduction to be 2-D only and the temperature distribution to be radially symmetric in the soil immediately surrounding the tube. Figure 21 illustrates the temperature distribution in the soil under the following simplifying assumptions:

1. soil thermal conductivity is uniform and constant
2. heat conduction parallel to the ground coils is negligible and the temperature profile in the surrounding soil is radially symmetric to a radius of 1 m
3. the temperature profile does not vary along the length of the coil
4. the soil temperature at a 1 m radius is constant and is considered to be equal to the undisturbed soil temperature at the coil burial depth [101]
5. thermal interaction between adjacent coils is negligible
6. contact resistance between the coil and the soil is negligible

Assumption 4 is a modification of the method of Mei [80] based on the experimental measurements of Freund & Whitlow [101] which found that the thermal effects of a ground coil did not extend beyond 1 m.

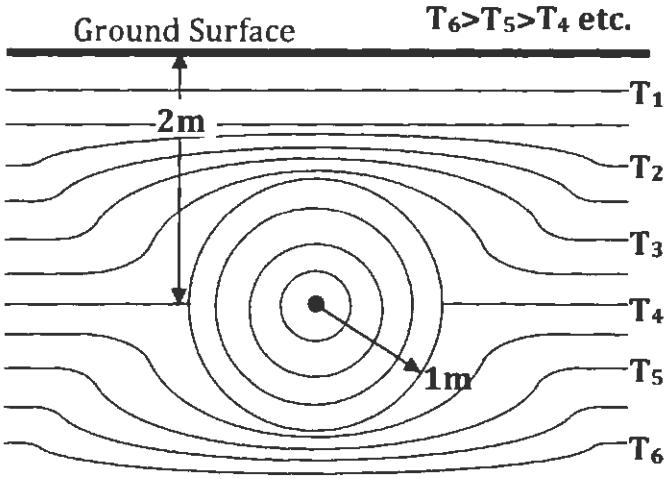

Figure 21. Assumed soil temperature distribution of the model

4.6. Cycle Performance and Thermal Efficiency

The preceding sections have focused on individual components of the CGHP. In this section, the system-level performance is addressed. At the system-level, a heat pump is evaluated by its thermal efficiency and by its rate of heat delivery (heating capacity). In general terms, thermal efficiency is defined as

$$\eta = \left[\frac{Desired\ Output\ Energy}{Energy\ Input}\right] \tag{54}$$

In the case of a heat pump the desired output is the heat rejected, the input is the compressor work, and this ratio is generally greater than one. To distinguish this from the decimal efficiency of a power cycle, heat pump efficiency is given the label of Coefficient of Performance as described in the Introduction. Using the component

inlet and outlet states determined by the simulation the coefficient of performance is given by:

$$COP = \left[\frac{h_2 - h_3}{h_2 - h_1}\right] \tag{55}$$

and the heating capacity is calculated as follows:

$$\dot{Q}_{cap} = \dot{m}_c(h_2 - h_3) \tag{56}$$

Since the CGHP system is being investigated for the purpose of water heating, the output could also be evaluated from the perspective of amount of hot water delivered, or hot water delivery temperature. However, since the gas cooler is assumed to be adiabatic, the energy gained by the water is equal to the energy rejected by CO_2.

4.7. Secant Method

The Secant Method is an iterative root finding technique which uses a linear interpolation technique to estimate the root of a function [102]. Figure 22 shows the iterative procedure using the simulation model's evaluation of P_2 as a sample. The function's derivative is approximated as shown below:

$$f'(x_i) = \frac{f(x_i) - f(x_{i-1})}{x_i - x_{i-1}} \tag{57}$$

The root of the function is obtained through iteration, where the next prediction for the root is calculated as follows:

$$x_{i+1} = x_i - f(x_i) \cdot \left(\frac{x_i - x_{i-1}}{f(x_i) - f(x_{i-1})}\right) \tag{58}$$

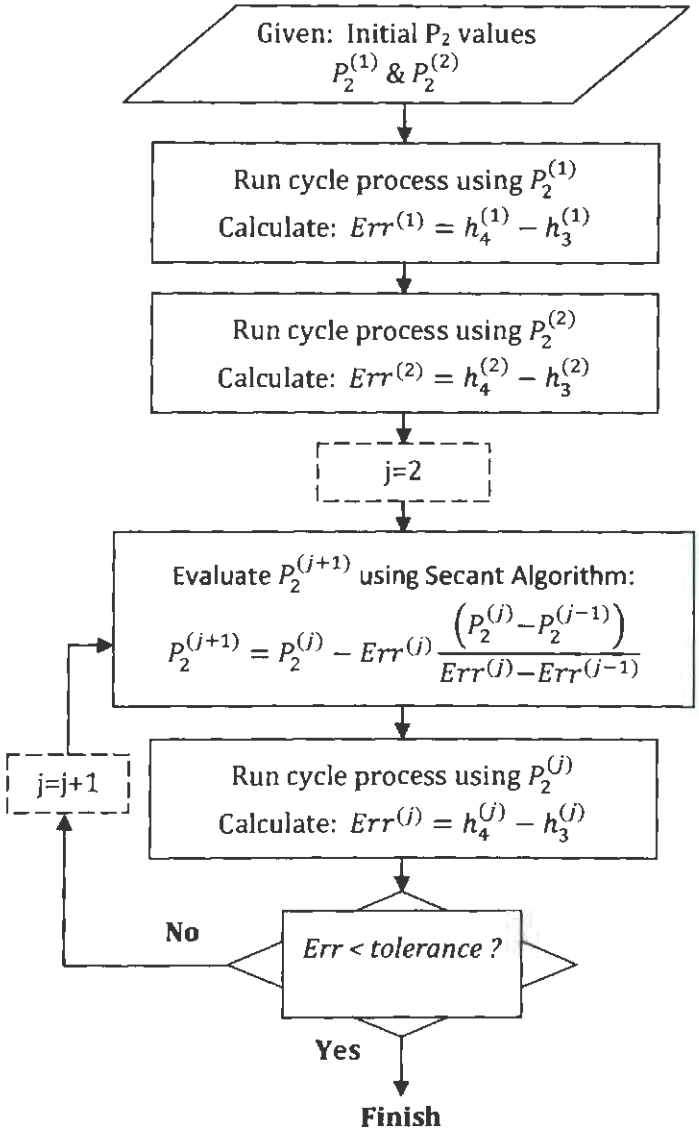

Figure 22. Flow diagram of Secant Method iteration procedure using P_2 solution as a sample

Equation (58) reveals that in the Secant Method two values are needed to evaluate the next value of x. Hence, two initial guesses are required to begin the procedure. The Secant Method converges quadratically, but convergence is not guaranteed [102].

4.8. Error Analysis

In order to compare the simulation results to the experimental work of previous studies a method of error accounting must be defined. In all comparisons the mean absolute deviation is used. Mean absolute deviation (%) is defined as:

$$|e| = 100 \cdot \frac{1}{n} \sum \left| \frac{(x_i - z_i)}{z_i} \right| \tag{59}$$

where x_i is the theoretical value of the i^{th} data point, z_i is the experimental value of the data point and n is the total number of data points. The mean absolute deviation provides a means to evaluate how well the predicted values of the simulation agree with the experimental values of previous studies.

4.9. Refinement of Heat Exchanger Control Volume Elements

The division or discreetization of the heat exchangers (evaporator & gas cooler) into finite control volume elements improves the accuracy of the simulation. In order to determine the appropriate element length, a refinement was performed on both heat exchangers separately. The evaporator refinement procedure consisted of running the full simulation with successively smaller evaporator control volume elements. The relative changes in the output parameters were then evaluated. Gas cooler refinement proceeded in like fashion.

The appropriate control volume element length was selected at the value for which further refinement produced insignificant change in output parameters. The refinement process resulted in a gas cooler control volume element length of 0.1m, and an evaporator element length of 0.5m. It is reasonable that the evaporator element length is much longer than that of the gas cooler since: (i) heat flux is lower

in the evaporator; (ii) variation in property values and heat transfer characteristics are less dramatic in the evaporator; (iii) mass flux is lower in the evaporator.

5. PARAMETRIC STUDIES

5.1. Simulation of the System

Utilizing the theory and methods developed in Chapter 4, a computer code was written using MATLAB software to simulate the performance characteristics of the CGHP system. The MATLAB code is presented in Appendix B. The simulation approximates the system's steady state operating conditions based on design and operating parameters determined by the user. The operating parameters which are input at the start of a simulation include: compressor speed, degree of superheat at the evaporator outlet, soil temperature, water inlet temperature and water flow rate. In addition, design parameters such as the HX geometries may be adjusted. All of these values remain constant throughout a simulation.

A heat pump system maintains steady state operation by adjusting the ratio between gas cooler (or condenser) and evaporator pressure. In a geothermal heat pump, the evaporation temperature and pressure remain relatively constant in the short-term since the ground temperature varies gradually over the heating season. In light of this, it is appropriate in the simulation to maintain constant evaporator pressure and to attain stead state operation by varying the gas cooler inlet pressure (P_2). To summarize, P_1 and T_1 are simulation inputs which remain constant and P_2 is adjusted to attain steady state system operation. Determination of P_2 occurs by iteration using the Secant Method, which requires two initial pressure estimations. The Secant Method was described in Section 4.7 and Figure 22 showed the use of the method for the determination of P_2.

Figure 23 shows the flow diagram of the simulation procedure. To begin a simulation, the operating parameters are input including two initial estimates of P_2. The compression, gas cooling and evaporation models are then called upon to determine the inlet/outlet conditions of each process. Fluid properties required throughout each model are evaluated using REFPROP 8.0 [10]. Finally, the model evaluates the difference between the inlet and outlet enthalpy of the expansion process, h_3 and h_4. Note that h_3 is calculated as the outlet of the gas cooling model and h_4 is calculated as the inlet of the evaporation model. If the difference between h_3 and h_4 is greater than the specified level of tolerance, the model will update P_2 and a new iteration begins. When the difference in enthalpy at the expansion valve reaches a value less than the error tolerance, the simulation is complete and the current operating conditions are considered steady state. The simulation outputs the inlet and outlet conditions for all components as well as the heating capacity, compressor power, heat extraction rate of the GHX and the COP.

5.2. Model Validation

A model validation is necessary in order to ensure that the simulation results agree with the values of previous experimental studies. However, to the author's knowledge no experimental or theoretical results have been published on a CGHP system. Instead, model validation was conducted by separately investigating the gas cooling and evaporation models in isolation from the system. These two processes were selected since they present the most challenge in terms of modeling and are perhaps the most critical to overall simulation accuracy.

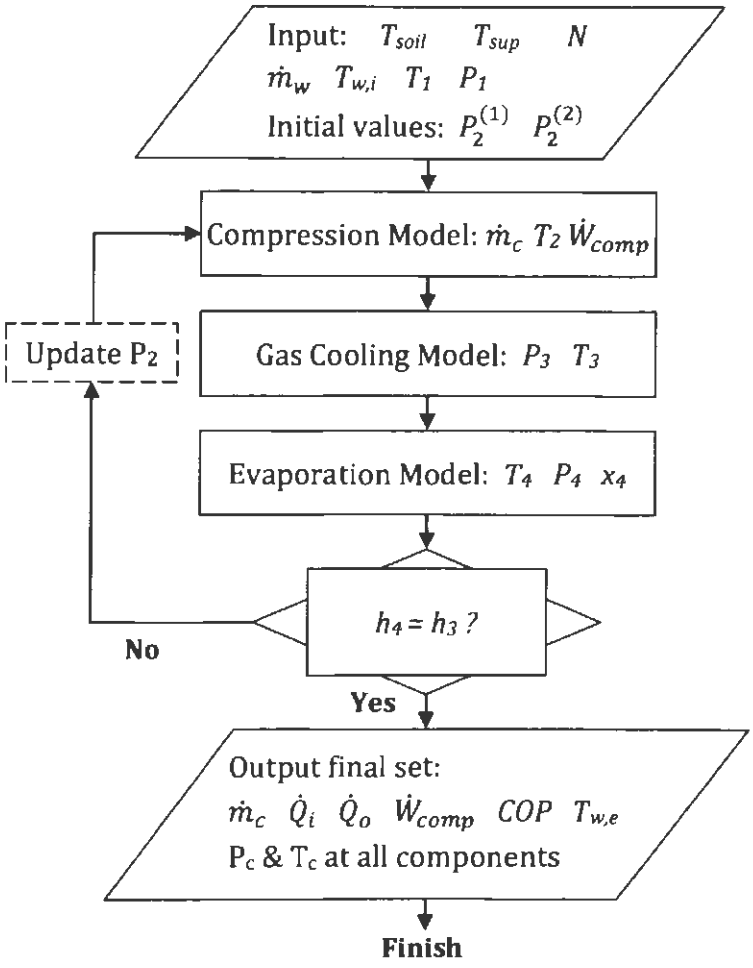

Figure 23. Flow diagram of the simulation procedure

The gas cooling model was verified by analyzing pressure drop and temperature distribution. The pressure drop predicted by the gas cooling model was compared to the experimental results of Yoon et al. [48] at various inlet pressures and mass flux rates. It can be observed in Figure 24 that the gas cooling model provides reasonable approximation of the experimental data. The mean absolute deviation was 15.8%.

Temperature distribution in the gas cooler was evaluated against the experimental results of Oh & Son [22]. Figure 25 shows the calculated and

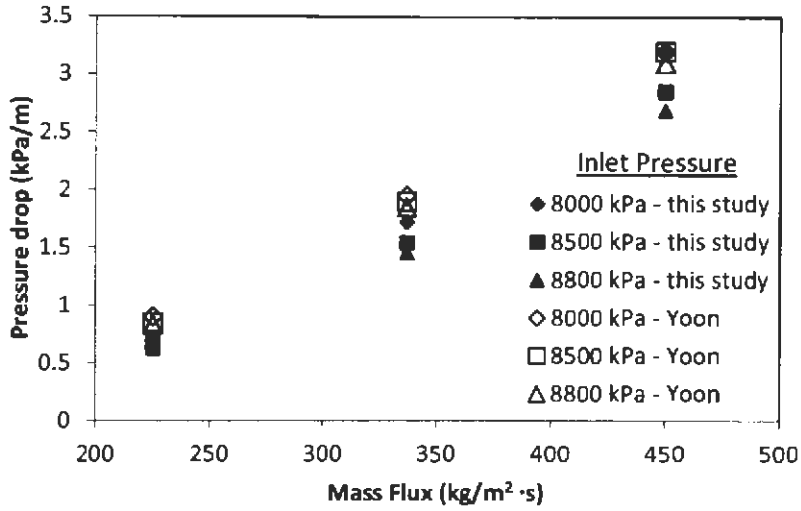

Figure 24. Gas cooler validation: predicted pressure drop vs. experimental results of Yoon et al. [48]

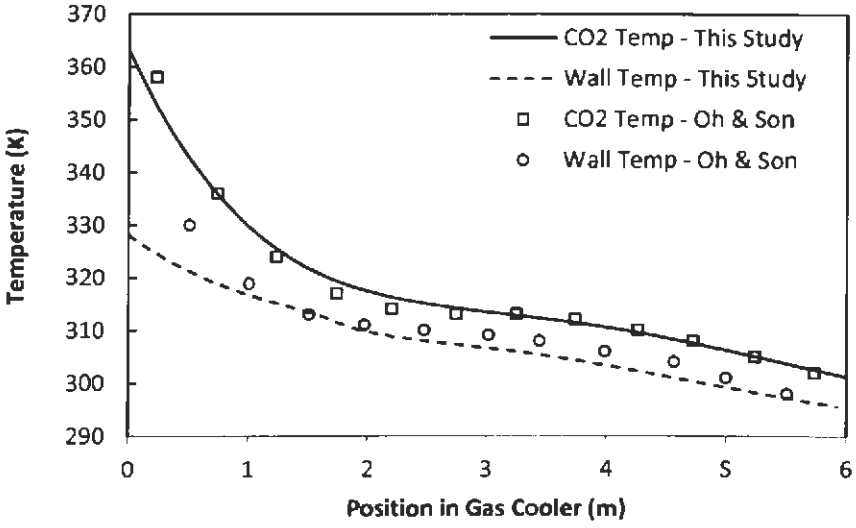

Figure 25. Gas cooler validation: predicted inner wall temperature and CO_2 bulk temperature vs. experimental results of Oh & Son [22] G=300 kg/m²·s

experimental temperature profiles of the CO_2 bulk temperature and the inner-wall temperature. As shown in the figure, good agreement exists between the data sets. Due to the large absolute temperature relative to the temperature range the mean

absolute deviation in this case was calculated as:

$$|e| = 100 \cdot \frac{1}{n} \sum \left| \frac{(x_i - z_i)}{z_{max} - z_{min}} \right| \tag{60}$$

The result is a mean absolute deviation of 6.3%.

Accuracy of the evaporation model was investigated using the reported data of Mastrullo et al. [71]. The calculated and experimentally determined local heat transfer coefficients, plotted in terms of vapor quality, are shown in Figure 26. The mean absolute deviation was 23%, and the model can be said to generally approximate the trend.

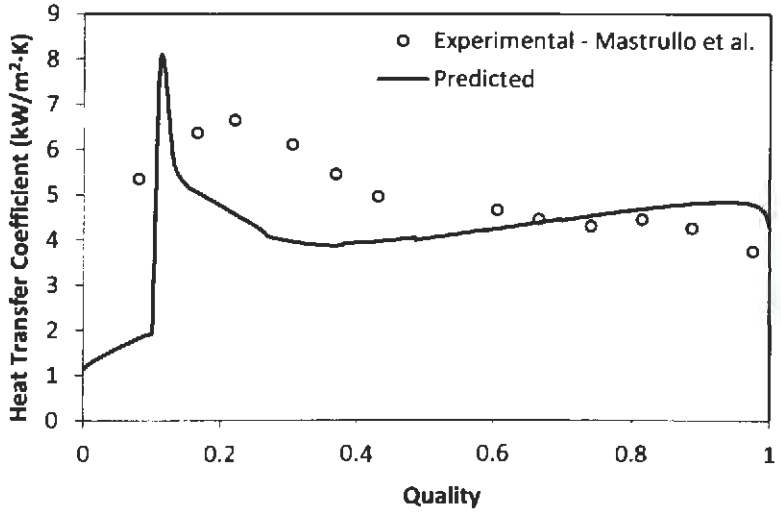

Figure 26. Evaporator validation: predicted local heat transfer coefficients vs. experimental results of Mastrullo et al. [71] G=201 kg/m²·s

The pressure drop characteristics of CO_2 in the evaporator were also analyzed by utilizing the results of Mastrullo et al. [71]. The comparison showed a mean absolute deviation of 13.8%. As shown in Figure 27, the predicted and experimental trends are similar.

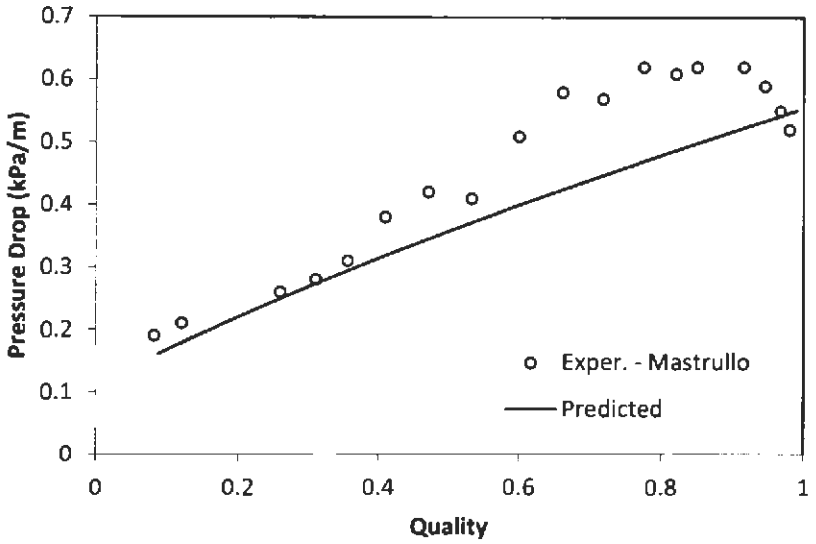

Figure 27. Evaporator validation: predicted pressure drop vs. experimental results of Mastrullo et al. [71] G=349 kg/m^2·s

Based on the validation results, the gas cooling and evaporation models can be said to provide reasonable prediction of actual gas cooler and evaporator performance. Reiterating that these are the most complex and perhaps most important elements of the model, the validation results lead to the conclusion that the accuracy of the total simulation model is sufficient for investigation of the system under study.

5.3. Baseline Simulation

A set of baseline simulation parameters was defined to serve as a point of reference during the parametric studies. The baseline conditions for the simulation are given in Table 2. The heat pump design parameters such as heat exchanger geometries were decided upon based on analysis and modification of parameters given in related studies [23,85]. The soil temperature and thermal conductivity correspond with the winter soil conditions in Fargo, North Dakota at a depth of 2m

[90,103]. The water inlet temperature is based on the temperature of water from a shallow well in the same location [104,105]. The baseline simulation showed a COP of 2.18 and a heating capacity of 10.5 kW. During the parametric studies, the baseline specifications shown in Table 2 were maintained for all simulations with the exception of the parameter(s) being studied.

Table 2. Baseline simulation parameters

Evaporator		**Gas Cooler**	
Inner diameter	9.5 mm	Inner-tube inner diameter	5 mm
Outer diameter	11.5mm	Inner-tube outer diameter	7 mm
Number of circuits	4	Outer-tube inner diameter	16 mm
Circuit length	120 m	Length	15 m
Soil temperature	279.2 K	Water inlet temperature	280 K
Soil thermal conductivity	1 W/ m·K	Water mass flow rate	0.06 kg/s
Superheat	5 K	**Compressor**	
$T_{ev,out}$	271.2 K	Swept volume	19.72 cm^3
		Speed	3000 rpm

5.4. Compressor Speed

Compressor speed is important for a heat pump system since it can be varied in order to match the heating load. The simulation was performed for compressor speeds ranging from 2400 to 6600. Increasing the compressor speed (N) produces the direct effect of increasing mass flow rate. Over the range simulated, $\dot{m}_c$ increased nearly linearly from 0.041 to 0.106 kg/s. The change in $\dot{m}_c$ produces several

secondary effects which will be detailed below, but the net effect is a decrease in COP as shown in Figure 28.

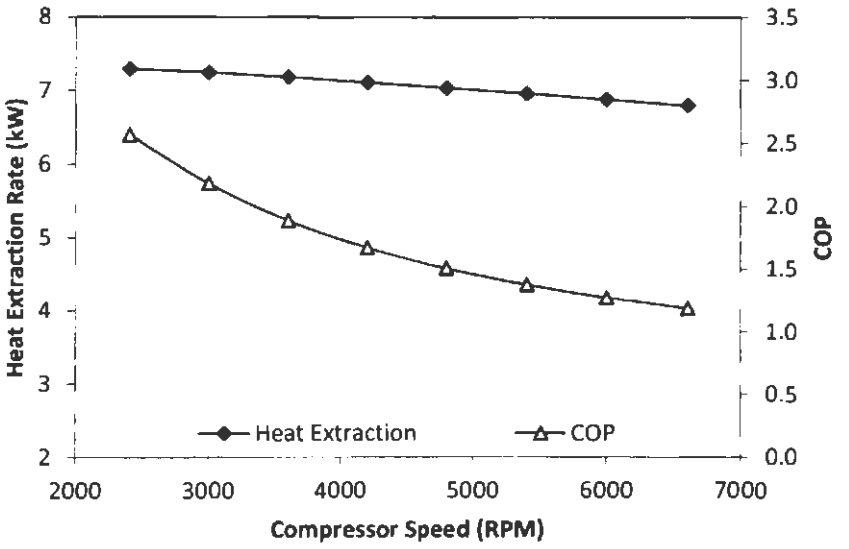

Figure 28. Heat extraction rate and COP versus compressor speed [106]

One of the effects of increased compressor speed is a slight decrease in the heat extraction rate. This effect, shown in Figure 28, was somewhat surprising since the additional turbulence caused by increasing $\dot{m}_c$ could be expected to increase the heat transfer rate. At the same time however, the change in $\dot{m}_c$ increases pressure drop in the evaporator. This results in an increased mean evaporation temperature ($\bar{T}_{ev}$), as illustrated in Figure 29. Heat extraction can be roughly calculated by:

$$\dot{Q}_i \cong \bar{\alpha} A (T_{soil} - \bar{T}_{ev}) \tag{61}$$

and thus $\dot{Q}_i$ decreases since $T_{soil} - \bar{T}_{ev}$ becomes smaller.

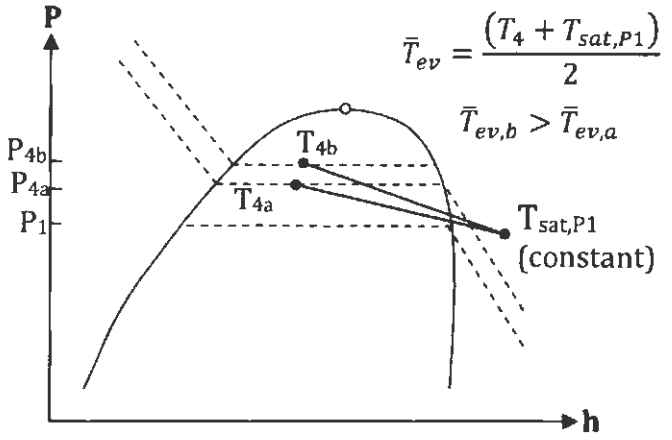

Figure 29. P-h diagram illustrating effect of pressure drop on mean evaporation temperature

The additional mass moving through the compressor increases the compressor power requirements. Figure 30 shows this effect along with the variation in heating capacity. Heating capacity increases at a rate slightly lower than the power, and this is due primarily to the decrease in heat extraction rate but also because of the

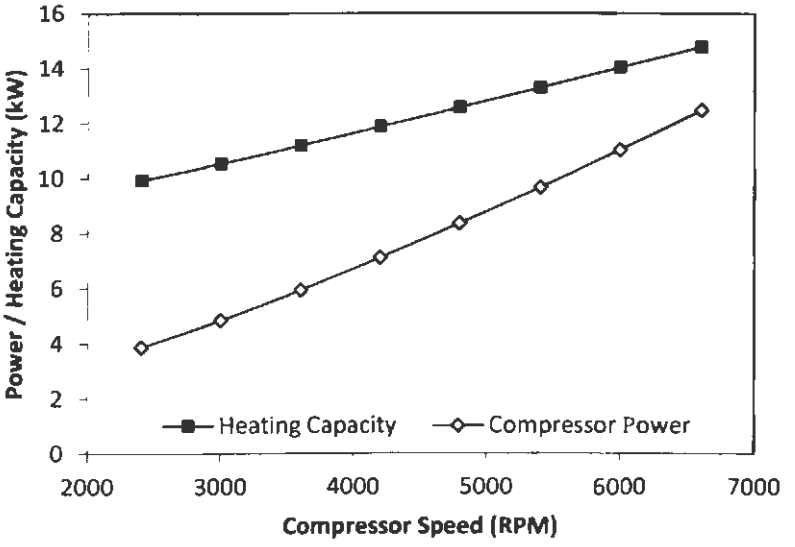

Figure 30. Change in compressor power and heating capacity versus compressor speed [106]

decreased compressor efficiency as the pressure ratio [P_2/P_1] increases. As mentioned above, the net effect of these changes on the coefficient of performance is a decreasing trend as compressor speed increases.

5.5. Effect of Evaporator Tube Diameter

As mentioned in Section 2.9, the diameter of the ground heat exchanger (evaporator) tubes can influence the performance of a DX-GHP by effecting the flow velocity, pressure drop and heat transfer area. In order to investigate these effects in a system using CO_2, the inner diameter of the evaporator coil was varied from 5.5 to 23.5 mm while maintaining a constant wall thickness.

Figure 31 shows evaporative pressure drop and mean evaporation temperature. As expected the pressure drop decreases significantly as tube diameter increases, even approaching zero at the upper range of tested diameters. Wang et al. [84] reported a pressure drop of 2 kPa/m in a vertical U-Tube using R134a. The simulation results show that, except for the 5.5mm diameter, the CO_2 pressure drop per meter is significantly lower than that of R134a. The change in mean evaporation pressure is also very low for all but the smallest tube diameter.

Figure 32 shows impact of tube diameter on COP, heating capacity and heat extraction rate. As tube diameter increases from 5.5 to 23.5 mm, heat extraction rate increases from 5.2 to 8.6 kW and heating capacity increases from 8.3 to 12.0 kW. Compressor power (not shown) also increases but to a lesser degree. It can be said that the majority of the capacity increase is due to the improved heat extraction rate. The increased heat extraction rate is because with larger diameters the heat flux is

being absorbed over a larger area. Also shown in Figure 32 is the influence of tube diameter on COP. The net effect of the trends listed is an increase in COP.

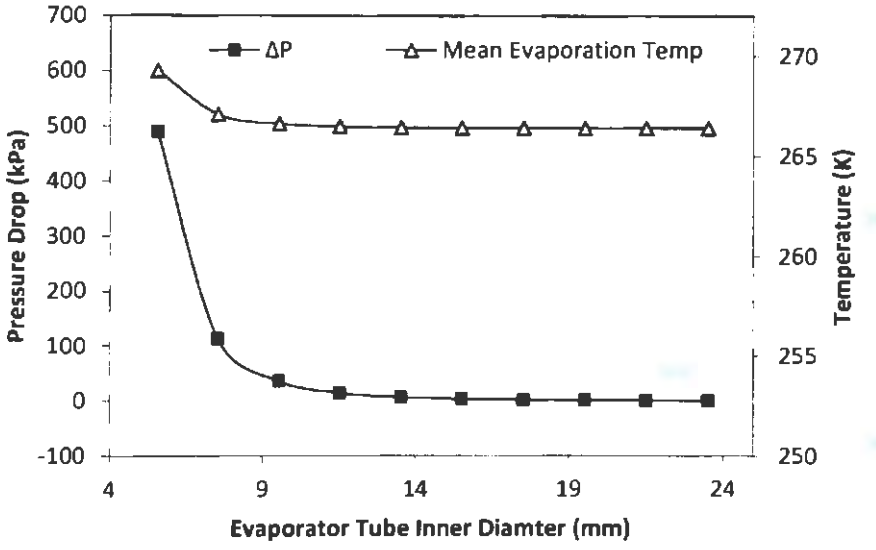

Figure 31. Evaporative pressure drop and mean evaporation temperature versus evaporator tube diameter

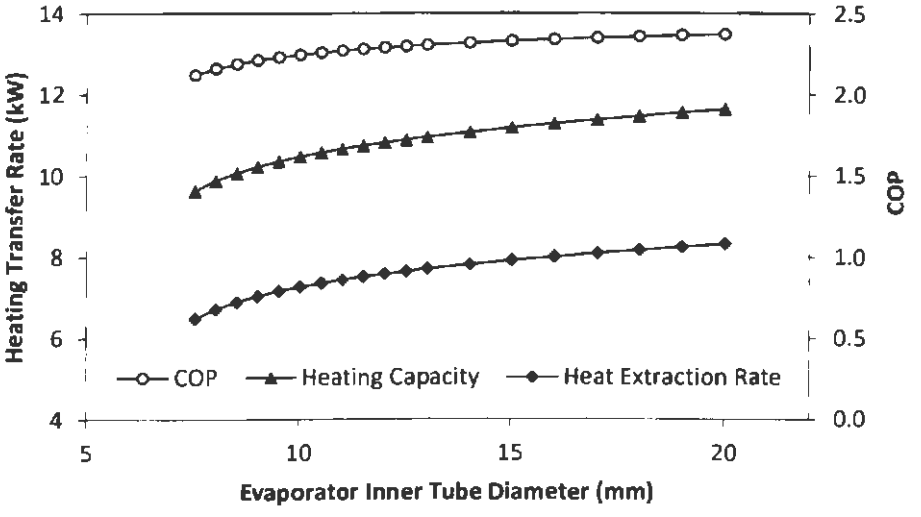

Figure 32. Effect of evaporator tube diameter on COP, heating capacity and heat extraction rate [106]

5.6. Evaporator Length and Number of Circuits

Coil length in the GHX is an important design parameter for conventional geothermal heat pumps, and this holds true for DX-GHPs as well. It is intuitive that as evaporator coil length increases more heat will be absorbed in the GHX and heating capacity of the system will increase. The simulation results support this conclusion. On the other hand, the effect of coil length on COP is more complex. Figure 33 reveals that as evaporator coil length increases, COP also increases to an optimal value of 2.28 when coil length is 140 m. Further increase beyond the optimal length results in declining COP values. The decrease at longer coil lengths is the result of increasing compressor pressure ratio which is also shown in Figure 33. It is clear that the pressure ratio increases more sharply beyond the optimal length. This, in turn, causes $\dot{W}_{comp}$ to increase. Ultimately, the trends shown in Figure 33 are due to an imbalance between evaporator and gas cooler capacities. Beyond the optimal length, the evaporator is oversized with respect to the gas cooler. The interaction between evaporator and gas cooler will be discussed further in Section 5.10.

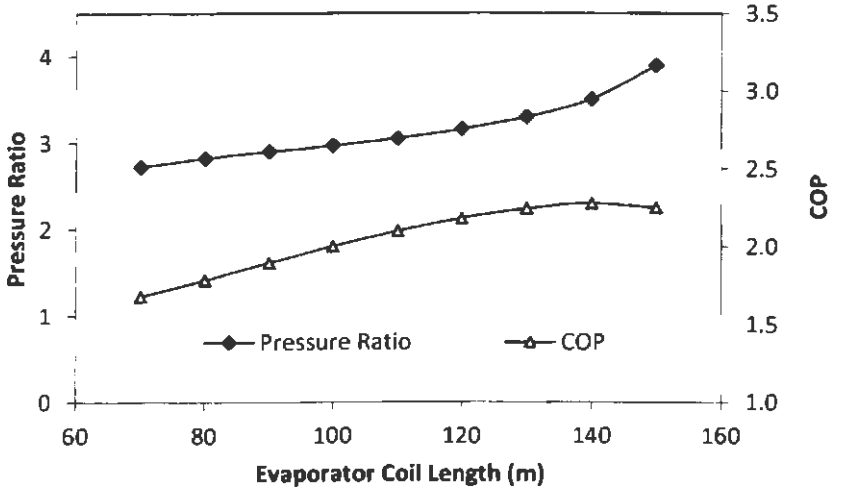

Figure 33. Effect of evaporator length on COP and P_2/P_1

Also of interest is the interaction between total GHX length and number of circuits. To analyze this connection, the number of evaporator circuits was varied while maintaining a total evaporator length of 480m. As illustrated in Figure 34, both heating capacity and COP reach a maximum value for a system with six circuits, after which both values gradually decrease. Hence, the simulation reveals that for constant total evaporator length there exists an optimum number of coils for which both COP and heating capacity are maximized.

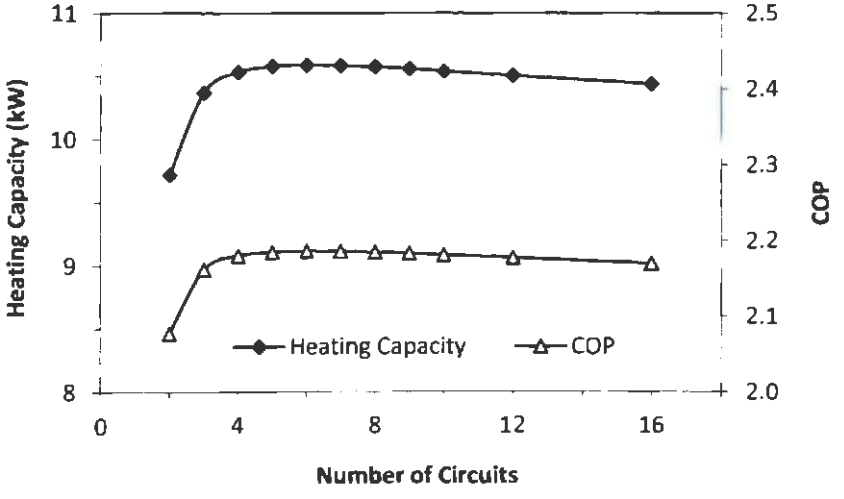

Figure 34. Variation of heating capacity and COP versus number of evaporator circuits for constant total evaporator length (L= 480 m)

It is believed that the trend in heating capacity is due to the combined effects of pressure drop and mass flow rate through the evaporator. As the number of circuits increases (and circuit length decreases), pressure drop across the evaporator is reduced. This decreases the average temperature in the evaporator, which results in an increased heat transfer rate because $T_{soil} - T_{ev}$ is greater. Meanwhile, the trend in mass flow rate produces a counter effect. The total mass flow is nearly constant, but

as the number of circuits increases mass flow in each circuit decreases. This leads to a decrease in turbulence and hence heat transfer rate. Since $\dot{W}_{comp}$ remains nearly constant during the trials, COP is essentially a function of heating capacity only. This explains why the trends are similarly aligned.

5.7. Mean Evaporation Temperature

As mentioned in the previous section, the rate at which the GHX absorbs heat from the surrounding soil is partially dependant on the difference between the soil temperature (T_{soil}) and the temperature of CO_2 in the evaporator coil. Since CO_2 temperature varies through the evaporator, the mean evaporation temperature is utilized to determine the overall heat transfer rate of the GHX. Mean evaporation temperature ($\bar{T}_{ev}$) is defined by,

$$\bar{T}_{ev} = \frac{\left(T_{inlet} + T_{sat,P_{outlet}}\right)}{2} \tag{62}$$

where T_{inlet} is the evaporator inlet temperature and $T_{sat,P_{outlet}}$ is the saturation temperature at the evaporator outlet pressure. The impacts of T_{soil} - $\bar{T}_{ev}$ were analyzed by varying $\bar{T}_{ev}$ from 264.6 to 270.7 K while T_{soil} is constant at 279.2K. As discussed previously, the soil temperature corresponds with the winter average at 2m depth for Fargo, ND.

Figure 35 shows the variation in heating capacity and COP plotted in terms of T_{soil} - $\bar{T}_{ev}$. It can be observed that as the temperature difference (ΔT) increases, the heating capacity increases. This is due to the increased heat transfer rate between the soil and CO_2. Similarly, as ΔT increases, the COP improves up to an optimum ΔT =14K above which the COP begins to decline. This is caused by a substantial increase in

pressure ratio and hence $\dot{W}_{comp}$ when ΔT is greater than the optimum. From the simulation results it can be concluded that the mean evaporation temperature should be optimized for the surrounding soil temperature.

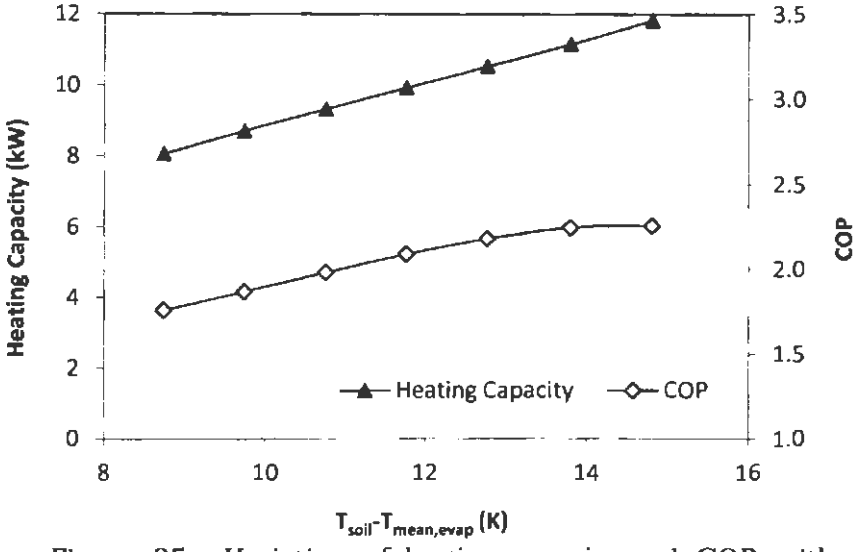

Figure 35. Variation of heating capacity and COP with change in $\bar{T}_{ev}$ for T_{soil} = 279.2K; plotted in terms of T_{soil} - $\bar{T}_{ev}$

5.8. Soil Temperature Variation

Temperatures in the soil surrounding a GHX decrease gradually over the course of a heating season. Given the results of the previous section, it is clear that this temperature decline will adversely impact CGHP performance if evaporator parameters are held constant. This occurs because as T_{soil} decreases, the optimum mean evaporation temperature also decreases.

The importance of optimizing $\bar{T}_{ev}$ with soil temperature can be better understood by observing Figure 36. The figure shows the impact of seasonal soil temperature variation for two operating schemes: (i) $\bar{T}_{ev}$ is constant; (ii) $\bar{T}_{ev}$ adjusted such that T_{soil} - $\bar{T}_{ev}$ is constant. Operating under the former constraint, both heating

capacity and COP decrease as soil temperature decreases. In the latter case, as T_{soil} decreases, heating capacity decreases only slightly while COP actually increases slightly.

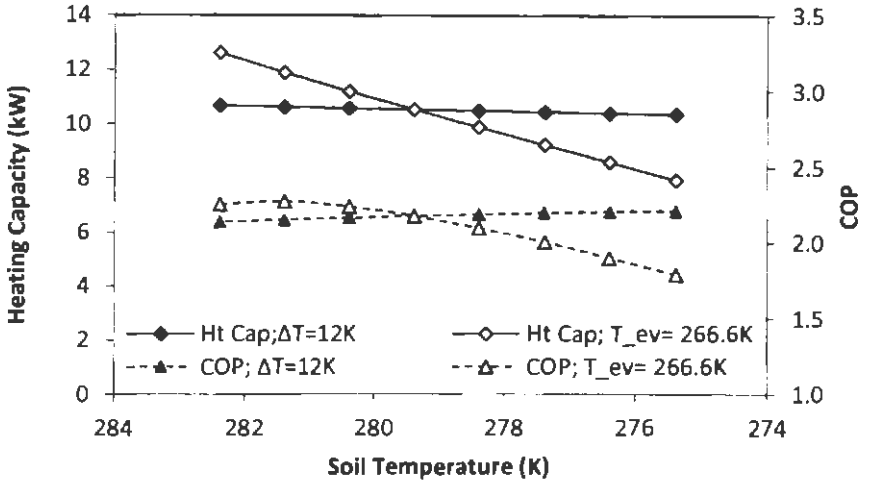

Figure 36. Impact of soil temperature on heating capacity and COP for: (i) $\bar{T}_{ev}$=constant; (ii) T_{soil} - $\bar{T}_{ev}$=constant

The COP increases only 3% as soil temperature decreases from 282.4 K to 275.4 K, but this trend is somewhat counter-intuitive. The effect can be explained by a decrease in CO_2 vapor density as the evaporator outlet temperature decreases. This reduced density at the compressor inlet results in a lower mass flow rate, and correspondingly, lower power required by the compressor. The end result is a slight improvement in COP as T_{soil} decreases.

From this simulation it is clear that to maintain the performance over the heating season, mean evaporation temperature must be adjusted (decreased) in correspondence with soil temperature. This result is in agreement with the findings

of Goulburn and Fearon [86] as mentioned in Section 2.9. The goal is to maintain operation at the optimum mean evaporation temperature.

5.9. Degree of Superheat

The effect of the degree of superheat was also numerically simulated. While some superheat is desirable in order to ensure no vapor reaches the compressor, it is worthwhile to investigate the impact of excessive superheat. The simulation was performed for T_{sup} ranging from 1 to 7K while $\tilde{T}_{ev}$ was constant at 266.6K. As can be observed in Figure 37, T_{sup} does not have a significant impact on CGHP performance; however, close inspection reveals that as T_{sup} increases, the heating capacity does decrease slightly, while COP increases marginally.

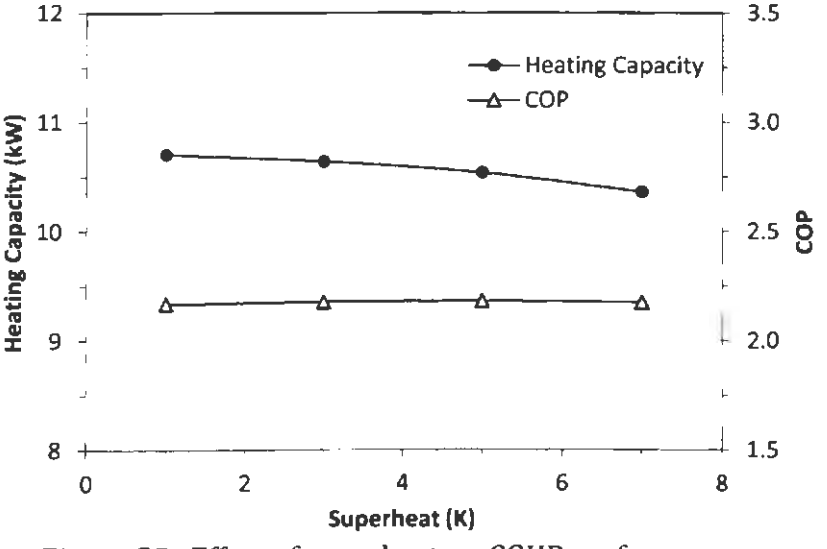

Figure 37. Effect of superheat on CGHP performance

5.10. Balancing Evaporator and Gas Cooler Capacity

The results of Section 5.6 indicate that the system COP is adversely impacted by a poor match between the evaporator and gas cooler capacities. This portion of the study looks more closely at this phenomenon. The respective heat exchanger

capacities were analyzed by varying their length, which roughly captures the effect of increasing or decreasing the capacity. The simulation was performed for evaporator coil lengths ranging from 80 to 160m. For each evaporator length the gas cooler length was varied through an appropriate range.

The simulation results reveal that gas cooler length has little effect on CGHP heating capacity but that the COP is significantly impacted. Figure 38 shows COP versus gas cooler length for each of the evaporator lengths tested. It can be observed that for each evaporator length there is an optimal gas cooler length which provides the greatest COP. Furthermore, as the evaporator length increases the optimal gas cooler length also increases. Thus it can be said that the heat exchanger capacities should be properly balanced. It is noteworthy that COP decreases sharply for gas cooler lengths below the optimum, whereas the decrease is gradual for lengths greater than the optimum. This reveals that an undersized gas cooler is more detrimental to performance than an oversized unit.

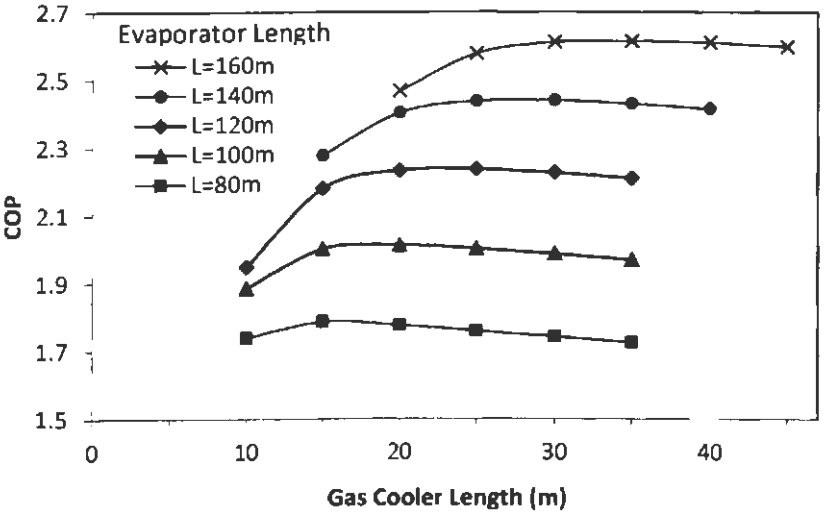

Figure 38. COP versus gas cooler length for various evaporator coil lengths

5.11. Effect of Water Flow Rate

Figure 39 shows the impact of changing water flow rate on heating capacity, compressor power and COP. As flow rate is varied from 2.4 to 5.4 liter/min, both heating capacity and compressor power decrease. The decline in power is due to a decrease in pressure ratio from 4.6 to 2.8 over the range. Pressure ratio effects power directly, but also indirectly due to the increase in compression efficiencies. The change of heat extraction is marginal (>50W) so the decrease in heating capacity can be attributed almost completely to the change in power. However, it can be observed that the change in power larger in magnitude than the capacity change. The difference results from compressor inefficiencies. The COP increases over the range as a net effect of the power and capacity variation.

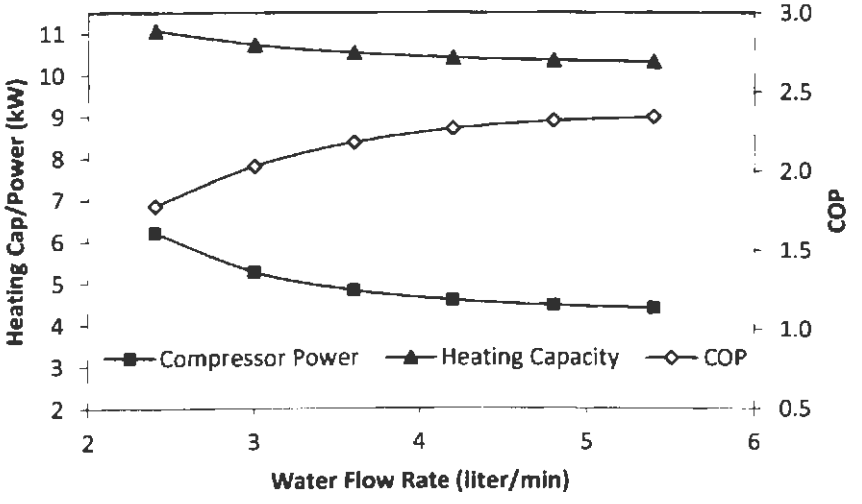

Figure 39. Effect of water flow rate on heating capacity, COP and compressor power

5.12. Approach Temperature Difference

The difference between the fluid temperatures at the outlet of a heat exchanger is known as the approach temperature difference (ΔT_{app}). In a counter-

flow heat exchanger there are two conditions of interest: the hot-side ΔT_{app} and the cold-side ΔT_{app}.

The approach temperature difference is an indicator of the heat exchanger performance and can provide insights into the gas cooler operation. In the case of the gas cooler it is desirable to have a small approach temperature difference on both hot and cold sides. On the hot side, minimizing ΔT_{app} results in a greater water output temperature. On the cold side, a small ΔT_{app} leads to a lower gas cooler outlet temperature, which, as discussed in Section 2.5, improves COP.

Two system parameters were analyzed with respect to the gas cooler's approach temperature difference: gas cooler length and water flow rate. Figure 40 shows the effect of gas cooler length on both hot-side and cold-side ΔT_{app}. As can be observed, the gas cooler length has a much greater impact on the hot-side ΔT_{app} which decreases from 62 to 33K as length increases from 10 to 35 m. Cold-side ΔT_{app} also decreases, but the change is much smaller.

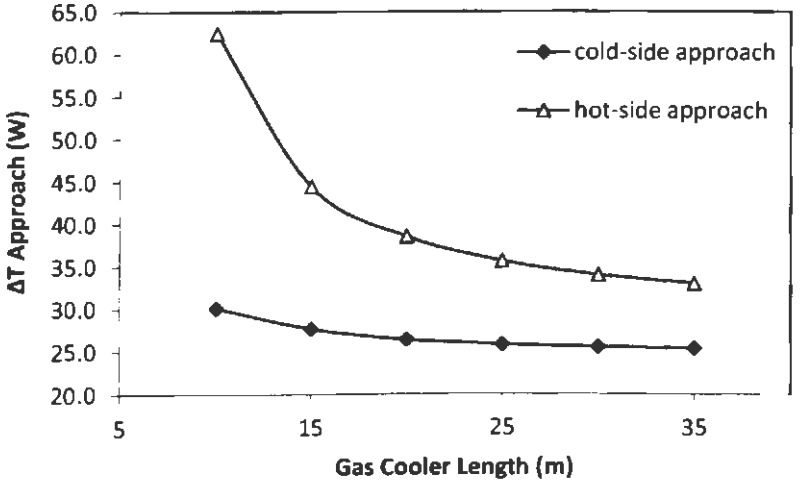

Figure 40. Effect of gas cooler length on hot-side and cold-side approach temperature difference

The impact of water flow rate on hot and cold side ΔT_{app} is shown in Figure 41. As flow rate increases from 2.4 to 3 liter/min there is a significant decrease in hot-side ΔT_{app}; however, the change then levels out and beyond 4.2 liter/min the approach temperature difference actually increases. On the cold end of the heat exchanger, ΔT_{app} increases slightly from 2.4 to 3 liter/min and then gradually decreases from 29.5 to 24.9K as flow rate is further increased.

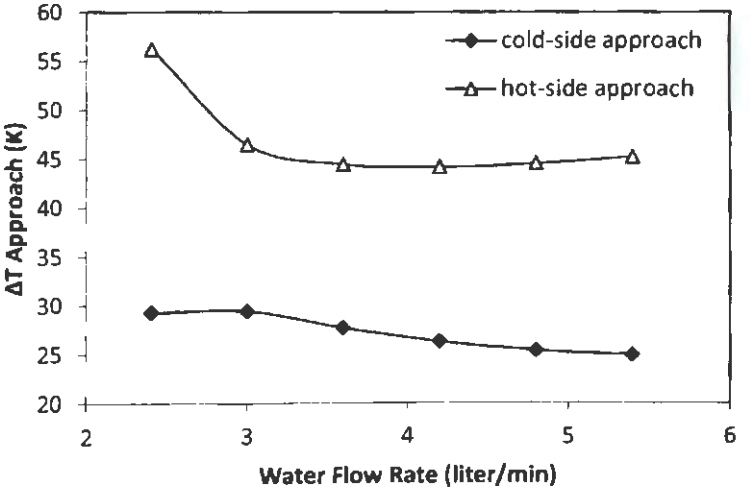

Figure 41. Effect of water flow rate on hot-side and cold-side approach temperature difference

5.13. Performance of Optimized System

Using the knowledge gained from the parametric study, the model was used to simulate the performance of an optimized CGHP system. The following parameters were optimized: gas cooler length, mean evaporation temperature, superheat, number/length of evaporator circuits with respect to the parameters tested. Other parameters including the total GHX length remained at baseline values. Table 3 shows the optimized and system parameters with the baseline values provided for

reference. The heating capacity of the optimized CGHP increased 17% to 12.3kW. The COP was 2.58, an 18% improvement over the baseline.

Table 3. Optimized system parameters (changes shown bold, baseline in parenthesis)

Evaporator		**Gas Cooler**	
Inner diameter	9.5 mm	Inner-tube inner diameter	5 mm
Outer diameter	11.5mm	Inner-tube outer diameter	7 mm
Number of circuits	**6** (4)	Outer-tube inner diameter	16 mm
Circuit length	**80m** (120m)	**Length**	**30 m** (15m)
Soil temperature	279.2 K	Water inlet temperature	280 K
Soil thermal conductivity	1 W/ m·K	Water mass flow rate	3.6 kg/min
Superheat	**2 K** (5 K)	**Compressor**	
$\overline{T}_{ev}$-T_{soil}	**16 K** (13K)	Swept volume	19.72 cm^3
		Speed	3000 rpm

5.14. Performance Comparison

It is of interest to compare the performance of a DX-GHP using CO_2 to that of a similarly sized system using a different refrigerant. With this goal in mind, the simulation model was used to predict the performance of a CGHP under the conditions tested in an experimental study reported by Minea [85]. The experimental DX-GHP used R-410A in a large greenhouse heating system. The ground heat exchanger consisted of 14 horizontal circuits, each 120 m long. Some of the experimental parameters were unknown; hence, the experimental and simulated

systems are not perfectly analogous. Some estimation, for instance, was required in the case of the compressor size and gas cooler size.

Given these uncertainties and the assumptions that go into the model, the results of the comparison should be viewed with some caution. Still, the simulation provides a rough benchmark for comparison purposes.

The simulation results show that under similar conditions the CO_2 system performed with reasonable COP but lower than the R-410A system. The COP results are shown in Table 4. The table also shows the normalized heat extraction rate and heating capacity (heat per meter of ground coil length). As can be seen, CO_2 actually had higher extraction and delivery rates. The comparison indicates that with optimization CO_2 may be used in DX-GHP systems with similar performance to that of other refrigerants.

Table 4. DX-GHP performance comparison CO_2 vs. R-410A

	CO_2- simulation [106]	**R-410A - Minea [85]**
COP	2.42	3.07
Heat extraction / meter of GHX length	16.5 W/m	14.4 W/m
Heat capacity /meter of GHX length	22.4 W/m	21.7 W/m

5.15. Monthly Performance Variation

Since the soil temperatures vary throughout the year, the system performance will vary as well. In the case of space heating, clearly one is only interested in the soil temps during the heating season, but for tap water heating the system will be used all year. The simulation was performed using the optimized parameters defined in

Section 5.13 and the average soil temperatures for each month of the year, which are given in Table 5.

Table 5. Monthly average soil temperatures for Fargo, ND

Jan	Feb	Mar	Apr	May	Jun	Jul	Aug	Sep	Oct	Nov	Dec
6.2°C	5.0°	4.3°	4.2°	5.8°	7.9°	10.2°	12.2°	13.2°	12.6°	11.2°	8.8°

Monthly COP is shown in Figure 42. COP is greatest in the months with the lowest temperatures, which agrees with the results of Section 5.8. To reiterate, the reason COP is greater at lower soil temperatures is due to the decreased CO_2 density at the compressor-inlet, which decreases $\dot{m}_c$ and hence compressor work.

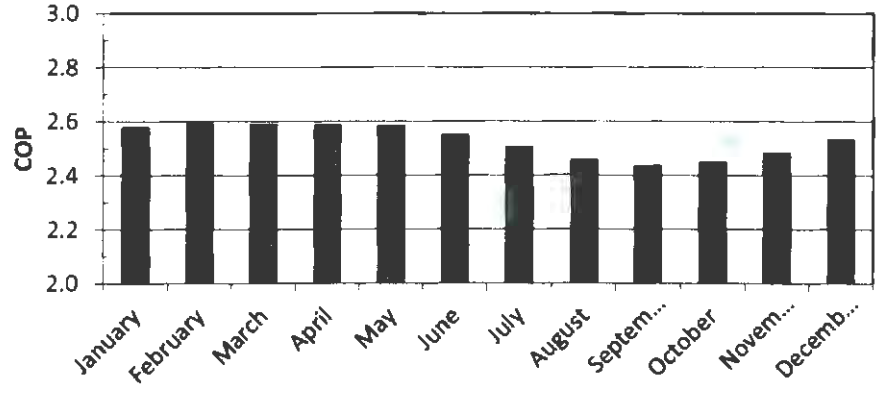

Figure 42. Monthly system COP based on average soil temperatures at 2 m depth for Fargo, ND

Heating capacity shows the opposite trend, with the greatest values in the months with highest soil temperatures (Figure 43). It is important to note that the peak heating capacity occurs in September/October due to the time lag between maximum ambient temperatures and maximum soil temperatures.

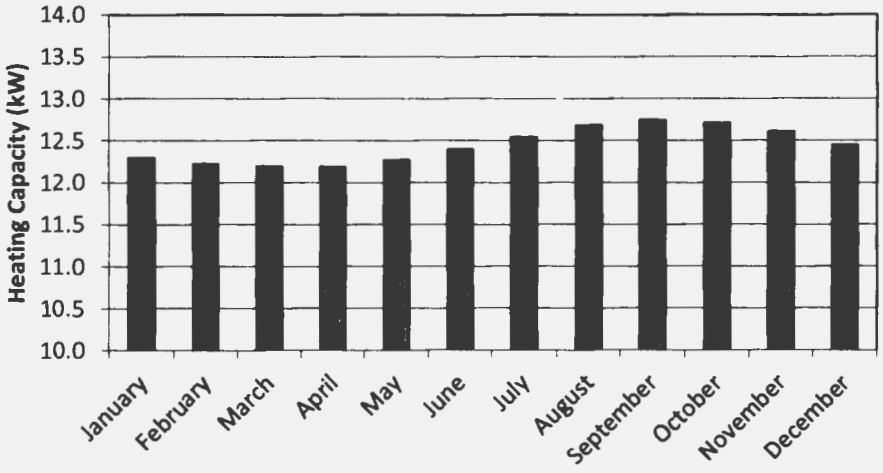

Figure 43. Monthly heating capacity based on average soil temperatures at 2 m depth for Fargo, ND

5.16. Water Outlet Temperature

To this point, system output has focused on the heating capacity without discussion of water delivery temperature. Since the gas cooler is assumed to be adiabatic with the surroundings, the rate at which energy is absorbed by the water is equal to the heating capacity. Furthermore, since water inlet temperature and flow rate were maintained during all simulations, the water outlet temperature is simply a function of the heating capacity and trends in $T_{w,e}$ and $\dot{Q}_o$ will be similar. Still, it is of value to investigate the trends in $T_{w,e}$ since various applications require different temperatures.

The most practical options for managing the water temperature are to adjust the compressor speed or the water flow rate. In the latter case, adjustment could be made by means of a thermostatically controlled valve that meters the flow of water based on outlet temperature. To analyze these methods of temperature control, the data from the previous parametric studies is revisited.

Figure 44 shows how changing water flow rate changes the delivered hot water temperature. As expected, $T_{w,e}$ decreases. The change is non-linear because the heating capacity is also decreasing non-linearly with the change of flow rate.

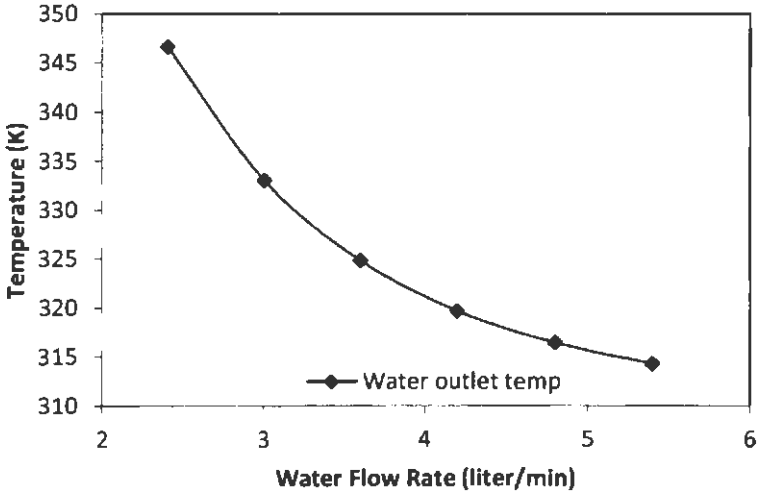

Figure 44. Variation of water outlet temperature with respect to water flow rate

Figure 45 shows the trend in $T_{w,e}$ as compressor speed is varied. Similar to the trend in heating capacity shown in Figure 30, the water outlet temperature increases roughly linearly with increasing RPM.

Both methods of control produced roughly the same change in water delivery temperature over the ranges simulated, but effects on COP are different. With compressor speed control, a 31 K temperature increase led to a 54% reduction in COP. When controlling water flow, a 32 K gain resulted in a 24% penalty in COP. It can be concluded that adjusting water-flow is a superior method of controlling water delivery temperature.

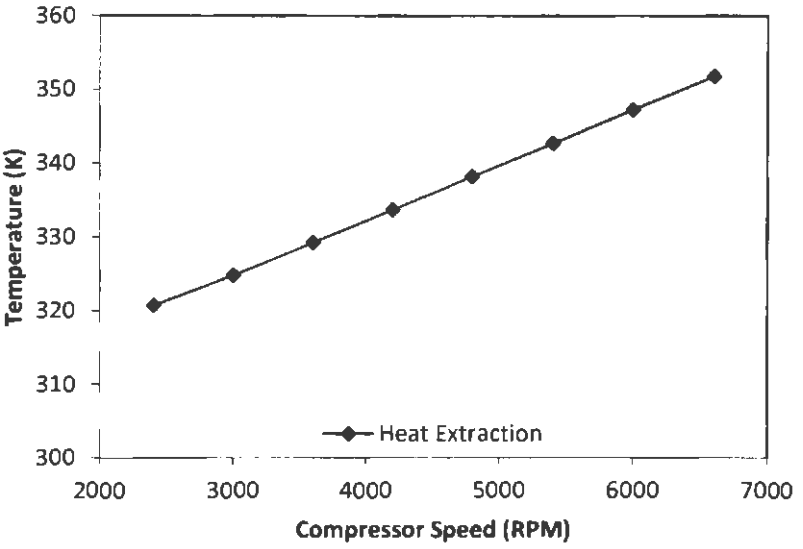

Figure 45. Variation of water outlet temperature with respect to compressor speed

Without implementing a method of control, the water delivery temperature will vary annually as the soil temperature changes. Figure 46 shows the monthly variation in $T_{w,e}$. As expected, the temperatures reflect the same trends as heating capacity (Figure 43).

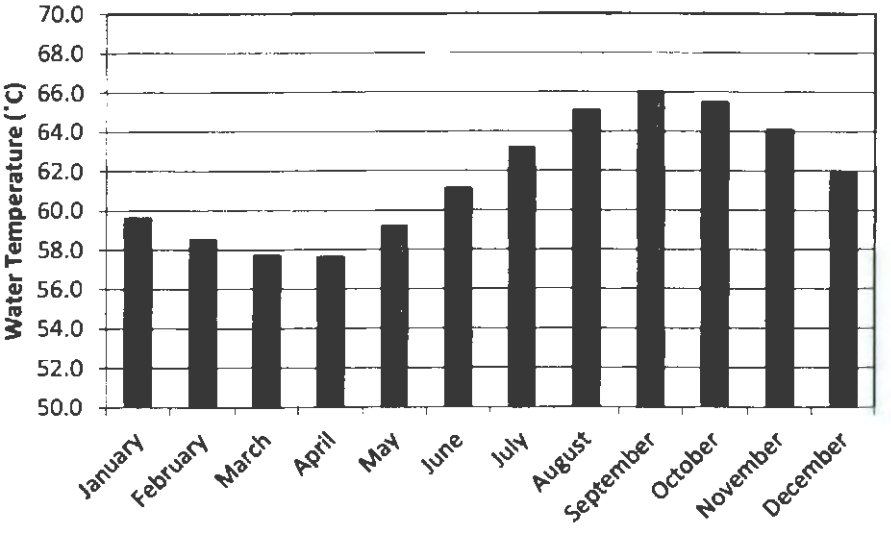

Figure 46. Monthly hot water delivery temperatures

6. CONCLUSIONS & FUTURE RESEARCH

This study has focused on the performance of a direct-expansion transcritical CO_2 geothermal heat pump used for water heating. The analysis has been carried out through use of a numerical model which was developed to simulate the steady state operation of the system. Predictions obtained from the gas cooler and heat exchanger portions of the model were compared to experimental results of previous studies [22,48,71] with reasonable agreement. This indicates the simulation can provide a reasonable representation of the actual system.

Using the simulation model, the study investigated the impacts of various design and operating parameters on overall system performance. The simulation has revealed several key design and operating characteristics of a CGHP system:

1. As the total length of the ground heat exchanger (evaporator) increases, the heating capacity increases and the COP increases to a certain length, but if the total length is fixed, there exists an optimum number of evaporator circuits with respect to both COP and heating capacity.

2. Mean evaporation temperature is important to optimizing system performance. The optimum value is dependent on the temperature of the surrounding soil and optimum $\bar{T}_{ev}$ will decreases as soil temperature decreases.

3. The relationship between gas cooler and evaporator capacities has significant effect on system performance of a CGHP. COP is maximized when the two heat exchangers are properly matched. System COP is significantly reduced by a gas cooler which is undersized with respect to the evaporator capacity, while an oversized condition is less detrimental

4. Water delivery temperature can be controlled by adjusting the water flow rate or the compressor speed but water flow rate control is superior since it has less impact on system COP.

In addition, the simulation results provide other insights regarding CGHP operation and the applicability of CO_2 in this application:

1. It was observed that the evaporative pressure drop of CO_2 is smaller than that of R134a, resulting in a smaller change in evaporation temperature.

2. Hot-side approach temperature difference is consistently and significantly larger than that of the cold-side. Furthermore, increasing the gas cooler length has a much larger effect on reducing the hot-side approach temperature difference.

The findings of the parametric study were then used to design an optimized CGHP. Simulation results for this system showed that COP and heating capacity improved 18% and 17% respectively over the baseline system.

The model was also used to compare the performance of CO_2 in a DX-GHP to that of an R410A system under the same conditions. The CO_2 system achieved greater heat extraction and delivery rates (normalized) compared to the R410A system, but CO_2's COP was lower. The CO_2 and R410A COP values were 2.42 and 3.07 respectively.

Finally, the monthly variation in performance due to the cyclic change in soil temperature was studied. The heating capacity ranged from a low of 12.2kW in April to 12.7kW in September. With constant water flow rate and no control on the outlet temperature, water delivery temperatures reflected the same trends as the heating capacity. The delivery temperatures ranged from 57.6 to 66.0°C.

6.1. Future Research

To improve the feasibility of a direct expansion CO_2 geothermal heat pump, more thorough studies must be conducted. Possible future studies include:

- Theoretical studies which analyze system modifications may indicate the benefit of additional components. In particular a suction line heat exchanger may be of benefit in this application. As discussed in the Literature Review, an SLHX reduces vapor quality at the evaporator inlet and superheats the vapor prior to compression. This allows evaporation to take place over the maximum length of the ground heat exchanger coils.
- The technical feasibility of the direct expansion transcritical CO_2 geothermal heat pump simulated in this study should be confirmed by experimentation. The experimental study is useful for validation of the theoretical results as well as to shed light on practical issues not captured in the simulation.
- An economic investigation of the equipment, installation and operating costs of a CGHP should be done in order to quantify the economic feasibility of this type of system.
- This study has focused on heating applications only. Many geothermal heat pumps use a reversing valve to operate the system in cooling mode, with the ground heat exchanger rejecting heat to the ground. The transcritical operation of a CGHP complicates this type of reversible operation, but research should be conducted analyzing this possibility.
- There is a potential for a reduction in the hot and cold-side approach temperature difference values in the gas cooler. Theoretical and experimental studies targeting

this goal could potentially lead to improved system performance and increased water outlet temperature. Studies may look at new gas cooler designs or implementation of existing designs in this new application.

REFERENCES

[1] U.S. Environmental Protection Agency. (2010) "High GWP gases and climate change." [Online]. http://www.epa.gov/highgwp/scientific.html

[2] "Directive 2006/40/EC of the European Parliament and of the Council of 17 May 2006 relating to emissions from air-conditioning systems in motor vehicles and amending Council Directive 70/156/EEC." Official Journal of the European Union 161 (June 14, 2006).

[3] Legislation Summaries. (September 25, 2007). "Emissions from air conditioning systems in motor vehicles." [Online] http://europa.eu/legislation_summaries/internal_market/single_market_for_goods/motor_vehicles/interactions_industry_policies/l24280_en.htm

[4] Lorentzen, G. "Trans-critical vapour compression cycle device." (1990) Patent WO/07683.

[5] IEA Heat Pump Centre Newsletter. "EcoCute tops one million units." 13 (2007).

[6] R744.com (November 26, 2009). "EcoCute shipments exceed 2 million landmark." [Online]. http://www.r744.com/articles/2009-11-26-eco-cute-shipments-exceed-2-million-landmark.php

[7] Hepbasli, A, and Y Kalinci. "A review of heat pump water heating systems." Renewable and Sustainable Energy Reviews 13 (2009): 1211-1229.

[8] American Society of Mechanical Engineers. (May 8, 1980). "The Equitable Building Heat Pump System Dedication Ceremony Program." [Online]. http://files.asme.org/ASMEORG/Communities/History/Landmarks/5541.pdf

[9] Sonntag, R.E., C. Borgnakke, G.J. Van Wylen. "Fundamentals of Thermodynamics, 6th ed." John Wiley & Sons Inc; Hoboken, NJ (2003).

[10] Lemmon E.W, Huber M.L, McLinden M.O. "NIST Standard Reference Database 23, Reference Fluid Thermodynamic and Transport Properties (REFPROP), Version 8.0." National Institute of Standards and Technology (2007).

[11] Pearson, A. "Carbon dioxide - new uses for an old refrigerant." International Journal of Refrigeration 28 (2005): 1140-1148.

[12] Calm, J.M. "The next generation of refrigerants - Historical review, considerations, and outlook." International Journal of Refrigeration 31 (2008): 1123-1133.

[13] Lorentzen, G., and J. Pettersen. "A new, efficient and environmentally benign system for car air-conditioning." International Journal of Refrigeration 16 (1993): 4-12.

[14] Pettersen, J. "An efficient new automobile air conditioning system based on carbon dioxide vapor compression." ASHRAE Transactions 100 (1994): 657-665.

[15] BeyondHFCs. (March 20, 2010). "BeyondHFCs position paper on CO2 vending machines." [Online]. http://www.beyondhfcs.org/search.result.php?Keyword=BeyondHFCs+position+paper+on+CO2+vending+machines

[16] Neksa, P. "CO2 heat pump systems." International Journal of Refrigeration 25 (2002): 421-427.

[17] U.S. Secretary of Commerce. (2008). "Thermophysical Properties of Fluid Systems." [Online]. http://webbook.nist.gov/chemistry/fluid

[18] Kim, M. H., J. Pettersen, and C. W. Bullard. "Fundamental process and system design issues in CO2 vapor compression systems." Progress in Energy and Combustion Science 30 (2004): 119-174 .

[19] Pettersen, J. Flow vaporization of CO_2 in microchannel tubes. PhD Thesis, Norwegian University of Science and Technology, Norway (2002).

[20] Pettersen, J., A. Hafner, and G. Skaugen. "Development of compact heat exchangers for CO2 air-conditioning systems." International Journal of Refrigeration 21 (1998): 180-193.

[21] Yang, Junlan, Yitai Ma, Shengchun Liu, and Xianyang Zeng. "Comparison investigation on the heat transfer characteristics for supercritical CO2 fluid and conventional refrigerants." 7th IIR Gustav Lorentzen Conference on Natural Working Fluids. Trondheim, Norway. (2006).

[22] Oh, H.K., C.H. Son. "New correlation to predict the heat transfer coefficient in-tube cooling of supercritical CO_2 in horizontal tubes." Experimental Thermal and Fluid Science, 34 (2010): 1230-1241.

[23] Sarkar, J., S. Bhattacharyya, and M.R. Gopal. "Simulation of a transcritical CO2 heat pump cycle for simultaneous cooling and heating applications." International Journal of Refrigeration 29 (2006): 735-743.

[24] Kauf, F. "Determination of the optimum high pressure for transcritical CO2-refrigeration cycles." International Journal of Thermal Sciences 38 (1999): 325-330.

[25] Liao, S.M., T.S.Zhao, and A. Jakobsen. "A correlation of optimal heat rejection pressures in transcritical carbon dioxide cycles." Applied Thermal Engineering 20 (2000): 831-841.

[26] Zhang, X.P., X.W. Fan, F.K. Wang, and H.G.Shen. "Theoretical and experimental studies on optimum heat rejection pressure for a CO2 heat pump system." Applied Thermal Engineering 30 (2010)2537-2544.

[27] Taira, S. "The Development of Heat Pump Water Heaters Using CO2 Refrigerant." Daikin Industries Ltd Japan (No Date).

[28] White, S.D., M.G.Yarrall, D.J. Cleland, and R.A. Hedley. "Modeling the performance of a transcritical CO2 heat pump for high temperature heating." International Journal of Refrigeration 25 (2002): 479-486.

[29] Neksa, P., H. Rekstad, G.R. Zakeri, and P.A. Schiefloe. "CO2 heat pump water heater: characteristics, system design and experimental results." International Journal of Refrigeration 21 (1998): 172-179.

[30] Anstett, P. "Measurement of the performance of an air/water heat pump using CO2 or R744 for the production of hot water for use in a hospital." IEA Heat Pump Centre Newsletter 24 (2006): 35-38.

[31] Sarkar, J., S. Bhattacharyya, and M.R. Gopal. "Natural refrigerant-based subcritical and transcritical cycles for high temperature heating." International Journal of Refrigeration 30 (2007): 3-10.

[32] Hihara, E. "Performance test of a carbon dioxide heat pump for combined domestic hot water and floor heating." IEA Heat Pump Centre Newsletter 24 (2006): 21-23.

[33] Laipradit, P., J. Tiansuwan, T. Kiatsiriroat, and L. Aye. "Theoretical performance analysis of heat pump water heaters using carbon dioxide as refrigerant." International Journal of Energy Research 32 (2007): 356-366.

[34] Fernandez, N., Y Hwang, and R. Radermacher. "Comparison of CO2 heat pump water heater performance with baseline cycle and two high COP cycles." International Journal of Refrigeration 33 (2010): 635-644.

[35] Cecchinato, L., M. Corradi, E. Fornasieri, and L. Zamboni. "Carbon dioxide as refrigerant for tap water heat pumps: a comparison with the traditional solution." International Journal of Refrigeration 28 (2005): 1250-1258.

[36] Stene, Jorn. "Residential CO2 heat pump system for combined space heating and hot water heating." Int. Journal of Refrigeration 28 (2005): 1259–1265.

[37] Byrne, P., J. Miriel, and Y. Lenat. "Design and simulation of a heat pump for simultaneous heating and cooling using HFC or CO2 as a working fluid." International Journal of Refrigeration 32 (2009): 1711-1723.

[38] Cho, H., C. Ryu, Y. Kim, and H.Y. Kim. "Effects of refrigerant charge amount on the performance of a transcritical CO2 heat pump." International Journal of Refrigeration 28 (2005): 1266-1273.

[39] Robinson, D.M., and E.A. Groll. "Efficiencies of transcritical CO2 cycles with and without an expansion turbine." International Journal of Refrigeration 21 (1998): 577-589.

[40] Kim, S.G., Y.J. Kim, G. Lee, and M.S. Kim. "The performance of a transcritical CO2 cycle with an internal heat exchanger for hot water heating." International Journal of Refrigeration 28 (2005): 1064-1072.

[41] Chen, Y., and J. Gu. "The optimum high pressure for CO2 transcritical refrigeration systems with internal heat exchangers." International Journal of Refrigeration 28 (2005): 1238-1249.

[42] Tamura, T., Y. Yakumaru, and F. Nishiwaki. "Experimental study on automotive cooling and heating air conditioning system using CO2 as a refrigerant." International Journal of Refrigeration 28 (2005): 1302-1307.

[43] Richter, M.R., S.M. Song, J.M. Yin, M.H.Kim, C.W. Bullard, and P.S. Hrnjak. "Experimental results of transcritical CO2 heat pump for residential application." Energy 28 (2003): 1005-1019.

[44] Krasnoshchekov, E.A., I.V. Kuraeva, and V.S. Protopopov. "Local heat transfer of carbon dioxide at supercritical pressure under cooling conditions." Translated from: Teplofizika Vysokikh Temperatur 7 (1970): 856-862.

[45] Baskov, V.L., I.V. Kuraeva, and V.S. Protopopov. "Heat transfer with turbulent flow of a liquid at supercritical pressures in tubes under cooling conditions." Translated from: Teplofizika Vysokikh Temperatur 15 (1977): 81-86.

[46] Petrov, N.E., and V.N. Popov. "Heat transfer and resistance of carbon dioxide being cooled in the supercritical region." Thermal Engineering 32(1985): 131-134.

[47] Petukhov, B.S., and V.N. Popov. "Theoretical calculation of heat exchange and frictional resistance in turbulent flow in tubes of an incompressible fluid with thermophysical properties." High Temperature I (1963): 69-83.

[48] Yoon, S.H., J.H. Kim, Y.W. Hwang, M.S. Kim, K. Min, and Y. Kim. "Heat transfer and pressure drop characteristics during the in-tube cooling process of carbon dioxide in the supercritical region." International Journal of Refrigeration 26 (2003): 857-864.

[49] Pitla, S.S., E.A. Groll, and S. Ramadhyani. "New correlation to predict the heat transfer coefficient during in-tube cooling of turbulent supercritical CO2." International Journal of Refrigeration 25 (2002): 887-895.

[50] Dang, C., and E. Hihara. "In-tube cooling heat transfer of supercritical carbon dioxide, Part 1. Experimental measurement." International Journal of Refrigeration 27 (2004): 736-747.

[51] Pettersen, J., R. Rieberer, and A. Leister. "Heat transfer and pressure drop characteristics of supercritical carbon dioxide in microchannel tubes under

cooling." Preliminary Proceedings of the 4th IIR-Gustav Lorentzen Conference on Natural Working Fluids. Purdue, Indiana. (2000): 99-106.

[52] Kuang, G., M.M. Ohadi, and Y. Zhao. "Experimental study on gas cooling heat transfer for supercritical CO2 in microchannels." Second International Conference on Microchannels and Minichannels. Rochester, New York. (2004): 325-332.

[53] Huai, X.L., S. Koyama, and T.S. Zhao. "An experimental study of flow and heat transfer of supercritical carbon dioxide in multi-port mini channels under cooling conditions." Chemical Engineering Science 60 (2005): 3337-3345.

[54] Huai, X.L., and S. Koyama. "Heat transfer characteristics of supercritical CO2 flow in small-channeled structure." Experimental Heat Transfer 20 (2007): 19-33.

[55] Liao, S.M., and T.S. Zhao. "Measurement of heat transfer coefficients from supercritical carbon dioxide flowing in horizontal mini/micro channels." Journal Heat Transfer 124 (2002): 413-420.

[56] Olson, D.A. "Heat transfer of supercritical carbon dioxide flowing in a cooled horizontal tube." Proceedings of 4th IIR-Gustav Lorentzen Conference on Natural Working Fluids. Purdue, Indiana. (2000): 251-258.

[57] Kuang, G., and M. Ohadi. "Semi-empirical correlation of gas cooling heat transfer of supercritical carbon dioxide in microchannels." HVAC&R Research 14 (2008): 861-870.

[58] Kim, J.H., M.S. Yoon, and Y. Kim. "An experimental investigation of heat transfer characteristics during in-tube gas cooling process of carbon dioxide." (IIF-IIR Commission B1) B6 (2001): 17-21.

[59] Dittus, F.W., Boelter, L.M.K. University of California Publications on Engineering 2 (1930): 433.

[60] Gnielinski, V. "New equations for heat and mass transfer in turbulent pipe and channel flow." International Journal of Chemical Engineering 16 (1976): 359-368.

[61] Petukhov, B.S. "Heat transfer and friction in turbulent pipe flow with variable physical properties." Advances in Heat Transfer. Academic Press, New York. (1970).

[62] Yoon, S.H., E.S. Cho, Y.W. Hwang, M.S. Kim, K. Min, and Y.Kim. "Characteristics of evaporative heat transfer and pressure drop of carbon dioxide and correlation development." International Journal of refrigeration 27 (2004): 111-119.

[63] Bredesen, A.M., A.H. Hafner, J. Pettersen, P. Neksa, and K. Aflekt. "Heat transfer and pressure drop for in-tube evaporation of CO2." IIF-IIR-Commission B1 with E1 & E2, College Park. (1997).

[64] Cho, J. M., and M.S. Kim. "Experimental studies on the evaporative heat transfer and pressure drop of CO2 in smooth and micro-fin tubes of the diameters of 5.00 and 9.52 mm." International Journal of Refrigeration 30 (2007): 986-994.

[65] Yun, R., Y. Kim, M.S. Kim, and Y. Choi. "Boiling heat transfer and dryout phenomenon of CO2 in horizontal smooth tube." International Journal of Heat and Mass Transfer 46 (2003): 2353-2361.

[66] Zhao, X., and P.K. Bansal. "Flow boiling heat transfer characteristics of CO2 at low temperatures." International Journal of Refrigeration 30 (2007): 937-945.

[67] Oh, H.K., H.G. Ku, G.S. Roh, and S.J. Park C.H. Son. "Flow boiling heat transfer characteristics of carbon dioxide in a horizontal tube." Applied Thermal Engineering 28 (2008): 1022-1030.

[68] Park, C.Y., and P.S. Hrnjak. "CO2 and R410A flow boiling heat transfer, pressure drop, and flow pattern at low temperatures in a horizontal smooth tube." International Journal of Refrigeration 30 (2007): 166-178.

[69] Wu, X.M., H.Y. Zhao, W.C. Wang, L. Jing, and L. Zhang. "Experimental study on evaporating heat transfer of CO2 in thin tube." Journal of Engineering Thermophysics 26 (2005): 823-825.

[70] Schael, A.E., and M. Kind. "Flow pattern and heat transfer characteristics during flow boiling of CO2 in a horizontal micro-fin tube and comparison with smooth tube data." International Journal of Refrigeration 28 (2005): 1186-1195.

[71] Mastrullo, R., A.W. Mauro, A. Rosato, G.P. Vanoli. "Carbon dioxide heat transfer coefficients and pressure drops during flow boiling: Assessment of predictive methods." International Journal of Refrigeration 33 (2010): 1068-1085.

[72] Cheng, L., G. Ribatski, Q. Moreno Quiben, and J.R. Thome. "New prediction methods for CO2 evaporation inside tubes: part I - a two-phase flow pattern map and a flow pattern based phenomenological model for two-phase flow frictional pressure drops." International Journal of Heat and Mass Transfer 51 (2008): 111-124.

[73] Jung, D.S., R. Radermacher. "Prediction of evaporation heat transfer coefficient and pressure drop of refrigerant mixtures in horizontal tubes." International Journal of Refrigeration. 16 (1993): 201-209.

[74] Jung, D.S., R. Radermacher, M. McLinden, D. Didion. "A study of flow boiling heat transfer with refrigerant mixtures." International Journal of Heat and Mass Transfer 32 (1989): 1751-1764.

[75] Stephan, K. & M. Abdelsalam. Heat transfer correlations for natural convection boiling. International Journal of Heat and Mass Transfer 23 (1980): 73-87.

[76] "Annual Geothermal Heat Pump Manufacturers Survey." U.S. Energy Information Administration, Form EIA-902 (December, 2010).

[77] C. H. Coogan, Jr. "Heat Transfer Rate." Mechanical Engineering 71 (1949): 495.

[78] D. M. Vestal, Jr., J. Fluker. "Earth as Heat Source and Sink for Heat Pumps." ASHVE Trans 63(1957): 41.

[79] F. C. Hooper. "An Experimental Residential Heat Pump." Canadian Journal of Technology 30 (1952): 180-97.

[80] Mei, V.C. "Horizontal Ground-Coil Heat Exchanger Theoretical and Experimental Analysis." Oak Ridge National Laboratory, Report (1986).

[81] Halozan, H., O. Svec. "Heat pump systems with direct expansion ground coils." Final Report of IEA Annex 15, Paris. 107 (1993).

[82] Halozan, H., R. Rieberer. "Direct-expansion ground-coupled heat pumps." IEA Heat Pump Centre Newsletter 23 (2005): 30-32.

[83] EarthLinked Technologies. (2011) "Frequently Asked Questions." [Online]. http://www.earthlinked.com/commercial/faq

[84] Wang, X., C. Ma, and Y. Lu. "An experimental study of a direct expansion ground-coupled heat pump system in heating mode." International Journal of Energy Research 33 (2009): 1367-1383.

[85] Minea, V. "Combined radiant floor and forced air heating with direct expansion GSHP in a northern greenhouse." International Congress of Refrigeration. Washington D.C. (2003).

[86] Goulburn, J.R., J. Fearon. "Deep ground coil evaporators for heat pumps." Applied Energy 4 (1978): 293-313.

[87] Johnson, W.S., B.A. McGraw, F. Conlin, S.D. Wix, R.N. Baugh. "Annual performance of a horizontal-coil ground-coupled heat pump." ASHRAE Transactions 92 (1986): 173-185.

[88] Johnson, W.S. "Field tests of two residential direct exchange geothermal heat pumps." ASHRAE Transactions: Part 2 108 (2002): 99-106.

[89] Prairie Energy Solutions. (2010). "Direct Expansion Heat Pumps." [Online]. http://www.pesdistributors.com/prod_detail.asp?ID=7097

[90] Dyrdahl, D. Personal interview. (February 25, 2011).

[91] North Dakota State Climate Office. (2010) "2010 Fargo Station Daily Deep Soil Temperatures." [Online]. http://www.ndsu.edu/ndsco/soil/farg/farg.htm

[92] Goulburn, J.R., J. Fearon. "Domestic heat pump with deep hole ground source evaporator." Applied Energy 14 (1983): 99-113.

[93] Demir, H., A. Koyun, G. Temir. "Heat transfer of horizontal parallel pipe ground heat exchanger and experimental verification." Applied Thermal Engineering 29 (2009): 224-233.

[94] Philippe, M., M. Bernier, D. Marchio. "Validity ranges of three analytical solutions to heat transfer in the vicinity of single boreholes." Geothermics 38 (2009): 407-413.

[95] Esen, H., M. Inalli, M. Esen. "Numerical and experimental analysis of a horizontal ground-coupled heat pump system." Building and Environment 42 (2007): 1126-1134.

[96] Pulat, E., S. Coskun, K. Unlu, N. Yamankaradeniz. "Experimental study of horizontal ground source heat pump performance for mild climate in Turkey." Energy 34 (2009): 1284-1295.

[97] Oritz, T.M., D. Li, and E.A. Groll. "Evaluation of the performance potential of CO2 as a refrigerant in air-to-air air conditioners and heat pumps: System modeling and analysis." ARTI Final Report (2003).

[98] Petukhov, B.S., Roizen, L.I. "Generalized Relationships for heat transfer in a turbulent flow of a gas in tubes of annular section." High Temperature-USSR 2(1964): 65-68.

[99] Blasius, H. Forsch. Geb. Ingenieurwes. 131 (1913).

[100] McAdams, W.H., W.K. Woods, L.C. Heroman Jr. "Vaporization inside horizontal tubes-II: Benzene-oil mixtures." ASME Transactions, 64 (1942): 193.

[101] Freund, E.A., G.S. Whitlow. "Earth Source Heat Pump: Characteristics, Design and Operation." Jor of the American Institute of Electrical Engineering (1959).

[102] Rao, S.S. "Applied Numerical Methods for Engineers and Scientists." Prentice Hall; Upper Saddle River, NJ (2002).

[103] Schmidt, W.L., W.D. Gosnold, J.W. Enz. "A decade of air-ground temperature exchange from Fargo, North Dakota." Global and Planetary Change 29 (2001): 311-325.

[104] Kasenow, M. "Applied ground-water hydrology and well hydraulics." Water Resources Publications; Highlands Ranch, Colorado (2001).

[105] North Dakota State Climate Office. (2010). "North Dakota Annual Average Temperature." [Online]. www.ndsu.edu/ndsco/temp/monthly/2010.html

[106] Austin, B.T., Sumathy, K. "Modeling a direct expansion geothermal heat pump using carbon dioxide in a transcritical cycle." Proceedings of the 2011 Renewable Energy World Conference & Expo. Tampa, Florida. (March 8-10, 2011).

Table 6. System data and experimental results from previous DX-GHP studies

Author	GHX-type/ Outer Dia	# of circuits/ length (borehole depth)	COP	Heating Capacity	Heat extraction per coil-length (per borehole-length)	Refrig.
Goulburn & Fearon [92]	Vert./ 9.5mm	16/(10m)	3.0	8 kW	(30-36 W/m)	R12
Goulburn & Fearon [86]	Hor./ 9.5mm	1/15.3m (depth=1.22m)	2.38	874 W	30 W/m	R12
Goulburn & Fearon [86]	Vert./ 9.5mm	2/(8m)	2.49-3.0	874 W	(40-50 W/m)	R12
Wang et al. [84]	Vert./8,12mm	3/(30m)	3.55	6.43 kW	(51.5 W/m)	R134a
Johnson [88]	Hor./6mm	15/30.5m (depth=1.4m)	3.6	7.6 kW	12 W/m	R22
Johnson [88]	Spiral/11mm	5/(3m)	3.0	4.7 kW	(20 W/m)	R22
Minea [85]	Hor. /9.5mm	16/120m (depth=0.9m)	3.07	35.9 kW	14.4 W/m	R410a

APPENDIX B: PROGRAM CODE

1. Program Flow

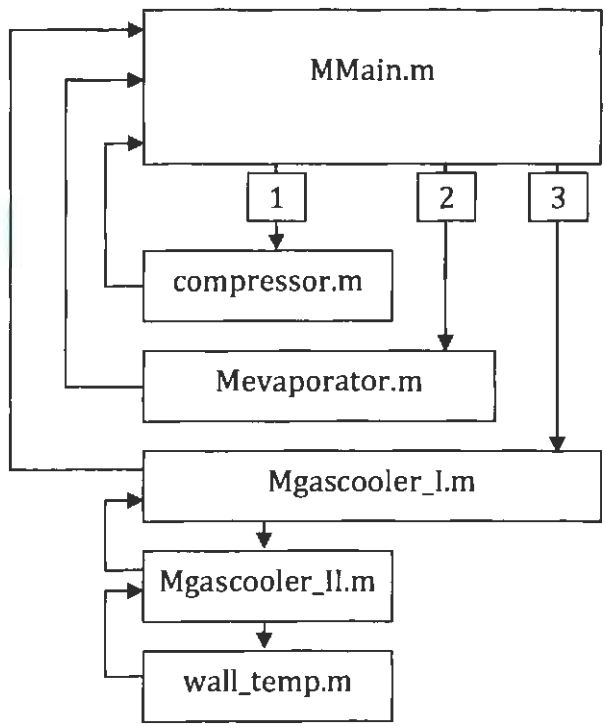

Figure 47. Flow diagram illustrating the order in which program functions are called

2. MATLAB Functions

a) Global System Model

Function Title: MMain.m

```
%This is the global model for the cycle analysis.  Program calls upon
each
%of the component-process models.  Compressor outlet pressure is updated
%using Secant Method until steady state condition is attained.


%Define Arrays
P2=zeros(3,1);
T2=zeros(3,1);
err=zeros(3,1);
T3=zeros(3,1);
h3=zeros(3,1);

%Input parameters
%-------Gas cooler parameters
    T_water_i=280.15;
    m_water=.035;
        viscosity=refpropm('V','T',T_water_i,'P',101.325,'WATER');
        Water_min_Re=m_water/(pi()*(.016^2-.007^2)/4)*(.016-
.007)/viscosity;
%-------Evaporator parameters
    Tsoil=279.39;
    minallow=8; %minimum allowable temperature difference between soil
and evaporator
    Tsup=5;

%compressor outlet pressure  this is the variable which will balance the
system
    P2(1)=12000;  %1st guess
    P2(2)=11000;  %2nd guess

        T1=Tsoil-minallow;
        P1=refpropm('P','T',(Tsoil-minallow-Tsup),'Q',1,'CO2');

%Component models run for compressor outlet pressure guess 1
[T2 m Wc]=compressor(T1,P1,P2(1));
[P4 T4 h4 x4 minRe_Evap]=Mevaporator(P1,T1,m,Tsoil);
[T3 P3 h3 Twout minRe_GC]=Mgascooler_I(T2,P2(1),m,T_water_i,m_water);
%Steady state check?
err(1)=h3-h4        %enthalpy difference between gas cooler outlet and
evaporator inlet

%Component models run for compressor outlet pressure guess 2
[T2 m Wc]=compressor(T1,P1,P2(2));
[P4 T4 h4 x4 minRe_Evap]=Mevaporator(P1,T1,m,Tsoil);
[T3 P3 h3 Twout minRe_GC]=Mgascooler_I(T2,P2(2),m,T_water_i,m_water);
%Steady state check?
```

```
err(2)=h3-h4        %enthalpy difference between gas cooler outlet and
evaporator inlet

i=2;

%secant method use to solve for discharge pressure
while abs(err(i))>.1
    i=i+1;

    P2(i)=P2(i-1)-err(i-1)*(P2(i-1)-P2(i-2))/(err(i-1)-err(i-2))

%Component models run for compressor new iteration
        [T2 m Wc]=compressor(T1,P1,P2(i));
        [P4 T4 h4 x4 minRe_Evap]=Mevaporator(P1,T1,m,Tsoil);
        [T3 P3 h3 Twout
minRe_GC]=Mgascooler_I(T2,P2(i),m,T_water_i,m_water);
  %Steady state check?
       err(i)=h3-h4    %enthalpy difference between gas cooler outlet and
evaporator inlet
end
P_2=P2(i);
%Once error is small enough in above loop and all associated functions
%the inlet and outlet states of all components are considered Ss.
%Thus the COP, work input and heating capacity can be calculated.  Also
%the outlet temperature of the water is retrieved

%Output Conditions:
P2_1=P2(i);
h1=refpropm('H','T',T1,'P',P1,'CO2');
h2=refpropm('H','T',T2,'P',P_2,'CO2');
h3=refpropm('H','T',T3,'P',P3,'CO2');
h4=h3;
CO2massflowrate=m;
Wateroutlettemperature=Twout;
Compressorwork=Wc;
COP=m*(h2-h3)/Wc;
Heatoutput=m*(h2-h3);
Heatabsorbed=m*(h1-h4);
Water_min_Re
minRe_GC
minRe_Evap
format short e
Output=[P1;P2_1;P3;P4;x4;T1;T2;T3;T4;CO2massflowrate;Wateroutlettemperatu
re;Compressorwork;COP;Heatoutput;Heatabsorbed]
format short

% Nomenclature
% err       J kg     enthalpy difference across throttle valve
% h3        J kg     gas cooler outlet enthalpy
% h4        J kg     Evap inlet enthalpy
% i                  counter
% m kg s             CO2 mass flow rate
% m_water   kg s     water mass flow rate
% minallow  K        min temp difference soil evap outlet
% minRe_Evap         minimum CO2 reynolds in Evap
```

```
% minRe_GC           minimum CO2 reynolds in gas cooler
% P1         kPa     compressor inlet pressure
% P2         kPa     compressor outlet Pressure
% P3         kPa     Gas cooler outlet press
% P4         kPa     Evap inlet press
% T_water_i K       Water inlet temp
% T1         K       compressor inlet temp
% T2         K       compressor outlet Temperature
% T3         K       gas cooler outlet temp
% T4         K       Evap inlet temp
% Tsoil      K       soil temperature
% Tsup       K       degree of superheat at evap outlet
% Twout      K       Water outlet temp
% viscosity Pa*s     water viscosity
% Water_min_Re       minimum water Reynolds #
% W          W       Compressor power
% x4                 Evap inlet quality
```

b) Compression Model

Function Title: compressor.m

```
function [T2 m Wc]=compressor(T1,P1,P2)
%calculates the ref mass flow, Compressor power, and the discharge
%temperature based on an assumed discharge pressure

%Known Parameters
N=50;
Vs=.00001972;

% -calculate efficiencies from from Pritz, Li and Stoll P. 142
n_v=0.9207-0.0756*(P2/P1)+0.0018*(P2/P1)^2; %volumetric efficiency
n_tot=-0.26+0.7952*(P2/P1)-0.2803*(P2/P1)^2+0.0414*(P2/P1)^3-
0.0022*(P2/P1)^4;    %total effic: isentropic*mechanical
n_m=0.9083-0.0884*(P2/P1)+0.0051*(P2/P1)^2;%mechanical efficiency of
compressor

[h1 s1 rho1]=refpropm('HSD','T',T1,'P',P1,'CO2'); %properties at
compressor inlet [J kg,, [J kg*K,, [kg m^3]
s2s=s1;                                  %ideal discharge entropy [J kg*K]
h2s=refpropm('H','P',P2,'S',s2s,'CO2');  %ideal discharge enthalpy [J kg]
m=n_v*rho1*Vs*N;                          mass flow [kg s]
Wc=m*(h2s-h1)/n_tot;                 %power input required by compressor [W
Loss=(1-n_m)*Wc;
h2=h1+(Wc-Loss)/m;                  %real discharge enthalpy[J kg]
T2=refpropm('T','P',P2,'H',h2,'CO2');     %discharge temp [K]
end

% Compressor Nomenclature
% T1          [K]      inlet temp
% P1          [kPa]    inlet pressure
% n_v                  volumetric efficiency
% n_tot                total efficiency
% n_m                  mechanical efficiency
% h1          [J kg]   inlet enthalpy
% s1          [J/kgK]  inlet entropy
% rho1        [kg/m^3] inlet CO2 density
% s2s         [J kgK]  discharge isentropic compression entropy
% h2s         [J kg]   discharge isentropic compression enthalpy
% Loss        [W]      Losses of compressor
% N           [Hz]     compressor speed
% Vs          [m^3]    swept volume
% P2          [kPa]    discharge pressure
% T2          [K]      discharge temp
% m           [kg s]   mass flow rate of CO2
% Wc          [W]      compressor power
% h2          [J/kg]   actual outlet enthalpy
```

c) Evaporation Model

Function Title: Mevaporator.m

```
function [P4 T4 h4 x4 minRe]=Mevaporator(P1,T1,m_tot,Tsoil)
%This model solves for the inlet conditions of the evaporator based on
the
%known conditions at the evaporator outlet and the mass flow which was
%determined by the compressor model.  Model can calculate heat transfer
%conditions for liquid, two-phase & superheated vapor conditions.

%divide total mass flow by number of circuits
m=m_tot/4;

%Evaporator dimensions
L=120;
di=.009525;
do=.011525;
N=L/.5;
ktube=400;
ksoil=1;
far_dia=2;
B=35;    %contact angle

%Calculated parameters
l=L/N;                          % segment length [m]
A_r=pi()*di*l;                  %CO2 side segment area [m^2]
G=m/((pi()/4)*di^2);             %mass velocity of CO2 [kg m^2*s]

%define arrays
T=zeros(N+1,1);      %nodal temperature array
P=zeros(N+1,1);      %nodal pressure array
Q=zeros(N,1);        %segment heat transfer
x=zeros(N+1,1);      %nodal quality
h=zeros(N+1,1);      %nodal enthalpy
alpha=zeros(N+1,1);
htcoef_tot=zeros(N,1);

P(1)=P1;
T(1)=T1;
n=1;
h(1)=refpropm('H','T',T(1),'P',P(1),'CO2');
hv=refpropm('H','T',T(1),'Q',1,'CO2');
Reynolds_min=10000000;

%___single-phase vapor flow in the evaporator_____ ___
while h(n)>=hv && n<=N
    [u den k cp]=refpropm('VDLC','T',T(n),'P',P(n),'CO2');
    Re=G*di/u;                                  %Reynolds
        if Reynolds_min>Re
            Reynolds_min=Re;
        end
    Pr=u*cp/k;              %Prandl
%Pressure drop
```

```
    fp=.0791*Re^-.25;           %pressure friction factor (Blasius)
    del_P=2*fp*l*G^2*.001/(den*di);  %pressure change (Darcy Weisbach
    P(n+1)=P(n)+del_P;                          %segment inlet pressure

%heat transfer
    f=(.79*log(Re)-1.64)^-2;    %friction factor (Petukhov's formula)
    Nu=(f/8)*(Re-1000)*Pr/(1.07+12.7*(f/8)^.5*(Pr^(2/3)-1));    %Nusselt
correlation of Gnielinski
    alpha(n)=Nu*k/di;           % 1 phase CO2 heat transfer coefficient

UA=(1/(alpha(n)*A_r)+log(do/di)/(2*pi()*l*ktube)+log(far_dia/do)/(2*pi()*
l*ksoil))^-1;
    T(n+1)=-exp(UA/cp/m)*Tsoil+exp(UA/cp/m)*T(n)+Tsoil;
    Q(n)=UA*((Tsoil-T(n+1))-(Tsoil-T(n)))/log((Tsoil-T(n+1))/(Tsoil-
T(n)));
    h(n+1)=h(n)-Q(n)/m;
    n=n+1;
    hv=refpropm('H','T',T(n),'Q',1,'CO2');
        if T(n)>Tsoil
            error('Evaporator temperature greater than soil temp')
        end
end

hl=refpropm('H','T',T(n),'Q',0,'CO2');
x(n)=(h(n)-hl)/(hv-hl);

%_____two-phase flow-boiling in the evaporator_____
 while h(n)<hv && n<=N && h(n)>hl
    [uv pv]=refpropm('VD','P',P(n),'Q',1,'CO2'); %CO2 vapor properties at
inlet pressure
    [ul pl kl cpl sften]=refpropm('VDLCI','P',P(n),'Q',0,'CO2'); %CO2
liquid properties at inlet pressure
    Re_lo=G*di/ul;
            if Reynolds_min>Re_lo
                Reynolds_min=Re_lo;
            end
    Prl=ul*cpl/kl;              %Prandl # at sat liq condition
    Xtt=((1-x(n))/x(n))^.9*(pv/pl)^.5*(ul/uv)^.1; %Lockhart-Martinelli
factor
%L-M not used in dP correlation but needed for Jung correlation

%_____2-phase pressure drop
    f_lo=.0791*Re_lo^-.25;      % Fanning friction factor correlation of
Blasius
    phi_squared=(1+(pl/pv-1)*x(n))/(1+(ul/uv-1)*x(n))^.25;  %two-phase-
multiplier of McAdams for total flow turbulent and total flow as liquid
turbulent
    del_P=2*l*f_lo*G^2*phi_squared*.001/(di*pl);
    P(n+1)=P(n)+del_P;
    [T(n+1)]=refpropm('T','P',P(n+1),'Q',1,'CO2');%Temperature at next
node

%_____2phase heat transfer coefficient
    bd=.0146*B*(2*sften/(9.81*(pl-pv)))^.5;
    Fp=2.37*(.29+1/Xtt)^.85;
```

```
    htfus=hv-hl;
    coef_l=.023*kl/di*(Re_lo*(1-x(n)))^.8*Prl^.4;

    %first iteration
    qguess(1)=100000 ;
    Boil=qguess(1)/(G*htfus);
    if Xtt<1
        NN=4048*Xtt^1.22*Boil^1.13;
    else
        NN=2-.1*(Xtt)^.28*Boil-.33;
    end

coef_sa=207*kl/bd*(qguess(1)*bd/(kl*T(n)))^.745*(pv/pl)^.581*Prl^.533;
    alpha_1(1)=NN*coef_sa+Fp*coef_l;

UA=(1/(alpha_1(1)*A_r)+log(do/di)/(2*pi()*l*ktube)+log(far_dia/do)/(2*pi(
)*l*ksoil))^-1;
    qcalc(1)=(UA*((Tsoil-T(n+1))-(Tsoil-T(n)))/log((Tsoil-T(n+1))/(Tsoil-
T(n))))/(l*di*pi());
    err(1)=qguess(1)-qcalc(1);

    %second iteration
    qguess(2)=qguess(1)-100;
    Boil=qguess(2)/(G*htfus);
    if Xtt<1
        NN=4048*Xtt^1.22*Boil^1.13;
    else
        NN=2-.1*(Xtt)^.28*Boil-.33;
    end

coef_sa=207*kl/bd*(qguess(2)*bd/(kl*T(n)))^.745*(pv/pl)^.581*Prl^.533;
    alpha_1(2)=NN*coef_sa+Fp*coef_l;

UA=(1/(alpha_1(2)*A_r)+log(do/di)/(2*pi()*l*ktube)+log(far_dia/do)/(2*pi(
)*l*ksoil))^-1;
    qcalc(2)=(UA*((Tsoil-T(n+1))-(Tsoil-T(n)))/log((Tsoil-T(n+1))/(Tsoil-
T(n))))/(l*di*pi());
    err(2)=qguess(2)-qcalc(2);

    j=2;
    %solution using secant method
    while abs(err(j))>.001
        j=j+1;
        qguess(j)=qguess(j-1)-err(j-1)*(qguess(j-1)-qguess(j-2))/(err(j-
1)-err(j-2));
        Boil=qguess(j)/(G*htfus);
        if Xtt<1
            NN=4048*Xtt^1.22*Boil^1.13;
        else
            NN=2-.1*(Xtt)^.28*Boil-.33;
        end

coef_sa=207*kl/bd*(qguess(j)*bd/(kl*T(n)))^.745*(pv/pl)^.581*Prl^.533;
        alpha_1(j)=NN*coef_sa+Fp*coef_l;
```

```
UA=(1/(alpha_1(j)*A_r)+log(do/di)/(2*pi()*l*ktube)+log(far_dia/do)/(2*pi(
)*l*ksoil))^-1;
        qcalc(j)=(UA*((Tsoil-T(n+1))-(Tsoil-T(n)))/log((Tsoil-
T(n+1))/(Tsoil-T(n))))/(l*di*pi());
        err(j)=qguess(j)-qcalc(j);
    end
    htcoef_tot(n)=UA;
    alpha(n)=alpha_1(j);
    Q(n)=A_r*qcalc(j);
    h(n+1)=h(n)-Q(n)/m;

    hv=refpropm('H','P',P(n+1),'Q',1,'CO2');
    hl=refpropm('H','P',P(n+1),'Q',0,'CO2');
    n=n+1;
    x(n)=(h(n)-hl)/(hv-hl);
            if T(n)>Tsoil
                failpressure=P(n)
                segment=n
                error('Evaporator temperature greater than soil temp')
            end
 end

x4=x(n);
%_____subcooled CO2 in the evaporator_____
while n<=N && h(n)<=hl
    [u den k cp]=refpropm('VDLC','T',T(n),'P',P(n),'CO2');

    %heat transfer
    Re=G*di/u;                              %Reynolds
        if Reynolds_min>Re
            Reynolds_min=Re;
        end
    Pr=u*cp/k;                              %Prandtl
    Nu=.023*Re^.8*Pr^.4;    %Dittus-Boelter correlation
    alpha(n)=Nu*k/di;

UA=(1/(alpha(n)*A_r)+log(do/di)/(2*pi()*l*ktube)+log(far_dia/do)/(2*pi()*
l*ksoil))^-1;    %overall ht trnsf coef * area  CO2 bulk temp to outer
tube temp.
    T(n+1)=-exp(UA/cp/m)*Tsoil+exp(UA/cp/m)*T(n)+Tsoil;
    Q(n)=UA*((Tsoil-T(n+1))-(Tsoil-T(n)))/log((Tsoil-T(n+1))/(Tsoil-
T(n)));
    h(n+1)=h(n)-Q(n)/m;
    P(n+1)=P(n);
    n=n+1;
                if T(n)>Tsoil
                    error('Evaporator temperature greater than soil
temp')
                end
end

T4=T(n);
P4=P(n);
h4=h(n);
```

```
x4=x(n);
minRe=Reynolds_min;

end

%Nomenclature
% A_r          m^2          CO2-side segment area
% alpha        W/m^2*K      CO2 convective heat transfer coefficient
% B            deg          contact angle
% bd                        Bond number
% Boil                      Boiling Number
% coef_sa      W/m^2*K      Nucleate pool boiling ht trans coef of Stephan &
Abdelsalam
% cp           J/kg*K       specific heat of CO2
% cpl          J/kg*K       specific heat of CO2 (liquid)
% del_P        kPa          pressure drop
% den          kg/m^3       density
% di           m            inner diameter of tube
% do           m            outer diameter of tube
% err          J/kg         enthalpy difference across throttle valve
% f_lo                      liquid only friction factor
% far_diameter  m           diameter of constant temp cyclindar
% fp                        friction factor
% Fp                        heat transfer enhancement factor
% G            kg/m^2*s     mass flux
% h4           J/kg         Evap inlet enthalpy
% hl           J/kg         saturated liquid enthalpy
% htcoef_tot   W/m^2*K      total ht trans coef
% hv           J/kg         saturated vapor enthalpy
% k            W/m*K        therm cond CO2
% kl           W/m*K        therm cond CO2 (liquid)
% ksoil        W/mK         therm cond. Soil
% ktube        W/mK         thermal conductivity of tube
% L            m            circuit length
% l            m            segment length
% m            kg/s         CO2 mass flow rate in each circuit
% m_tot        kg/s         total system CO2 mass flow rate
% minRe_Evap                minimum CO2 reynolds in Evap
% N                         number of segments
% n                         counter
% NN                        Nucleate boiling factor
% Nu                        Nusselt
% P1           kPa          compressor inlet pressure
% P4           kPa          Evap inlet press
% phi_squared               2-phase multiplier
% pl           kg/m^3       density (liquid)
% Pr                        Prandl
% pv           kg/m^3       density (vapor)
% Q W                       local heat transfer rate
% q_calc       W/m^2        local calculated heat flux
% Re                        Reynolds
% sften        N/m          surface tension
% T1           K            compressor inlet temp
% T4           K            Evap inlet temp
% Tsoil        K            soil temperature
```

```
% u          Pa*s        viscosity
% UA         J/K         overall ht conductance
% ul         Pa*s        viscosity (liquid
% uv         Pa*s        viscosity (vapor)
% x                      local quality
% x4                     Evap inlet quality
% Xtt                    Lockhart-martinelli factor
```

d) Gas Cooling Model: Part 1

Function Title: Mgascooler_I.m

```
function [T3 P3 h3 Twater minRe]=Mgascooler_I(T2,P2,m,T_water_i,m_water)
%this model solves for the outlet conditions of CO2 and water
%in the gas cooler.  The function determines the water outlet temp by
iterative
%proceedure using secant method.

%define arrays
T_wi=zeros(3,1);
T_wo=zeros(3,1);
err=zeros(3,1);

%water outlet temperature initial estimations
T_wo(1)=T2-2; %1st guess
T_wo(2)=T2-4; %2nd guess

%send simulation info to other function
secant=Mgascooler_II(T2,P2,m,m_water);

%call upon function to determine the temp press distribution across GC
%using first guess for water outlet
[T_wi(1) T3 P3 h3 minRe]=secant(T_wo(1));
    err(1)=T_water_i-T_wi(1);  %calculated water inlet = actual??
%using 2nd guess for water outlet
[T_wi(2) T3 P3 h3 minRe]=secant(T_wo(2));
    err(2)=T_water_i-T_wi(2);   %calculated water inlet = actual??
    j=2;
    while abs(err(j))>.001
        j=j+1;
        %determine next value of water outlet temp
    T_wo(j)=T_wo(j-1)-err(j-1)*(T_wo(j-1)-T_wo(j-2))/(err(j-1)-err(j-2));
        %solve for CO2 outlet using current value of water outlet temp
        [T_wi(j) T3 P3 h3 minRe]=secant(T_wo(j));
            err(j)=T_water_i-T_wi(j);  %calculated water inlet=actual??
    end
Twater=T_wo(j);
end
%Nomenclature
% T3          K        co2 outlet temp
% P3          kPa      co2 outlet pressure
% h3          kJ kg    co2 outlet enthalpy
% Twater      K        final water outlet temp
% minRe                minimum CO2 reynolds #
% T_wi        K        calculated water inlet temp
% T_wo        K        assumed water outlet temp
% err         K        difference
% m           kg s     co2 mass flow rate
% m_water     kg/s     water mass flow rate
% T2          K        co2 inlet temp
% P2          kPa      co2 inlet press
% T_water_i   K        actual water inlet temp
```

e) Gas Cooling Model: Part 2

Function Title: Mgascooler_II.m

```
function secant=Mgascooler_II(T2,P2,m,m_w)
secant=@shooting;
    function [T_w_calc T3 P3 h3 min_reynolds]=shooting(Two)
%calculates the gas cooler temperature pressure drop distribution across
%the gas cooler.  Outputs a calculated value of water inlet temp and the
%co2 outlet temp and pressure.  Calls upon to wall_temp to estimate the
co2
%side wall temperature for calculation purposes.

%Gas cooler dimensions
L=15;
l=.1;       % mesh size or segment length [m]
N=L/l;
di=.005;
do=.007;
D=.016;
ktube=400;

%calculated parameters
A_r=pi()*di*l;                  %CO2 side segment area [m^2]
A_w=pi()*do*l;                  %water side segment area [m^2]
Dh_w=D-do;                      %hydraulic diam of water tube [m]
G_w=m_w/(pi()*(D^2-do^2)/4);    %mass velocity of water [kg/m^2*s]
G=m/(pi()/4*di^2);              %mass velocity of CO2 [kg/m^2*s]

%define arrays
T=zeros(N+1,1);    %temperature gradient arrays
T_w=zeros(N+1,1);
P=zeros(N+1,1);    %pressure gradient array
Q=zeros(N,1);      %Heat transfer for each ht-ex segment
h=zeros(N+1,1);
alpha_r=zeros(N+1,1);

T(1)=T2;             %CO2 temp at inlet
T_w(1)=Two;          %assign water temp at outlet
Outletguess=Two;
min_reynolds=10000000;    %Dummy value to start
P(1)=P2;
diff_est=20; %this variable is used to estimate dT between wall and bulk
                      %temp on CO2 side; this is a dummy value to start
for n=1:N

  if T_w(n)<274, break, end %will go to solid phase so break from loop

%----Water-Side----
    [Cp_w visc_w cond_w]=refpropm('CVL','T',T_w(n),'P',101.325,'WATER');
    Re_w=G_w*Dh_w/visc_w;           %Reynold number of water
    Pr_w=visc_w*Cp_w/cond_w ;        %Prandl number of water
```

```
    % water-side heat transfer coefficient
    ffw=(0.79*log(Re_w)-1.64)^-2;
    Nu_w=((ffw/8)*(Re_w-1000)*Pr_w)/(1.07+12.7*(ffw/8)^.5*(Pr_w^(2/3)-
1));
    CF=.86*(do/D)^(-.16); %correlation correction factor for annular flow
    alpha_w=CF*Nu_w*cond_w/Dh_w; %heat transfer coeficient for water-side

%CO2-side heat trasfer-------
        %use func to determine the wall temp on CO2 side of tube &
        %associated local ht trans coef
    [alpha_r(n)
Twall]=wall_temp(T(n),T_w(n),P(n),di,do,l,ktube,G,alpha_w,diff_est);

    diff_est=T(n)-Twall;%update temperature difference estimator at inlet
                        %of current segment  for use on next segment
    UA=(1/(A_r*alpha_r(n))+1/(A_w*alpha_w)+log(do/di)/(2*pi()*l*ktube))^-
1;
    [Cp_rb]=refpropm('C','T',T(n),'P',P(n),'CO2');
    Cr=m*Cp_rb;
    Cw=m_w*Cp_w;
    Cmin=min(Cr,Cw);
    Cmax=max(Cr,Cw);
    C=Cmin/Cmax;
    NTU=UA/Cmin;
    eff=(1-exp(-NTU*(1-C)))/(1-C*exp(-NTU*(1-C)));
    T_w(n+1)=(eff*Cmin*T(n)/Cw-T_w(n))/(eff*Cmin/Cw-1);
    Q(n)=eff*Cmin*(T(n)-T_w(n+1));
    T(n+1)=T(n)-Q(n)/Cr;

%CO2-Pressure-drop
    [dens visc]=refpropm('DV','T',T(n),'P',P(n),'CO2');
    Re=G*di/visc;                   %Reynold number CO2 at bulk temp
                if min_reynolds>Re
                    min_reynolds=Re;
                end
        if Re>=20000
            ee=.184*Re^-.2;  %Darcy friction factor using Blasius
        elseif Re<=20000 && Re>=2300
            ee=.316*Re^-.25;   %Darcy friction factor using Blasius
        else
            disp 'Laminar CO2 flow.'
            ee=64/Re;
        end
    del_P=.001*ee*G^2*l/(2*dens*di);     %Pressure drop:  Darcy-Wesibach
    P(n+1)=P(n)-del_P;

end

%this 'if' loop determines if water is close to solid phase and estimates
%the input water temp if the water has gone to solid phase
    if T_w(n)<274
        T_w_calc=(N+1-n)*((T_w(1)-T_w(n))/n); %water inlet estimation
        %output assignments
        P3=P(n);     % dummy value to pass
        T3=T(n);     % dummy value to pass
```

```
        h3=h(n);     % dummy value to pass
    else

%real output value assignments
    T_w_calc=T_w(N+1);
    P3=P(N+1);
    T3=T(N+1);
    h3=refpropm('H','T',T3,'P',P3,'CO2');
    end
end
end

%Nomenclature
% A_r            m^2          co2-side tube wall surface area
% A_w            m^2          water-side tube wall surface area
% alpha_r        W m^2*K      local co2 ht trans coef
% alpha_w        W/m^2*K      local water ht trans coef
% CF                          correction factor for annular flow
% Cmax           kJ/s*K       max heat capacity rate
% Cmin           kJ/s*K       min heat capacity rate
% cond_w         kg/m^3       water thermal conductivity
% Cp_rb          kJ/kg*K      co2 specific heat at bulk temp
% Cp_w           kJ/kg*K      water specific heat
% Cw             kJ/kg*K      water specific heat
% D              m            outer tube inner-diameter
% del_P          kPa co2      pressure drop
% dens           kg/m^3       co2 density @ bulk temp
% Dh_w           m            water-side hydraulic diameter
% di             m            inner-tube inner diameter
% do             m            inner tube outer-diameter
% ee                          co2 friction factor
% eff                         heat exchanger effectiveness
% err            K            difference
% ffw                         water-side friction factor
% G_w            kg/s*m^2     water mass flux
% G_w            kg/s*m^2     co2 mass flux
% h              kJ/kg        co2 local enthalpy
% h3             kJ/kg        co2 outlet enthalpy
% ktube          W/m*K        thermal conductivity of tube
% L              m            Gas cooler length
% l              m            segment length
% m              kg/s         co2 mass flow rate
% m_w            kg/s         water mass flow rate
% min_reynolds                minimum CO2 reynolds #
% N                           Number of segements of mesh
% NTU                         number of transfer units
% Nu_w                        water Nusselt
% P              kPa          local co2 pressure
% P2             kPa          co2 inlet press
% P3             kPa          co2 outlet pressure
% Pr_w                        water-side Prandl
% Q              W            local heat transfer rate
% Re_w                        water-side Reynolds
% T              K            local co2 temp
% T_w            K            local water temp
```

```
% T_w_calc       K           calculated water inlet temp
% T2             K           co2 inlet temp
% T3             K           co2 outlet temp
% Twall          K           co2-side tube wall temperature
% Twater         K           final water outlet temp
% Two            K           assumed water outlet temp
% UA             W/K         overall heat conductance
% visc           Pa*s        co2 viscosity @ bulk temp
% visc_w         Pa*s        water viscosity
```

f) Gas Cooling Model: Part 3

Function Title: wall_temp.m

```
function [htcoef
wlltmp]=wall_temp(T_rb,Twater,P,di,do,l,k,G,alpha_w,diff_est)

%calculates the gas cooler inner wall temperature for the current segment
%and the heat transfer coefficient by iteration

    %Bulk properties-------
    [dens_rb Cp_rb visc_rb cond_rb]=
refpropm('DCVL','T',T_rb,'P',P,'CO2');
    Re_rb=G*di/visc_rb;                %Reynold number CO2 at bulk temp
    Pr_rb=visc_rb*Cp_rb/cond_rb;       %Prandl number CO2 at bulk temp
    f_b=(0.79*log(Re_rb)-1.64)^-2;
    Nu_b=((f_b/8)*(Re_rb-1000)*Pr_rb)/(1.07+12.7*(f_b/8)^.5*(Pr_rb^(2/3)-
1));

    %Wall temperature initial estimations
    T_rw(1)=T_rb-.5;               %1st estimation
    T_rw(2)=(T_rb+Twater)/2;       %2nd estimation

    %Calculate heat transfer coef using 1st estimation
    [dens_rw Cp_rw visc_rw
cond_rw]=refpropm('DCVL','T',T_rw(1),'P',P,'CO2');
    Re_rw=G*di/visc_rw;                %Reynold number CO2 at wall temp
    Pr_rw=visc_rw*Cp_rw/cond_rw;       %Prandl number CO2 at wall temp
    f_w=(0.79*log(Re_rw)-1.64)^-2;
    Nu_w=((f_w/8)*(Re_rw-1000)*Pr_rw)/(1.07+12.7*(f_w/8)^.5*(Pr_rw^(2/3)-
1));

    Nu=((Nu_b+Nu_w)/2)*cond_rw/cond_rb;%overall co2 Nusselt correlation
of Pitla et al
    alpha_r=Nu*cond_rb/di;              %co2 ht trans coeff

UA=(1/(pi()*l*di*alpha_r)+1/(pi()*l*do*alpha_w)+log(do/di)/(2*pi()*l*k))^
-1;
    Qc=UA*(T_rb-Twater);
    Twall=T_rb-Qc/(pi()*di*l*alpha_r);
    err(1)=Twall-T_rw(1); %error between actual and calculated wall temp

    %Calculate heat transfer coef using 2nd estimation
    [dens_rw Cp_rw visc_rw
cond_rw]=refpropm('DCVL','T',T_rw(2),'P',P,'CO2');
    Re_rw=G*di/visc_rw;
    Pr_rw=visc_rw*Cp_rw/cond_rw;
    f_w=(0.79*log(Re_rw)-1.64)^-2;
    Nu_w=((f_w/8)*(Re_rw-1000)*Pr_rw)/(1.07+12.7*(f_w/8)^.5*(Pr_rw^(2/3)-
1));

    Nu=((Nu_b+Nu_w)/2)*cond_rw/cond_rb;
    alpha_r=Nu*cond_rb/di;                        %co2 ht trans coeff
```

```
UA=(1/(pi()*l*di*alpha_r)+1/(pi()*l*do*alpha_w)+log(do/di)/(2*pi()*l*k))^
-1;
    Qc=UA*(T_rb-Twater);
    Twall=T_rb-Qc/(pi()*di*l*alpha_r);
    err(2)=Twall-T_rw(2);  %error between actual and calculated wall temp

    n=2;
    while abs(err(n))>.001 && n<=25
        n=n+1;
        %next estimation of wall temp
        T_rw(n)=T_rw(n-1)-(err(n-1)*(T_rw(n-1)-T_rw(n-2)))/(err(n-1)-
err(n-2));

        if T_rw(n)<Twater    % correction if updated wall temp is too low
            TooLow=T_rw(n)
            T_rw(n)=T_rw(1)
        end

        if n>25              % final value selected if too many iterations
            T_rw(n)=T_rb-diff_est;
            Bulk=T_rb
            estimate=T_rw(n)
        end
        %Calculate heat transfer coef using current wall temp
        [dens_rw Cp_rw visc_rw
cond_rw]=refpropm('DCVL','T',T_rw(n),'P',P,'CO2');
        Re_rw=G*di/visc_rw;              %Reynold number CO2 at wall temp
        Pr_rw=visc_rw*Cp_rw/cond_rw;      %Prandl number CO2 at wall temp
        f_w=(0.79*log(Re_rw)-1.64)^-2;
        Nu_w=((f_w/8)*(Re_rw-
1000)*Pr_rw)/(1.07+12.7*(f_w/8)^.5*(Pr_rw^(2/3)-1));

        Nu=((Nu_b+Nu_w)/2)*cond_rw/cond_rb;
        alpha_r=Nu*cond_rb/di;                          %co2 ht trans coeff

UA=(1/(pi()*l*di*alpha_r)+1/(pi()*l*do*alpha_w)+log(do/di)/(2*pi()*l*k))^
-1;
        Qc=UA*(T_rb-Twater);
        Twall=T_rb-Qc/(pi()*di*l*alpha_r);
        err(n)=Twall-T_rw(n);
    end
htcoef=alpha_r;
wlltmp=T_rw(n);
end



%Nomenclature
% alpha_r       W m^2*K     co2 heat transfer coefficient
% alpha_w       W/m^2*K     water heat transfer coefficient
% cond_rb       W m*K       co2 conductivity - bulk temp
% cond_rw       W/m*K       co2 conductivity - wall temp
% Cp_rb         kJ kg*K     co2 spec. heat - bulk temp
% Cp_rw         kJ kg*K     co2 spec. heat - wall temp
% dens_rb       kg/m^3      co2 density - bulk temp
```

```
% dens_rw        kg/m^3      co2 density   wall temp
% di             m           inner-tube inner-diameter
% diff_est       K           estimation of temp diff wall vs bulk
% do             m           inner-tube outer-diameter
% err            K           temp difference  estimated vs calculated
% f_b                        co2 friction factor   bulk
% f_w                        co2 friction factor   wall temp
% G              kg/s*m^2    co2 mass flux
% htcoef         W/m^2*K     final co2 ht trans coef
% k              W/m*K       thermal conductivity of tube wall
% l              m           segment length
% Nu                         co2 avg Nusselt
% Nu_b                       co2 Nusselt   bulk temp
% Nu_w                       co2 Nusselt   wall temp
% P              kPa         co2 pressure
% Pr_rb                      co2 Prandl #   bulk temp
% Pr_rw                      co2 Prandl #   wall temp
% Qc             W           overall heat transfer rate
% Re_rb                      co2 Reynolds #   bulk temp
% Re_rw                      co2 Reynolds #   wall temp
% T_rb           K           co2 bulk temperature
% T_rw           K           estimated co2 wall temperature
% Twall          K           calculated co2-side wall temp
% Twater         K           water temperature
% UA             W K         overall heat conductance
% visc_rb        Pa*s        co2 viscosity   bulk temp
% visc_rw        Pa*s        co2 viscosity   wall temp
% wlltmp         K           final co2 wall temperature
```

LIST OF PUBLICATIONS

1. Austin, B.T., Sumathy, K. Modeling a direct expansion geothermal heat pump using carbon dioxide in a transcritical cycle. Proceedings of the 2011 Renewable Energy World Conference & Expo; Tampa, Florida; March 8-10, 2011.
2. Austin, B.T., Sumathy, K. Thermophysical properties of supercritical CO_2 and their impacts on transcritical heat pump design. Proceedings of the 9th International Conference on Sustainable Energy Technologies; Shanghai, China, August 24-27; 2010.
3. Austin, B.T., Sumathy, K. Transcritical carbon dioxide heat pump systems: A review. Renewable and Sustainable Energy Reviews. (submitted November 4, 2010)
4. Austin, B.T., Sumathy, K. Parametric study on the performance of a direct expansion geothermal heat pump using carbon dioxide. Applied Thermal Engineering. (submitted April 20, 2011)